HIGH THROUGHPUT METHOD FOR THE DEVELOPMENT OF BULK LEAD FREE PIEZOELECTRIC CERAMICS

Dissertation

Zur Erlangung des Grades

des Doktors der Naturwissenschaften

der Naturwissenschaftlich-Technischen Fakultät III

Chemie, Pharmazie und Werkstoffwissenschaften

Der Universität des Saarlandes

Von

Aurélie Cardin

Saarbrücken

2009

Tag des Kolloqiums: 19.01.2009

Dekan: Prof. Dr. Ulli Müller

Berichterstatter: Prof. Dr. W. F. Maier

Prof. Dr. R. Clasen

Index

Index

Index

Nomenclature

HTE	High Throughput Experimentation
HTS	High Throughput Screening
MPB	Morphotropic phase boundary
PZT	$Pb(Zr,Ti)O_3$
KNN	$(K,Na)NbO_3$
D_{ij}	Dielectric displacement in i and j directions
ε_0	Dielectric permittivity of air
ε_{ij}	Dielectric permittivity of material in i and j directions
ε_r	Relative dielectric permittivity
P	Polarisatioon
P_r	Remanent polarisation
P_s	Saturation polarisation
E_{ij}	Electric field in i and j directions
d_{ijk}	piezoelectric constant in i, j or k directions
d_{33}^{*}	Large signal piezoelectric constant in Z-direction with electric field in Z-direction
tan δ	Dielectric losses
T	Stress
S	Strain
Kp	Planar coupling factor
Q	Mechanical factor
C	Capacitance
Tc	Curie temperature
t	Goldschmidt factor
R_A	Ionic radius large cation
R_B	Ionic radius small cation
R_O	Ionic radius oxygen
BT	$BaTiO_3$
PMN	$Pb(Mg,Nb)O_3$
PNN	$Pb(Ni,Nb)O_3$
EA	Earth alkali
TB	Tungsten-Bronze
SBN	$Sr_{1-x}Ba_xNb_2O_6$

Nomenclature

SCNN $(Sr,Ca)_{2-x}Na_xNb_5O_{15}$

KLN $K_3Li_2Nb_5O_{15}$

T_{O-T} Orthorhombic-Tetragonal phase transformation temperature

NN $NaNbO_3$

KN $KNbO_3$

BNT $(Bi,Na)TiO_3$

BKT $(Bi,K)TiO_3$

SPS Spark plasma sintering

LT $LiTaO_3$

BNN $Ba_{2-x}Na_xNb_5O_{15}$

LKNNT $(Li,K,Na)(Nb,Ti)O_3$

I. Introduction

1. Preamble

Piezoelectricity is the ability of certain crystalline materials to develop an electric charge proportional to a mechanical stress. The materials having this ability possess also the reverse effect, i.e. generate mechanical strain proportional to an applied voltage, this is called inverse piezoelectric effect[1]. The word "piezoelectric" is derived from the Greek word "piezein" which means to press or squeeze.

2. Historical introduction

Piezoelectricity was first observed on a quartz crystal by J. and P. Curie in 1880 but it is only almost 40 years later that Cady used it as radio frequency oscillator. A few years later the discovery of the barium titanate by Hippel *et al.* and the discovery of the poling process lead to the use of $BaTiO_3$ in phonograph pickers. The discovery of lead zirconate-titanate (PZT) by Jaffe *et al.* in 1954 opened a wide field of applications to piezoelectric ceramics[2].

Both, the direct and the inverse piezoelectric effect can be used for devices or they can be used simultaneously[3].

The devices using the direct piezoelectric effect are basically used in 2 applications: detection of large or small signals. The detection of large signals is used to generate high voltage and can be applied to power generators. The devices based on the detection of small signals are basically used in the detection of sound, ultrasound, force, acceleration or pressure. Small changes in pressure for example can be easily detected by some piezoelectric materials at high frequency inducing a change in the electric signal produced, which makes these materials very effective for sensors.

Both the direct and the inverse piezoelectric effect can be used in devices like frequency filters, acoustic delay line, sonar sensors or transformers.

The inverse piezoelectric effect is used for devices like actuators, motors, ink jet printer heads or sound and ultrasound transducers. The accuracy, the force, the repeatability of the strain produced by certain piezoelectric material make them suitable for such applications.

Piezoelectric ceramics can be employed for a lot of industrial applications. However the use of lead is strictly limited as lead is a heavy element and a potent neurotoxin. The European Council Directive on Waste from Electrical and Electronic Equipment" (WEEE) proposes restrictions on the use of lead among other materials in electronic products[4]. An exception was temporarily made about PZT as no other material was found to replace it for actuators. However, alternative lead-free ceramics should be investigated. The Japanese industry is rather active and lead-free ceramics with performances comparable to those of PZT are already available[5]. Therefore new development methods should be carried out to make the market pressure.

3. *High Throughput Experimentation*

The period between the generation of an idea and the moment it reaches the market is known under "time to market". A short time to market is one of the key success factors of any industrial product. The time to market of piezoelectric devices could be successfully shortened by the application of High Throughput Experimentation (HTE) combined with High Throughput Screening (HTS) to their development. As the name suggests these methods permit the production and the properties screening of a high volume of samples by significantly increasing the speed at which new materials are engineered. HTE was developed in the early 1990's in the drug industry and is implemented at present in the development of catalysts, or polymers and pharmaceutical products[6].

The generic workflow of HTE is shown in figure 3. The data collected from these processes is subsequently analysed through data mining techniques. HTE and HTS exist in different size, scale and form, depending on the material researched. However the same general steps are followed for each technology.
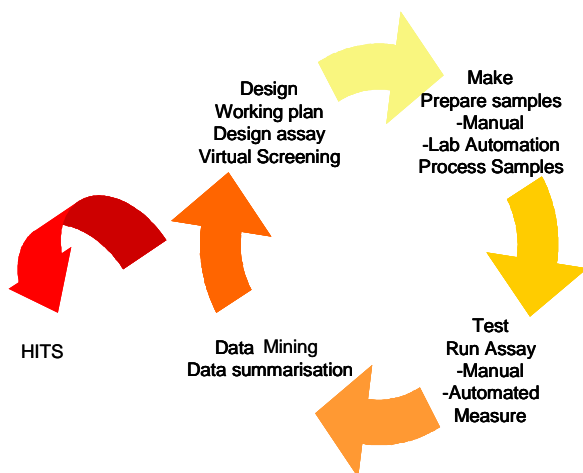
Fig. 1: Generic HTE workflow

a. Design

Although the HTE method allows the production of a significant amount of samples, the experiences should be designed in accordance with the selected experimental model. This model varies with the platform which is dependent on the type of material evaluated. The design of experiments optimises the efficiency of the method.

b. Make

The make phase has three main components: starting materials or sources, formulations and samples production. This depends on the type of material evaluated: films, bulk…

c. Test

The test phase evaluates the key properties. These properties are conditioned by the application of the material researched. Often new equipment specific to the material and the application must be designed for the test phase.

d. Data Mining

During the data mining step the data are compiled and analysed. With the results collected during a run, the design of experiments for the next run can be better oriented and new areas of interest can be explored.

Various technologies can be used to produce the samples; and different technologies can be used in parallel, depending on the throughput desired and the state of the research. To screen a large compositional area, fully automated methods producing small size samples are used, such as the sol-gel method. As the screening progresses the quantity of samples can be reduced and their size increased.

Liquid handling systems are often used for the first screening as the precision of the automated solution is quite high and the manufacturing of samples can be quite easy. A piping robot can mix different substances and coat them on a substrate. This type of method was first used to discover new dielectrics in 1995[7]. Samples were coated on a silicium wafer coated with platinum and sintered together. Then their key properties are screened.

Generally materials with interesting properties that can be screened on a wafer can be engineered by this method. The test method depends on the material investigated (for catalyst IR is often used, for luminescent materials a spectrometer will be used etc…).

Solid handling systems are not so widely used as the dosing system is not trivial. Moreover the handling of solid samples on one plate is sometimes not so simple due to the necessity of mixing the powders together. In the case of ceramics and in particular for piezoelectric ceramics, these should be often grinded or the powders employed must have a very fine grain size, which makes the automated dosage more difficult.

4. High Throughput Experimentation for the Development of new Piezoelectric Ceramics

As explained above the fast development of new piezoelectric ceramics is crucial for the market but on the other hand HTE solutions are quite difficult to set up for piezoelectric ceramics due to the long preparation time needed. The aim of this work is to find an efficient compromise between the sample quality and the rapidity of the production and evaluation of new materials.

At present only partial HTE solutions are developed for the production of piezoelectric ceramics[8], therefore a workflow should be developed and then an improvement cycle for each step should be carried out.

The work during the project was divided in two parts. First new lead-free dielectrics should be identified with a sol-gel method; the sol-gel method which has a very high throughput is set up to identify new materials with a high dielectric constant. After this phase the materials identified should be processed through the mixed-oxide route where the throughput is lower but other parameters like sintering temperature or doping could be adjusted. This work is based only on the mixed-oxide route as both parts were handled independently.

First the classical preparation must be evaluated and innovative production solutions should be met. Then for the qualification of the new materials, the key properties should be chosen and an adapted measurement solution developed. The focus on different properties depends on the application. The aim of this project is to find a lead-free material for actuators; therefore the emphasis is put on the indirect piezoelectric properties, especially materials having the highest strain for a given electric field. In the following section the definitions of the key properties are given, before proceeding with the description of the state of the art in the field of piezoelectric lead-free ceramics.

5. Scientific project and Goals

As stated before the market of piezoelectric ceramics for actuator applications is rather important. The most employed material is PZT which contains almost 60 weight % lead and due to environmental concerns the use of lead should be reduced in the next years. Therefore HTE method for the production and screening of bulk lead-free piezoelectric ceramics produced from a mixed-oxide route should be developed to accelerate the material development. This HTE method must also be focused on the processing and evaluation of bulk samples and moreover it should deliver complementary information regarding doping and/or sintering parameters.

The goals of this works were the following:

Set up of a HTE route for the synthesis of bulk piezoelectric ceramics

Set up of a HTE screening of key parameters of bulk piezoelectric ceramics

Discover new lead-free piezoelectric bulk ceramics

Optimise new lead-free piezoelectric bulk ceramics

The first two parts are treated in chapter IV. Thereafter the discovery of new lead-free piezoelectric ceramics is investigated in chapter VII and finally the optimisation is considered in chapter VIII.

The basics and the state of the art lead-free piezoelectric ceramics is first examined in chapters II and III.

II. Basics

1. Ferroelectricity and Antiferroelectricity

The ferroelectricity is the presence of a spontaneous electric moment in a crystal which can be changed in its orientation between two or more distinct crystallographic directions by applying an external electric field[9]. The term ferroelectricity is used in analogy with ferromagnetism in which materials exhibit a spontaneous magnetic moment. Another phenomenon similar can exist, the antiferroelectricity. An antiferroelectric state is defined as one in which lines of ions in the crystal are spontaneously polarized, but with neighboring lines polarized in antiparallel directions.
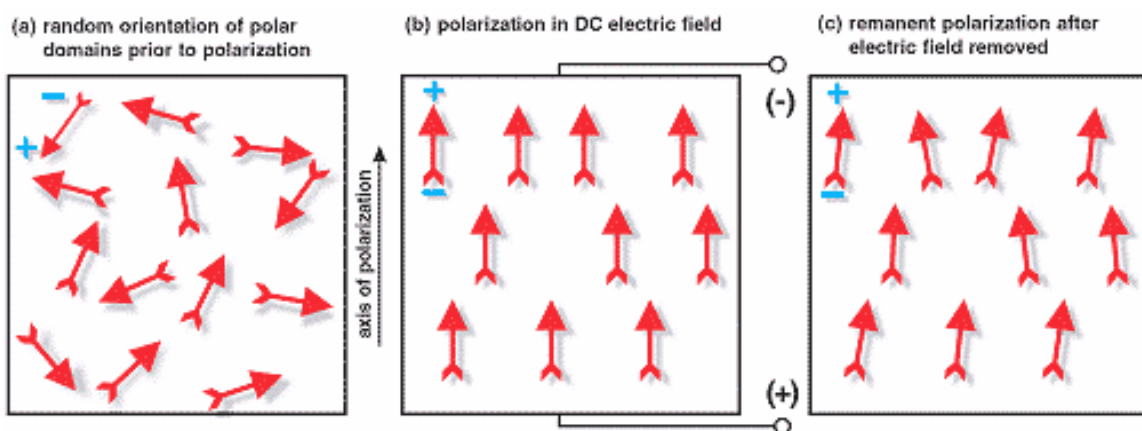
Fig. 2: Domains and polarisation in a ferroelectric material

From the thirty-two crystal classes, twenty-one are non symmetric and of these twenty are polar. If the dipole is reversible applying an electric field, the material is said to be ferroelectric. There are two types of ferroelectrics: displacive and order-disorder. The piezoelectrics are of the displacive type. When an ion is displaced from its equilibrium the internal electrical field forces increase faster than the elastic restoring forces creating an asymmetric shift and hence a dipole moment.

2. Ferroelectric polarisation

The polarisation is the result of the dipole moment in the crystals in the material. In a non-poled ceramic the total polarisation can be 0 as the dipoles can have different orientations but in a poled ceramics the dipole moments are aligned which results in a remanent polarisation [10] . The polarisation is the measure of the degree of ferroelectricity. The most frequent approach to measure the polarisation is the investigation of charge-field hysteresis as shown in Fig. 5.

D is the dielectric displacement and is equal to:

$$D = \varepsilon_o E + P \qquad\qquad\qquad (1.1)$$

where ε_0 is the dielectric permittivity of air and is equal to 8.85 10^{-12} F/m, E the electric field applied and P the polarisation. The remanent polarisation (Pr) is the polarisation (expressed in C/m²) that remains after an applied electric field is removed and the coercitive field (Ec) is the necessary field to switch the remanent polarisation to 0. When no further domain orientation can occur, the behaviour between the dielectric displacement and the electric field becomes linear. This linear response extrapoled to the polarisation axis (E=0) is the saturation polarisation (Ps).
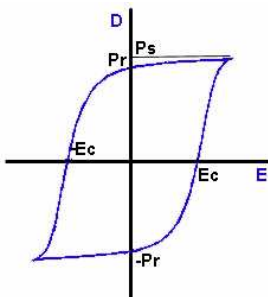
Fig. 3: Typical hysteresis loop of dielectric displacement vs. electric field[3]

3. The perovskite structure

The perovskite structure is the structure of $BaTiO_3$, which was the first piezoelectric ceramic discovered. Fig. 6 describes the dipole moment in a perovskite structure. The perovskite is a primitive cell with a large ion in A-site (barium for $BaTiO_3$), a small ion in B-site (titanium for $BaTiO_3$) and oxygen in the centre of the faces[11].
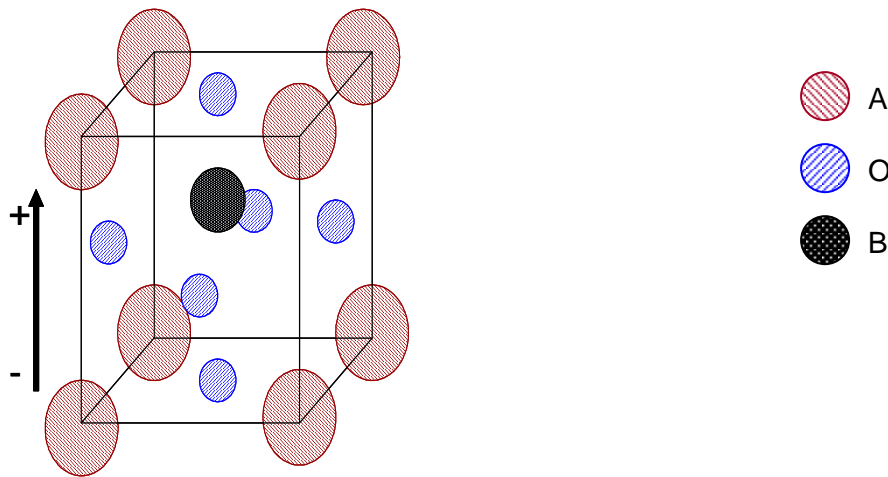
Fig. 4: Dipole moment in a tetragonal perovskite

Modification of the perovskite structure to enhance the properties of the material should be carried out according to the Goldschmidt tolerance factor t. The relationship 1.2 describes the ideal perovskite structure when t=1:

$$t = \frac{R_A + R_O}{\sqrt{2}\left(R_B + R_O\right)} \tag{1.2}$$

where R_A, R_B and R_O indicate the ionic radii of the large and small cations and the anions respectively. Generally for t<0.92 the antiferroelectric properties do not appear, for 0.92<t<1 the structure tends to be cubic and for t>1 the structures are generally ferroelectric.

4. *Dielectric constant and losses*[12]

The electric displacement in a dielectric material is related to the applied electric field by the relation:

$$D_i = \varepsilon_{ij} E_j \tag{1.3}$$

where ε_{ij} is the dielectric permittivity of the material, D_i the electric displacement and E_j the electric field component.

To characterise a material, it is usual to refer to the relative dielectric constant ε_r which is defined as the ratio between the charge stored on an electrode slab of the material and the charge stored on identical electrodes separated by air. The relation between the dielectric permittivity of the material and its relative dielectric constant is:

$$\varepsilon_{ij} = \varepsilon_0 \varepsilon_r \tag{1.4}$$

The permittivity of the material is a dimensionless unit. For practical measurement the capacitance (C) of the material is measured and is related to the permittivity ε_r through the equation:

$$C = \varepsilon_0 \varepsilon_r \frac{A}{d} \tag{1.5}$$

where A is the surface of the sample and d the distance between the electrodes. As the capacitance depends on the geometry of the sample, ε_r represents a material data and is commonly used to describe the material properties. ε_r refers often to the domain displacement. A high ε_r is the signal of a difficult but stable polarisation as a lower ε_r is the signal of an easily polarisable material but which is easy to depolarise.

To measure the relative dielectric constant of a material, alternative voltage is used. The alternative voltage has two components, a real one called in-phase and an imaginary one called out-of-phase. The dielectric losses characterise the ratio of the out-of-phase component to the in-phase component.

The dielectric losses in the material are often referred as tan δ which is the tangent of the loss angle or the ratio of parallel resistance to the parallel reactance, expressed in percent. For a material having interesting properties the losses should be as low as possible.

5. The piezoelectric tensor[13]

The equations of the state of the piezoelectric effect relate the elastic variables, stress and strain to the electric variables, field and displacement. The piezoelectric effect can be described by the results of different electrical behaviour of the material with the relation:

$$D_{ij} = d_{ijk} T_{jk} + \varepsilon_{ij}^T E_j \tag{1.6}$$

or the Hooke's Law can be used to define the reverse piezoelectric effect and in this case the relation used is:

$$S_{ij} = s_{ijkl}^E T_{kl} + d_{kij} E_k \tag{1.7}$$

where S_{ij} is the strain, s_{ijkl}^E the compliance, T_{kl} the stress and d_{kij} the piezoelectric constant. The piezoelectric constant is often used to define the performance of a material destined to actuator application. To measure it the direct piezoelectric effect or the reverse piezoelectric effect can be used. During this PhD the inverse piezoelectric

effect was used to quantify the performances of the new materials, therefore more attention will be paid to the equation 1.8.

The compliance and the piezoelectric constant are orientation dependant and the equation 1.7 can be replaced by:

$$
\begin{bmatrix} S_1 \\ S_2 \\ S_3 \\ S_4 \\ S_5 \\ S_6 \end{bmatrix} = \begin{bmatrix} s_{11}^E & s_{12}^E & s_{13}^E & 0 & 0 & 0 \\ s_{21}^E & s_{22}^E & s_{23}^E & 0 & 0 & 0 \\ s_{31}^E & s_{32}^E & s_{33}^E & 0 & 0 & 0 \\ 0 & 0 & 0 & s_{44}^E & 0 & 0 \\ 0 & 0 & 0 & 0 & s_{44}^E & 0 \\ 0 & 0 & 0 & 0 & 0 & s_{66}^E \end{bmatrix} \begin{bmatrix} T_1 \\ T_2 \\ T_3 \\ T_4 \\ T_5 \\ T_6 \end{bmatrix} + \begin{bmatrix} 0 & 0 & d_{31} \\ 0 & 0 & d_{31} \\ 0 & 0 & d_{33} \\ 0 & d_{15} & 0 \\ d_{15} & 0 & 0 \\ 0 & 0 & 0 \end{bmatrix} \begin{bmatrix} E_1 \\ E_2 \\ E_3 \end{bmatrix}
\tag{1.8}
$$

The annotations 1…6 refer to the axes as described in fig. 1. The axe 3 refers to the poling axe and the axes 1 and 2 refer arbitrarily to perpendicular axes.

The method of measurement chosen allow measuring the displacement in the poling direction, therefore S_3 is measured. The equation 1.6 becomes:

$$
S_3 = s_{31}^E T_1 + s_{32}^E T_2 + s_{33}^E T_3 + d_{33} E_3
\tag{1.9}
$$

To measure the free displacement of a ceramic no stress is applied on the sample and $T_{1...6}$ are equal to 0 and the equation 1.7 becomes:

$$
S_3 = d_{33} E_3
\tag{1.10}
$$
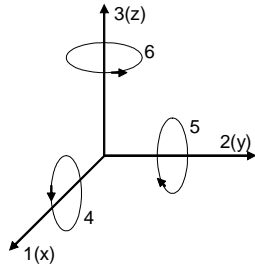
Fig. 5: Notation of axes

The piezoelectric coefficient d_{33} can also be defined as:

$$
d_{33} = \left(\frac{\partial S_3}{\partial E_3} \right)_T
\tag{1.11}
$$

This definition is employed to quantify the piezoelectric coefficient during the measurement as the stress is constant. The piezoelectric coefficient d_{33} is expressed in pm/V or C/N. The notation C/N is used in case of a direct piezoelectric effect measurement and pm/V is used in case of an inverse piezoelectric effect measurement. Thus the notation pm/V will be used in the rest of this work as the measurement method is the inverse piezoelectric effect.

6. Planar Coupling Factor k_p and Mechanical Quality factor Q^{14}

The energy to a piezoelectric body can be applied either by an electric field or stressing it. The response will be either mechanical or electrical. The planar coupling factor k_p is the square root of the mechanical energy applied transformed into electrical output or the square root of the applied electric energy converted into mechanical energy. Or in other word k_p is the power conversion efficiency. It is measured by a resonance method.

The mechanical quality factor Q characterises "the sharpness of the resonance" and is obtained from the 3dB bandwidth of the series resonance of a resonating system. Q is also interpreted as the ratio of total energy stored to the energy loss per cycle multiplied by a constant or the ratio of reactance to resistance.

Both properties were not systematically measured during the first screening but discrete samples were chosen to be evaluated.

7. Curie temperature

The Curie temperature is named after Pierre Curie. For ferromagnetic material it is the temperature at which it looses its permanent magnetic field. Due to the analogy between ferromagnetism and ferroelectricity, the Curie temperature is also used to describe the temperature where ferroelectric materials loose their spontaneous polarisation.

All piezoelectric properties as well as mechanic or elastic properties vary with the temperature. During the heating of the material a change occurs in the crystal lattices. Many of piezoelectric ceramics become cubic and they loose their polarisation. An effective method to measure the Curie temperature is measuring the dependence of the capacity with the temperature. Generally above this crystal structure transition the dielectric constant obeys the Curie-Weiss law:

$$\varepsilon_r - 1 = \frac{C}{T - T_c} \tag{1.12}$$

where C is a constant called the Curie constant, T the temperature and T_c the Curie temperature. Near the Curie temperature the crystal structure is often 'soft' and can be

polarised strongly with a small electric field. Therefore the permittivity of many of the useful ferroelectrics is very high in the vicinity of the Curie temperature[15]. For broad scope of application, materials having a high Curie temperature are often recommended. For the actuators in injectors for example, the engine service temperature is situated around 90°C. In case of overhea t, up to 130°C, the injectors should be able to run, therefore a material with a Curie temperature much over 130°C must be employed. An additional safty factor advises to employ materials having the double temperature, thus materials having a minimal Curie temperature of 260°C are generally employed for injectors.

III. State of the art of Lead-Free Piezoelectric Materials

1. PZT-based compositions

The most common piezoelectric material used at the moment is PZT. As discussed previously, PZT was discovered in 1954 by Jaffe and co-workers and it has attracted most research efforts carried out in the field of piezoelectric during the last half century. Nowadays PZT is widely used under its multiple forms and its production is well established. Before beginning with the state of the art of lead-free piezoelectric materials, a small introduction on lead-containing materials will be presented to establish a realistic comparison between both material classes.

$Pb(Zr, Ti)O_3$ is a solid solution between $PbTiO_3$, which is tetragonal and ferroelectric, and $PbZrO_3$, which is orthorhombic and antiferroelectric[16]. Around 52% $PbZrO_3$, there is a coexistence of both structures and a morphotropic phase boundary (MPB) is present. The highest piezoelectric effects are measured near the MPB. Early works show the benefits of modifications of PZT through isovalent substitutions of lead by increasing the piezoelectric constant [17]. Modifications are possible with elements compensating valence substitutions of A or B-sites. Other clases of additives are those which cause A or O-position vacancies. The additives causing A-positionsvacancies or "donor" substitutes are widely used to enhance the performances of PZT[18,19,20]. The characteristic properties of those additives are the increase of the dielectric constant, dielectric losses, mechanical coupling factor on one hand and the reduction of mechanical Q and coercive field on the other hand. The additives causing O-position vacancies or "acceptor" substitutions are not so widely used as they induce the opposite effects of the additives causing the A-position vacancies. Therefore a compensating valence substitution is often more successful than A or O-position vacancies.

Among the compensating valence substitutes of B-sites in PZT the best known are $(Mg_{1/3}Nb_{2/3})$[21] or $(Ni_{1/3}Nb_{2/3})$[22]. Both substitution couples can be used alone (PZT-PMN or PZT-PNN) or as a ternary system (PZT-PMN-PNN)[23]. The properties induced by this kind of substitutions are diverse, from low temperature sintering [24] to superior

piezoelectric properties [25]. The compensating valence substitution can be made between the A and B-site, i.e. introducing in A-position ion producing O-position vacancies and in B-sites ion producing A-position vacancies[26].

Table 1: Description of the properties of different PZT-based materials

Material	Doping	ε	tan δ [%]	d_{33}* [pm/V]	T_{curie} [°]	Year	Ref.
PZT	No	1700		223	386	1965	27
PNN-PZT	Compensating valence substitution			1100		2003	28
$Pb_{1-x}EA_x$ (Zr, Ti) O_3	Additive causing A-positions vacancies	1600	0.03	400	110	1994	29
Pb_{1-x}(Sr, K)$_x$ (Zr, Ti)$_{1-y}$Nb$_y$ O_3	Compensation valence substitution	1800		450	335	1999	30
PMN-PZT	Compensation valence substitution	1400	0.3	430	350	2003	26

2. Tungsten Bronze materials

The Tungsten-Bronze (TB) structure consists of a skeletal framework of MO_6 octahedra sharing corners from the three different types of tunnels parallel to the c-axis in the unit cell formula of $[(A1)_2(A2)_4C_4][(B1)_2(B2)_8]O_{30}$[31].
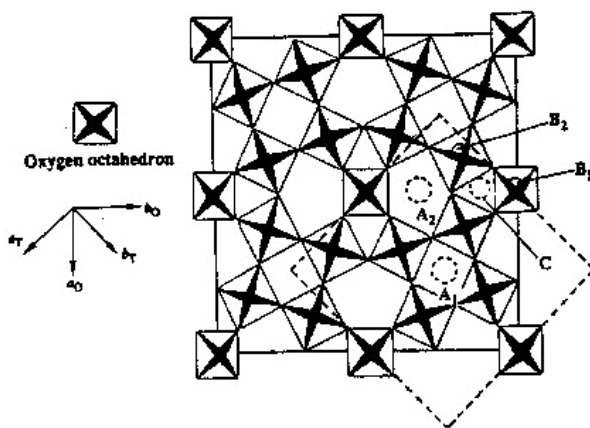

Fig. 6: Tungsten-Bronze structure

The compounds being piezoelectric have generally the formula AB_2O_6, like $PbNb_2O_6$, which was the first non-perovskite piezoelectric known[32]. In this TB the sites are occupied by Nb, the A-sites are 5/6 filled by Pb and the C-sites are not occupied at all

(see Fig. 6). The one cell TB should be $Pb_5Nb_{10}O_{30}$ which is simplified into $PbNb_2O_6$. One of its major properties is its high Curie temperature of 570°C and its ability to work in this temperature region without suffering depoling. One of the first applications of these materials were piezoelectric ceramic transducers. Later other ceramics having the tungsten-bronze structure have been produced as single crystals for electro-optic applications. The single crystal form is quite expensive to produce but for some devices like electromedical tomography the material cost is a trivial part of the total system, therefore TB single crystals can be used[33]. The properties of the TB, like those of other materials, differ significantly from the polycrystalline state to the single crystal state.

Other TB materials having the same structure as $PbNb_2O_6$ are the TB where the A-site is occupied not by lead but by earth-alkaline ions. One or a mix of two or three ions can reside in the A-sites while the C-site is empty. One of the most commonly used TB is $Sr_{1-x}Ba_xNb_2O_6$ (SBN). Its interest resides in the large pyroelectric current and large linear electro-optic coefficient[34]. The SBN sinters at quite high temperature or needs pressure sintering; therefore additives are often used like V_2O_5[35] to lower the sintering temperature because they induce a liquid phase sintering at low temperature. The control of the microstructure is also not so easy with SBN ceramics and abnormal grain growth is often seen [36]. However recent developments have facilitated the microstructure control and the orientation of these ceramics making them more interesting for new industrial applications[37]. The use of SBN as a replacement for PZT for the actuator material in the car industry would not be possible due to its low Curie temperature about 75°C [38].

In the same category the other widely researched ceramic is $Sr_{2-x}Ca_xNaNb_5O_{15}$ or SCNNx. The A1-sites are filled by Sr or Ca and A2-sites are occupied Na, C- sites are empty and B1 and B2-sites are filled by Nb. SCNNx is an interesting candidate to replace PZT as it exhibits a large piezoelectric signal of d_{33}=270 pC/N but under its single crystal form[39]. Single crystals are expensive to produce and therefore not used for industrial applications where the costs play a central part. Therefore improvement should be realised for the piezoelectric properties of polycrystalline SCNNx, one of its major problem being its density due to the evaporation of the alkali ion during the sintering. In polycrystalline ceramics the grain boundaries, crystal orientation and variations in composition did not allow to obtain the highest properties observed in the single crystals but a piezoelectric coefficient of d_{33}=100 pC/N could be measured[40]. An alternative sintering process evaluated was Spark Plasma Sintering (SPS) which leads to satisfying microstructure and properties, unfortunately, this process can not be used for industrial processing as it is too time-consuming[41].

Another class of TB are those where the C-site is fully occupied. Actually the C-site is larger than the A-site and it can be occupied by an alkali ion. This is the case for the potassium lithium niobate ($K_3Li_2Nb_5O_{15}$ or KLN) where all sites are occupied[42]. KLN is of great interest as monocrystal for non linear applications however the interesting form of KLN is the single crystal and the properties are largely dependant on the crystal direction but its completely filled structure allows a high resistance to laser damage[43]. Recent works improved the quality of KLN polycrystals to make them suitable for low cost applications[44].

3. Bismuth layered Structures

Bismuth layered structures are made up of two dimensional perovskite layers separated from each other by $Bi_2O_2^{2+}$ layers. This group of ferroelectric compounds is known since the 50's. It is interesting from the structural point of view but it presents weak piezoelectric effects in its ceramic form[45]. These compounds can be described by the general formula $Bi_2A_{x-1}B_xO_{3x+3}$ where x is the number of units in the perovskite layer.
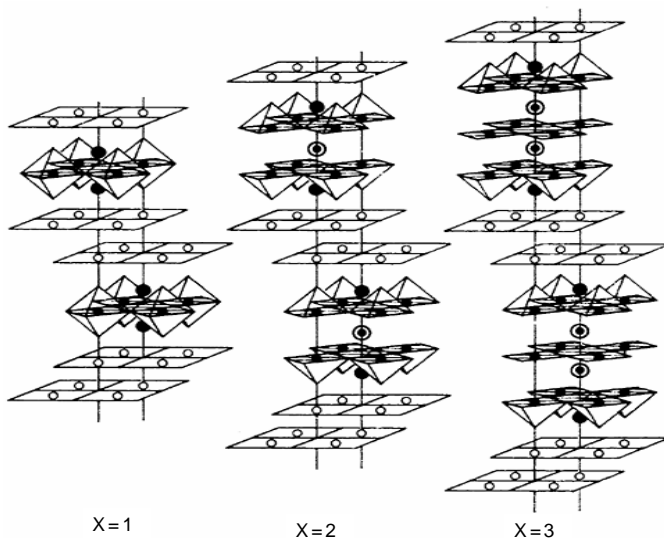
Fig. 7: Bismuth layer structures

Typically the Bi-layer structures are based on Bi_2O_3-TiO_2 compositions. The most investigated are $Bi_4Ti_3O_{12}$, $Bi_2Ti_3O_9$ and $Bi_2Ti_2O_7$ [46]. Modifications of these base compositions with earth-alkalis are also included in this family. The Bi-layer structures are characterised by high Curie temperature, low dielectric constant and large anisotropy in the electromechanical properties[47]. This anisotropy can be furthermore increased by grain orientation in the ceramic using reactive-templated grain growth

processing. Despite these attractive properties these compounds would never be used as actuators due to their poor piezoelectric coefficient not exceeding 45 pm/V after grain orientation[48].

4. Perovskite

The materials having the perovskite structure are of more common use for polycrystalline materials due to their superior performances. The perovskite structure is described in a previous section.

a. BaTiO$_3$

As stated before BaTiO$_3$ (BT) was the first piezoelectric ceramic which was developed. The causes of the piezoelectricity were soon discovered by Kay and Vousden in 1949, to be linked to a displacement of the Ti central ion toward to the adjacent oxygen ions by applying an electric field[49]. The BT possesses interesting dielectric properties which are highly dependent on the microstructure and the preparation method[50]. BT has two transition temperatures, the Curie temperature (T$_c$) at 130℃ and tetragonal-orthorhombic transition temperature (T$_{O-T}$) about 20℃. Depending on the purity of the material or the composition modifications theses temperatures can be shifted. Composition modifications of BT also allow the control of different processing parameters or properties. The substitution of the A-position by cations of the same valence except in the case of Pb, which tends to lower the Curie temperature for example. The replacement by strontium leads to an increase of ε and the addition of Ca raises the tetragonal temperature stability area. The B-position substitution by ions like Zr, Hf or Sn leads to a complete solid solution having different influences on the properties[51]. Although BT is the oldest piezoelectric ceramic known, it is still the object of numerous investigations to increase and understand its performances. The correlation between the preparation of BT and the dielectric properties is still the object of investigation. As different preparations lead to diverse microstructures, the morphology of ferroelectric domains is changed and that has an impact on the electric properties[52]. Doping of BT with elements having a different valence than barium and titanium induces A- or O-position vacancies which also influence the dielectric properties. Acceptor ions such as Co^{3+} or Al^{3+} for the A-position and Nb^{5+} for the B-position create A-position vacancies and allow the control the abnormal grain growth[53],

they also help the movement of the domain walls leading to special electric behaviour[54]. The influence of the doping with rare earth is not clear as it is difficult to determine if they will be situated in A- or B-position. The most important effect detected was the decrease of the resistivity for low doping levels and the increase for high doping levels [55, 56].

The doping of BT with other perovskite as potassium niobate was also intented. $NaNbO_3$ is antiferroelectric (see section below $(K,Na)NbO_3$-based ceramics) and the mixing of a ferroelectric and an antiferroelectric can lead to a high performance material as is the case for PZT. For high $NaNbO_3$ contents (>50 mol %) the material is antiferroelecric and for low contents (<7.5 mol %) the material is ferroelectric[57].

Others approaches to replace titanium in $BaTiO_3$ were studied. If titanium is replaced by the couple $(Li_{1/4}Nb_{3/4})$ or $(Cu_{1/3}Nb_{2/3})$, the Goldschmidt rule still applies (see equation 1.2) and t~1. $Ba(Li_{1/4}Nb_{3/4})O_3$ leads to the formation of a cubic structure at room temperature and $Ba(Cu_{1/3}Nb_{2/3})O_3$ has a highly tetragonal structure and is ferroelectric[58]. However the piezoelectric properties are not large enough to enable the use of this kind of materials for actuator purposes.

b. $(Bi, Na)TiO_3$-based materials

$(Bi,Na)TiO_3$ (BNT) is also a perovskite like BT where barium is alternatively replaced by bismuth and sodium. The crystal structure of BNT is rhombohedral. BNT is considered to be an interesting lead-free piezoelectric ceramic since many years due to its stable temperature dependence of the frequency constant and high mechanical coupling factor[59]. However BNT suffers of depoling at about 200°C. The depoling temperature must not be interpreted as the Curie temperature as no phase transition is visible. The origin of this phenomenon is not totally understood but some authors think that it corresponds to a ferroelectric-antiferroelectric phase transition[60]. The single crystal forms of BNT show interesting properties in regards to the use as actuators, with measured d_{33} about 500 pm/V[61].

As well as for the other ferroelectrics different works have been carried out in order to improve the properties of BNT. Different techniques can be used to increase the properties such as an improved sample preparation, the doping through A- or B-position valence substitutions or mixing BNT with other perovskites.

The preparation methods have a big influence on the later properties of piezoelectric ceramics. The purity and the grain size of the starting materials employed can be of

importance as impurities can lead to the formation of different phases in the ceramic and the grain size of the starting materials influences the calcination and the sintering or the density[62]. For BNT optimal parameters to optimise the density of the ceramic and thus its dielectric properties[63] have been found. Another method employed to optimise the performances of BNT is the non-stochiometric preparation. One of the major problems of the BNT like PZT is the evaporation of one of the elements during sintering, i.e. the control of the bismuth content in the BNT is crucial to maintain the stochiometry. Piezoelectric and dielectric measurements revealed that a deficiency of titanium leads to an increase in the piezoelectric coefficient, the dielectric constant ε, the dielectric losses as well as the electromechanical coupling coefficient, but at the same time the depolarisation temperature was shifted to lower temperatures. Exactly the contrary effects can be observed for an excess of titanium[64]. The other preparation method which can influence the properties is the microstructure development and the development of a texture in the ceramic. If the grains are oriented the dielectric properties are enhanced. The reactive templated grain growth is one of the current methods to give a microstructure orientation. In this method a precursor of a target compound is used as a reactive template, and a complementary compound for the target compound is mixed. A green sample containing the aligned reactive templates is produced via tape-casting. The sample is then calcined *in-situ* and sintered. The matrix alginates subsequently with the templates and the properties are enhanced due to the uniform grain orientation. In most of the cases the templates used for BNT are $Bi_4Ti_3O_{12}$[65]. This technique allows to increase the piezoelectric properties like d_{33} up to two times and a piezoelectric coefficient of 152 pC/N could be measured by Tani *et al.*[66].

For BNT as well as other ceramics the properties can be increased by the adjunction of dopants. The substitution of sodium through potassium and lithium is one of the most widely used substitutions. This kind of doping leads to a pure phase perovskite in BNT[67] with increased piezoelectric properties like a d_{33} value of up to 230 pm/V for 6 at.% Li[68]. Moreover, a MPB exists between BNT and $(Bi_{0.5}K_{0.5})TiO_3$ (BKT) at around 80 mol% BNT, which makes it a more suitable candidate to replace PZT, as the piezoelectric properties are better around the MPB similar to PZT. However the depolarisation temperature decreases up to 174℃ at th e MPB. Therefore compositions not in the MPB are also suitable to produce lead-free actuators like 0.7 BNT – 0.3 BKT which possesses a depolarisation temperature similar to BNT but with a higher d_{33} coefficient around 130 pm/V[69]. The classic doping of $Bi_{0.5}(Na,K)_{0.5}TiO_3$ with Pb, Li etc... is also possible.

The doping creating A- or O-position vacancies can be carried out with an excess of sodium or bismuth in the starting materials but also other elements can be used like rare earths. Doping BNT with rare earth like cerium shows beneficial to the properties due to a better densification of the ceramic[70].

A different doping strategy is doping with other elements which are not similar to the elements contained in BNT and therefore use the compensative valence substitution like using the alkaline instead of $(Bi_{0.5}Na_{0.5})$ or compounds like $MnCoO_3$. Mn and Co can take the A- or B-positions in the BNT leading to serious changes like a dramatic lowering of the Curie temperature but at the same time an enhancement of the electromechanical coupling factor as well as the resistivity[71]. The doping with earth alkaline elements such as Ca improves the piezoelectric coefficient[72]. If BNT is doped with barium, the resulting material corresponds to a mixture of two perovskites BNT and BT. This kind of modification can be also interpreted in a different manner under the form of a modification of BNT such as $[(Bi_{0.5}Na_{0.5})_{1-x}Ba_x]TiO_3$. In this section it will be treated in this first form, i.e. a mix of two perovskites BNT and BT.

A MPB between BNT and BT at a concentration of 6-8 mol% BT has been reported in 1991 by Takenaka *et al.*[73]. Some piezoelectric properties are increased as the planar coupling factor, the piezoelectric constant or the dielectric constant but the depolarisation temperature decreases up to 100°C [74]. The replacement of sodium by lithium in BNT-BT leads to interesting properties as piezoelectric properties have a different behaviour. The piezoelectric coefficient d_{33} and the relative dielectric constant ε increase linearly when BNT contains 7.5 at.% lithium and 8 mol% BT and moreover, the depolarisation temperature lightly decrease to 190°C [75]. The replacement of sodium by potassium in BNT-BT leads to BKT-BT. A MPB also exists between BKT and BT at approximately 40 mol% BKT but these ceramics are difficult to densify without additive due to the evaporation of potassium during sintering and possess lower piezoelectric properties than BNT-BT[76].

As stated before a MPB exists between BNT and BT as well as BNT and BKT therefore, Nagata *et al.* investigated the existence of a MPB between the three end-members BNT-BKT-BT[77]. They found the best piezoelectric properties for 0.852BNT-0.028BT-0.12BKT that means in the theoretically rhombohedral zone. The values measured for this composition were ε=1141, k_p=0.56, T_c=301°C and d_{33}=191 pC.N^{-1}. However, they did not give any value for the depolarisation temperature.
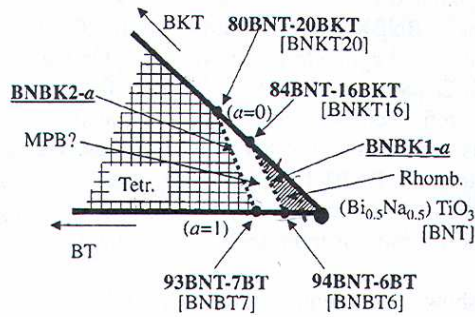
Fig. 8: Phase relationship of the $(Bi_{1/2}Na_{1/2})TiO_3$-$BaTiO_3$-$(Bi_{1/2}K_{1/2})TiO_3$ (BNBK) system around the MPB (from 85).

Other work from Li *et al.* were focussed on similar ternary compounds but with different ratios for the three end-members, and they found the best properties for 0.895BNT-0.035BT-0.07BKT with ε=850, d_{33}=150 pC.N^{-1}, T_d=120℃ and T_c=320℃ [78].

Other end-members possible to mix with BNT are different perovskite as $KNbO_3$ or $NaNbO_3$. The presence of a MPB between BNT and $KNbO_3$ was not clear before the work of Ishii *et al.* because dense ceramics were difficult to prepare due to the evaporation of the alkali element. In this study, high density by hot pressing of the samples was achieved and the MPB could definitely be investigated[79]. The MPB was found around 5 mol% $KNbO_3$ in solid solution in BNT. On the other hand the depolarisation temperature decreases with the amount of doping incorporated.

A MPB between BNT and $NaNbO_3$ was found at 90-98 mol% $NaNbO_3$ in solid solution into BNT[80]. These results were confirmed by Li *et al.* who found that the depolaristion temperature also was diffuse and did not exist anymore for high doping levels.

Table 2: summarisation of $(Bi_{1/2}Na_{1/2})TiO_3$-based materials

Material	Remark	d_{33} [pm/V]	T_d [℃]	Ref.
BNT		80	200	65
BNT-single crystal		450	200	67
BNT-textured	Templated Grain Growth with $Bi_4Ti_3O_{12}$ seeds	150	200	72
BNT-Li doped		230	190	74
BNT-K doped	MPB at 15 at.%K	130	174	75
BNT-BT	MPB at 8 mol% BT	120	100	80
BNT-BKT-BT	MPB	191	120	85
BNT-(K,Na)NbO$_3$	MPB around 5 mol% (K,Na)NbO$_3$	71		88

c. (K, Na)NbO$_3$-based materials

(K, Na)NbO$_3$ (KNN) is a piezoelectric formed by the ferroelectric KNbO$_3$ (KN) and the antiferroelectric NaNbO$_3$ (NN)[81]. To begin this part first both materials will be shortly separately presented.

KN is quite difficult to process to full densities by natural sintering for different reasons. The first is that the phase stability is limited to 1040℃ therefore high temperature sintering is not possible. Another important reason is the volatility of potassium oxide at low temperatures inducing slight stochiometry changes thus leading to the formation of impure phases[82]. However, production techniques for KN single crystals have been developed as KN is interesting for its photorefractive effect used for holographic data storage, phase conjugation, data processing or band wavelength filter[83]. KN presents different phase transitions similar to BT; these are cubic (above 400℃), tetragonal (between 400 and 230℃), orthorhombic (between 230 and -50℃) and rhombohedral (under -50℃).

In the research for new lead-free piezoelectric ceramics KN single crystals are widely investigated to optimise their performances as actuator. The domain engineering is one of the methods. If the domains are oriented and their size optimised the piezoelectric properties are better for transducer applications but for actuator applications the d_{33}^{*} values are too small[84]. The full poling of the material is also an important parameter to investigate to increase the performances of KN. Study shows that with an adapted poling some piezoelectric properties could be 5 times enhanced in comparison with a classical poling treatment[85]. Despite its properties as single crystal, the properties of polycrystalline KN are not without interest. A carefully preparation can produce samples with dynamic d_{33} up to 110 pm/V[86]:

As well as for other ceramics the properties of KN can be improved by the utilisation of dopants. One of the classical dopants is tantalum since KTaO$_3$ is ferroelectric[89]. The K(Nb,Ta)O$_3$ (KNT) as well as KN can also be grown as single crystal and used in electro-optical devices[87] or it can be used as polycrystalline ceramics for tunable applications[88]. KN in its polycrystalline form can be easily doped to improve its properties, which is not the case for single crystals as dopants disturb the crystallographic order. Among the most promising dopants for KN ceramics is the couple LaFeO$_3$ as almost all piezoelectric properties are enhanced by the addition of only 3mol% in solid solution: the density raises to 98.8% of the theoretical density, the remanent polarisation increases to values of single crystal KN, the dielectric constant,

the orthorhombic-tetragonal phase transition temperature and the Curie temperature stay unchanged and the d_{33} coefficient increases up to 98 pC/N [89].

NN as stated above is antiferroelectric with an orthorhombic structure at room temperature[89]. NN undergoes appreciatively the same phase transitions like KN. This phase transitions temperatures can however be easily influence by the introduction of dopants into single crystals, such as Mn[90]. Ferroelectric domains can appear as the result of polarisation creating piezoelectricity in NN although NN is antiferroelectric[91]. However this piezoelectric effect in NN is quite weak, ε and d_{33} are low despite of polarisation (respectively 200 and 50 pC/N).

Regarding the fabrication of NN it meets the same problems as KN due to the evaporation of sodium during its firing. Techniques such as spark plasma sintering (SPS) allow to fabricate high density NN. SPS is a process that uses microscopic electrical discharges between particles under pressure (about 30 MPa). The NN samples produced through SPS have interesting properties like a quite high remanent polarisation after poling (around 28µC.cm^{-2}) and its coupling factor remains stable at 18% over a wide temperature range (up to 300°C) [92]

KN and NN alone do not show piezoelectric properties good enough to compete with PZT but a solid solution of both like PZ and PT leads to higher performances.

KNN did not arouse enthusiasm of the scientific community due to its sinterability problems which are the same as KN and NN. It was though during a long time that KNN cannot be sintered by conventional technique[93]. However the limitation on the use of lead in consumable devices put the attention on lead-free materials a few years ago. In 2001 the European LEAF project proposed KNN as alternative material for PZT for certain industrial applications[94].

The addition of NN to KN increases the dielectric constant and ε values of KNN around 250 have been reported for $(K_{0.5}Na_{0.5})NbO_3$ prepared by a mixed-oxide route[95]. The Curie temperature is not too modified in comparison to the Curie temperature of pure NN and KN. The Curie temperature of KNN is around 400°C. One of the other characteristic of pure KNN is that it suffers also a phase transition around 200°C between orthorhombic and tetragonal (see Fig. 9).

The attention developed in the last years about KNN lead to a better observation of the influencing parameters permitting to reach higher performances. One of the first parameters to be controlled is the preparation. Often KNN is prepared through the mixed-oxide route from sodium and potassium carbonates. These carbonates are

sensitive to the ambient humidity and a false stochiometry of the final compound can be introduced if no attention is given to the dryness of the starting powders. The use of dried powder and a careful milling can increase the density and therefore the dielectric and piezoelectric properties[96]. However the maximal density reached by this route was only of 95% and a d_{33} around 80 pC/N was measured. To estimate the properties of a fully densified KNN other sintering process should be investigated like SPS which was already used for KN or NN. SPS leads to a density superior to 99% of the theoretical density (theoretical density of 4.51 g.cm^{-3}) for sintering temperatures inferior to the temperature of air sintering (920°C instead of 1140° C). The piezoelectric coefficient measured for the samples was 148 pC/N, nearly the double of the d_{33} measured on air-fired samples with the same composition[97]. Another preparation method of the powder from alkoxides leads to a very fine powder after calcination with a different morphology. This kind of preparation did not conduct to a KNN ceramic with interesting properties and is therefore not adapted for the production of bulk ceramics[98].
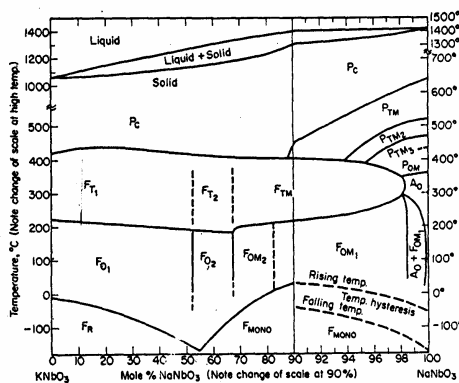
Fig. 9: phase diagram of (K,Na)NbO$_3$

The properties of pure KNN cannot satisfy the requirements of the industry for some applications. Thus an optimisation of the properties may be achieved through doping. The first part of the following review about KNN doping focuses on dopants with the same valence, the second part on mix with different perovskite and to finish the review dopants with different effects on the ceramic will be introduced.

Doping elements with valence 1 and 5 were the first investigated to improve the performances of KNN. The alkalis being critical elements the attention was put first on the insertion of lithium in A-position. This kind of modification can be also investigated as a ternary system with the three end-members KN, NN and LiNbO$_3$ (LN). LN has an ilmenite structure which is similar to the perovskite but due to the small diameter of lithium it is a heavily distorted perovskite. LN has also application for electro-optical

devices like KN. The insertion of lithium in the A-position allows to increase the dielectric constant ε at room temperature. This is due to the displacement of the orthorhombic-tetragonal phase transition temperature (T_{O-T}). For 5 mol% Li doping in KNN T_{O-T} moves from 200°C to 110°C, the incorporation of more Li decreases T_{O-T} up to temperature below room temperature for 7 mol% Li[99]. On the other hand the incorporation of Li into KNN leads to an improvement of the piezoelectric coefficient of 200 pm/V. This can be interpreted as a MPB between LN and KNN as described by Kakimoto *et al.* The limit of solid solution of LN into KNN was detected for 7 mol% of $LiNbO_3$. The incorporation of more than 7 mol% leads to the formation of a secondary phase identified as a tungsten-bronze. Another benefit of the incorporation of Li into KNN is the decrease of its sintering temperature[100]. Samples containing 5 mol% LN fired at 1040°C present higher d_{33} (150 pm/V) and coupling factor (37%) than samples fired at higher temperature or containing more LN.

The silver niobate and silver tantalate (respectively $AgNbO_3$ and $AgTaO_3$) also have a perovskite structure and are reported to be ferroelectric[101]. They possess a similar phase transition as potassium niobate and silver comes in mind as a dopant for KNN. Few references are available on the topic as the first studies reported poor piezoelectric properties[102].

It is natural to think about tantalum to replace niobium as they are neighbours in the periodic classification of the elements and have similar properties. Different cases can be investigated: the incorporation of Li and Ta independently or the insertion of $LiTaO_3$. It is interesting to begin by an independent content of Li and Ta to evaluate their properties. The addition of Li as stated above increases the piezoelectric coefficient d_{33} of pure KNN; the addition of Ta to LKNN increases even more d_{33} up to 300 pm/V for samples containing 20 mol% Ta and 3 mol% Li[103]. Li has quasi no influence on the Curie temperature, which sinks linearly with the addition of Ta. Moreover, Ta increases the sintering temperature. The maximal density measured on Li- and Ta- modified KNN was reached for higher sintering temperature but the absolute density was higher for samples doped with both elements[104]. Guo *et al.* have detected the existence of a MPB between $LiTaO_3$ (LT) and KNN around 5-6 mol%. Similarly to LN the limit of solid solution is situated at 7 mol% and an increase in LT content leads to the formation of a second phase having the tungsten-bronze structure[105]. Saito *et al.* reported another MPB between KNN and LT[106] as shown in Fig. 10. For low Li and Ta doping level, KNN stays orthorhombic (grey area). At higher doping level (for Li between 5 and 12 mol%, depending on the Ta content) the ceramics become tetragonal (white area) and for higher Li content (from 12 mol% Li) a tetragonal and a near phase coexist independently from the Ta content (dashed area).
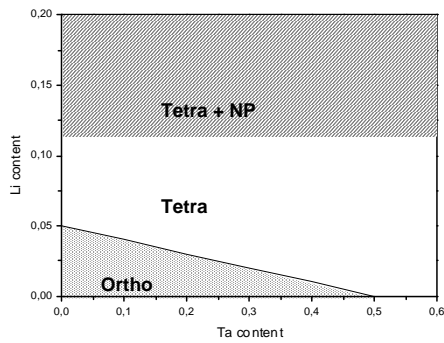
Fig. 10: MPB in LKNNT depending on Li and Ta content

Another element which can be inserted in B-position is antimony (Sb). The common oxidation numbers of antimony are -3, 3 and 5. If it is inserted into KNN due to its radius it will naturally be inserted in B-position and will take the oxidation number 5. $LiSbO_3$ (LS) is used as an electroceramic and is primarily used in its thin film form. The first effects of LS doping on KNN were reported by Zang et al.[107]. The effects of LS are even more important onto KNN than LT as the maximal piezoelectric coefficient was reported for 5.2 mol% LS in solid solution into KNN of 320 pC/V. A planar coupling factor around 51% was also measured and the Curie temperature does not suffer an important decrease but the T_{O-T} was shifted to 70-80°C. Another work from Yang *et al.* reported a MPB between 6 and 10 mol% of LS in solid solution into KNN. The values were quite different for d_{33} as the maximum reported was 171 pm/V and the T_{O-T} was only shifted to temperatures around 120°C.

In 2004 the scientific journal Nature presented a paper from Saito *et al.* which had an important impact on the piezoelectric scientific society. A lead-free piezoelectric ceramic with properties comparable to those of PZT via air- and pressure-less sintering was reported[108]. Their results are presented in Fig. 11. The compounds called LF 1-4 are from the family $(K_{1-x}Na_x)_{1-y}Li_y)(Nb_{1-z-w}Ta_zSb_w)O_3$. The compounds called LF 3-4T are the same composition as LF3 and 4 but with a texture created via templated grain growth techniques. As shown in Fig. 11 the properties of lead-free compounds are comparable to those of non-modified PZT and are superior to those of other known lead-free piezoelectrics, such as $BaTiO_3$, $(Bi,Na)TiO_3$ or non modified KNN.

The optimal composition was obtained for x=0.54, y=0.04, z=0.1 and w=0.04 with the following properties: ε=2000, d_{33}^*=290 pm/V, T_c=275°C. The orientation of the ceramic via templated grain growth leads to a d_{33}^* of 416 pm/V.

Complementary work of Yoo *et al.* shows the importance of the sintering parameters and poling conditions to achieve even better properties than those presented by Saito

et al.[109]. The addition of potassium carbonate in excess to reach better densities was reported. As the potassium is an element which has a high vapour pressure and can therefore easily vaporise during sintering, a compensation was done before sintering to reach a stochiometric KNN. The poling temperature of KNN was also centre of attention and they discovered that poling at high temperature (more than 100°C) leads to higher polarisation.
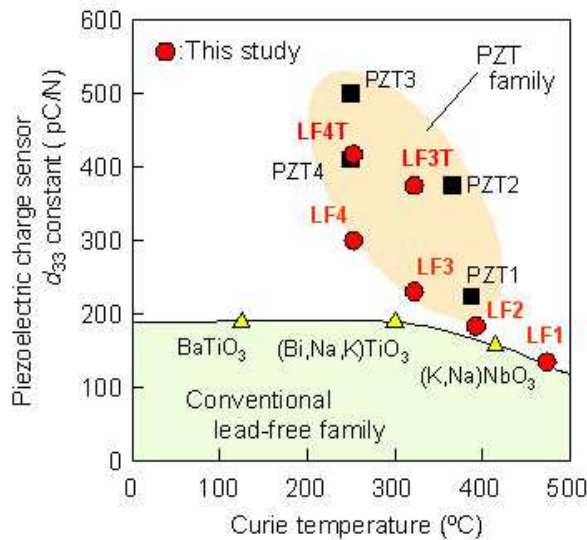
Fig. 11: d$_{33}$ coefficient vs. Curie temperature for different compounds from Saito *et al.*

After the results presented by Saito *et al.* KNN-based ceramics became the centre of attention since with appropriate doping the properties of a lead-free piezoelectric could reach those of PZT-based materials.

Another family of dopants for KNN are the earth-alkali elements such as barium, strontium, magnesium or calcium because of their large radius (almost as large as the alkali elements) and their low valence. The influence of 0.5 at.% of earth-alkali elements on KNN is noticeable. They mostly occupied the A-site; calcium and strontium promoted the densification and decrease the phase transition temperature (T_{O-T} as well as T_c) and the piezoelectric response is enhanced for air sintered samples. The introduction of magnesium leads to the contrary effects and the addition of barium conducts to the formation of a second phase[110]. The effects of potassium and sodium substitution by strontium and A-position vacancies were studied in details by Tashiro *et al.*[111]. The introduction of strontium and therefore, A-position vacancies leads to abnormal grain growth. Furthermore, the resistivity of the samples was too low and no sufficient electric field could be applied to measure piezoelectric properties. By

adding MnO the abnormal grain growth was inhibited, the resistivity increases and satisfying piezoelectric properties could be measured as d_{33}^* up to 150 pm/V.

To inhibit or control the formation of A-position vacancies an acceptor can be inserted on B-sites. One of the most employed in the literature is titanium; this leads to the insertion of compounds like $EATiO_3$ (EA=earth alkaline element) into KNN. Chang *et al.* reported improvement of the piezoelectric properties as well as a decrease of both transition temperatures[112]. The influences of $EATiO_3$ doping are similar to EA doping reported by Malic *et al.*, i.e. the doping with $SrTiO_3$ and $CaTiO_3$ leads to denser ceramics and a increase of the piezoelectric properties whereas, the KNN ceramics doped with $MgTiO_3$ and $BaTiO_3$ exhibit a secondary phase and lower piezoelectric performances. The KNN doping with $BaTiO_3$ was studied more in details by Guo *et al.* and they discovered the existence of a MPB between KNN and BT for 6 mol% $BaTiO_3$ in solid solution into KNN[113]. However, it is for only 2 mol% that the piezoelectric properties with a reported d_{33} equal to 106 pC/N were the most important. The addition of BT decreases the Curie temperature and leads to a diffuse phase transition temperature. The microstructure of KNN also is improved and the grain size distribution is mono-modal without abnormal grain growth. These results were confirmed by Shimojo *et al.*[114] who studied furthermore the doping of KNN with $SrTiO_3$ and came to the conclusion that the use of strontium to dope KNN provides better piezoelectric results as $SrTiO_3$ is paraelectric and $BaTiO_3$ ferroelectric at room temperature. Other groups from Japan cam to the same conclusion and also discovered the existence of a MPB at 6 mol% $SrTiO_3$ in solution in KNN. But they measured different piezoelectric coefficients, one of 90-96 pm/V[115] and the other of almost 200 pm/V[116]. The true value is difficult to know but it is sure that the piezoelectric properties are enhanced with the doping of $SrTiO_3$ in the MPB.

As stated above one of the major problems of KNN is its lack of density under air firing, therefore the addition of a secondary phase which fills the pores can improve the properties. Matsubara *et al.* discovered a sintering aid when they added copper oxide to KNN. In the presence of copper a second phase, namely $K_4CuNb_8O_{23}$ (KCN) is formed during the sintering, which promotes the densification. The addition of only 0.5 mol% KCN achieved the best performances, lower ε_r and tan δ (respectively 200 and 2%) higher d_{33}, kp and Q (180 pm/V, 0.4 and 1200)[117]. The modification of copper-doped KNN with tantalum leads to the formation of a similar liquid sintering phase, namely $K_{5.4}Cu_{1.3}Ta_{10}O_{29}$ (KCT). The quantity of KCT needed to achieve the best performances of KNN is only of 0.38 mol%[118]. Its performances are approximately as good as the properties of dense KNN prepared with KCN. The doping of KNN with

lithium and sintered with KCT leads to higher properties; ε_r, k_p, Q and d_{33} increased to respectively 400, 0.43, 2000 and 200 pm/V [119].

Other dopants like zinc, scandium, cadmium, cerium or tin were studied by Zuo *et al.*[120]. It was discovered, that the addition of tungsten, yttrium and cerium inhibits the densification during sintering and that elements like zinc promote it and high densities (>96% of theoretical density) were achieved at low temperature. The addition of 1 at.% Zn also promotes other properties like relative dielectric constant, coupling factor or piezoelectric coefficient which attained the values of respectively 650, 0.44, 117 pm/V without affecting the Curie temperature and the T_{O-T}. That confirms the work of Park *et al.*, who first discovered, that the addition of ZnO to KNN improves its performances[121].

Table 3: Summary of different KNN-based materials

Material	Doping	ε	d_{33} [pm/V]	T_c [°C]	Ref.
KNN air-sintered		250	80	400	96
KNN hot-pressed			150		100
KNN	Li		200		103
KNN	Li-Ta		300		107
KNN	Li-Sb		171		111
KNN	Li-Ta-Sb	2000	290	275	112
KNN	earth-alkali		95		114
KNN	EATiO$_3$		106		116
KNN	Cu; Cu containing compounds	200	200		123
KNN	Zn	650	117		126

IV. Method

1. Classical preparation

To develop new compositions of the multilayer ceramics, new materials are first treated individually as bulk materials. When the properties are considered acceptable multilayer techniques are developed. In the first part of the material development, bulk samples of one up to several millimetres are produced and investigated. The method described in this section was used to produce the first bulk samples before the multilayer technique was further developed. The classical preparation follows different stages which will be described step by step as well as the contribution of each individual step to the quality of the ceramic sample.

a. Dosage

The receipt of the ceramic is prepared and the weight of each ingredient is calculated (an example is given Chap 9). The chosen quantity for the classical preparation is of one mole, which represents a weight of powder around 300g for lead-based ceramics and around 500g for niobate-based ceramics. The significant amount of dosed powder has two reasons: one is to minimise the error induced by each component and the second is the possibility to vary parameters such as calcination or sintering temperature and time. In the classical method all the components are dosed per hand with a precision of 0.1 mg. The time invested in dosing varies with the number of compounds. Typically for a receipt with 6 compounds, the time taken for a complete dosing is 45 minutes.

The powders are weighted in PVC beakers of one litre and water or alcohol is used as cooling media depending of the solubility of the raw materials in water or alcohol.

b. First milling

To produce the bulk samples the powders are ground on a on a milling bank for 18h in the PVC beaker. At the beginning of the milling process the grain size of the different compounds is different and in many cases the distribution is heterogeneous.
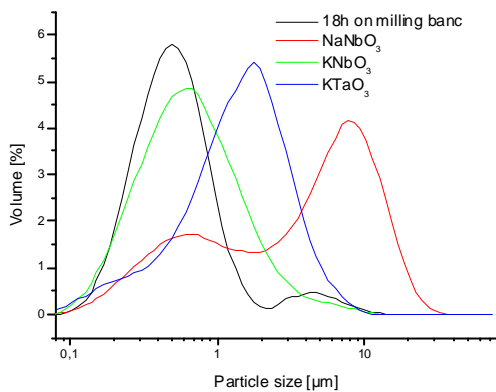
Fig. 12:Particule size distribution of different powders before and after milling banc

The milling achieves a unimodal grain size distribution ($d_{50} \approx 0.6 \mu m$) as well as an intimate mixing of the different compounds. These two parameters are important to optimise the calcination step which comes afterwards. Before the calcination the slurry is dried out by means of filtration and a drying furnace.

c. Calcination

During the calcination the perovskite structure is formed. The stochiometry of the ceramic will be determined during this step. The different compounds are transformed to give the final stochiometry (ABO_3 in the case of the perovskite). If carbonates are dosed, the carbon as well as the exceeding oxygen will be released. To form the perovskite structure, the compounds need a certain amount of energy which is given by the temperature. Typically for perovskite formation the calcination temperature is situated between 700 and 800°C.

As the calcination is a sensitive parameter the heating and cooling rate should not be too high to allow the different atoms to diffuse within the mixture. Typical heating and cooling rates are 3 K/min. The calcination takes up to 5 h and the total time taken is about 24h.

Once the perovskite structure has formed, the mixture must be milled another time to break the agglomerates which could impeach the densification during sintering.

d. Second milling

After the calcination the second milling takes place to break the agglomerates formed during the calcination. The second milling is also carried out in a one litre PVC beaker with water as cooling liquid. The second milling takes 18h. Afterward the slurry is filtered and dried in a furnace.

e. Pressing and debinding

The dried powder is then granulated with the addition of polyvinyl butyrate (PVB). PVB helps the powder to glue during the forming, that ensures the formation of pellets. The pellets are shaped in a uniaxial press with a maximal load of 8 bar. The pellets have a diameter of about 15mm and a thickness of about 1.5mm.

After the pressing, the pellets are put in a furnace for the debinding process. The PVB has to be burnt out to ensure a good densification of the sample. The process takes place at 550℃ for two hours.

f. Sintering

The sintering is the final step for the formation of the piezoelectric ceramic.

To avoid the diffusion of certain element in the sintering air, pellets are stacked. To investigate enough samples, 7 or 8 pellets are piled up, with the upper and the lower ones dismissed after sintering   (due to the diffusion between the sintering medium and support). This means that 5 or 6 samples are available to characterise a composition and a method of preparation.

To prevent the gluing of the pellets together a fine layer of ZrO_2 powder is placed between each pellet because zirconium ions have a low diffusivity in PZT.

There are three important parameters of the sintering phase that must be considered in detail:

Sintering temperature. A too high temperature can damage the ceramic. Diffusion can also be too fast and the pellets may glue together, even leading in extreme cases to

ceramic melt. A too low sintering temperature achieves poor density leading to poor properties. The sintering temperature has to be adjusted for each ceramic.

Heating rate. The sintering of a ceramic is carried out by different mechanisms. Six basic mechanisms are responsible for the sintering of the ceramic. They are illustrated in Fig. 13. Three of these mechanisms are related to surface transport and three to bulk transport. Surface and bulk transports are in fact complementary. The surface transport is responsible for the neck formation and the bulk transport for the growing of the neck. As the formation of the neck and its growth are time dependent, enough time must be allowed to produce the sample, otherwise it will be incorrectly sinter (high concentration of closed porosity for example), which will be detrimental for the poor properties.

Weight loss during sintering. If the weight loss is significant during sintering, the composition of the powers has to be adjusted accordingly during their elaboration. A weight loss of 2% for a PZT during the sintering must be compensated with the addition of 2% weight lead oxide in the initial powder composition because lead is the most volatile compound of the PZT. After the sintering the samples can be characterised.
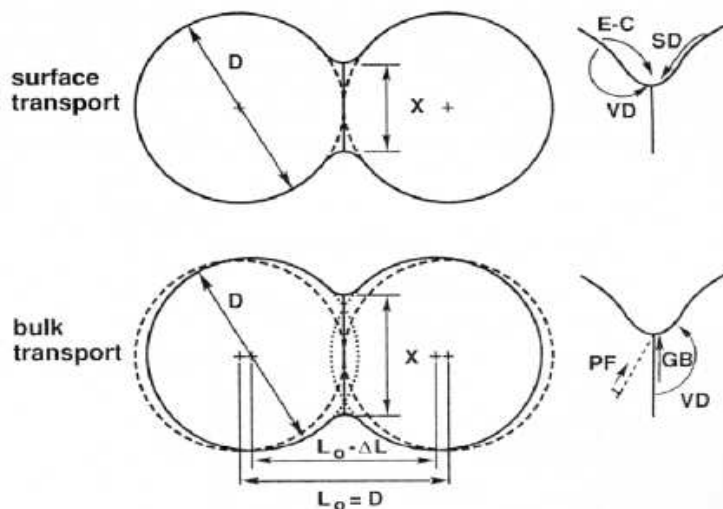
Figure 3.10. Two classes of sintering mechanisms as applied to the two-sphere sintering model. Surface transport mechanisms provide for neck growth by moving mass from surface sources (E-C, evaporation–condensation; SD, surface diffusion; VD, volume diffusion). Bulk transport processes provide for neck growth using internal mass sources (PF, plastic flow; GB, grain boundary diffusion; VD, volume diffusion). Only bulk transport mechanisms give shrinkage with the approach of the two particles.

Fig. 13 Sintering principle

g. Characterisation

i) **Sample preparation**

For the characterisation the surfaces of the samples have to be plane and parallel to allow a unidirectional transmission of the electric field in the ceramic. Parallel and plane surfaces are obtained by means of grinding. Samples are glued with wax on a plate to grind one surface and afterwards they are glued on the other side to grind the second surface. The surfaces are then washed with benzene to eliminate all traces of wax.

The samples need an electric contact to allow the dielectric characterisation. Different methods are available to make the contact: a metallic solution can be sprayed on the surface and the organics can be burnt off to provide a fine bed of metal on the surface. Alternatively the contacting metal can be sputtered on the surface. The second method was the standard at the lab and the equipment was available, so this was the method that was selected. The selected contact metal was Ag as it is the main component of the electrodes of the multilayer system; it is quite cheap and melts at low temperature.

The diameter of the samples is measured and they are placed in a support having an adequate diameter in order to keep as much ceramic surface as possible free of silver. This system allows having the maximum of the surface contacted with silver to avoid clamping as well as a heterogeneous field distribution in the sample during the characterisation. This mounting allows also the edge of the sample to stay free of silver to avoid short-circuit during the measurement without supplementary machining.

ii) **Properties screening**

For each sample the diameter and the thickness must be known. The dielectric constant of the material is calculated using the following formula:

$$C = \varepsilon * \varepsilon_0 * \frac{A}{d} \qquad\qquad (1.13)$$

C is the measured capacity, A the area of the surface, d the thickness and ε_0 the dielectric constant of the vacuum.

The samples are then poled in SF6 (isolating gas) and the dielectric constant is measured again. During the polarisation the dipole moments are all oriented in the same direction. The difference of dielectric constant after and before the poling gives a concrete reference to the ability of the piezoelectric domain to tilt. Typically samples within a MPB have a higher dielectric constant after the poling than those not having a MPB which have a comparable or deeper dielectric constant.

Afterwards the d_{33} or strain in the poling direction is measured. The system is home-made. The sample is held between two tips and a field is applied from the lower to the upper tip. The field is recorded at the input source and the elongation is measured with the upper tip which contains an inductive sensor and recorded. The d_{33} is the elongation of the sample (in pm) through the voltage applied for a sample having a thickness of one mm. For the application as multilayer this property is one of the most important. The measurement takes place typically 3 times at 2kV/mm and 2 times at 1kV/mm. During the polarisation the sample suffers a deformation. The first measurement poles the sample again and then during the second measurement only the piezoelectric property is measured.

2. High Throughput Method

To improve the time needed to prepare samples a few steps must be reconsidered and adapted to the HTE method.

a. Dosing

The first consideration that needs to be done is to reduce the quantity of powder dosed. The quantity of powder should be reduced in order to work in smaller milling cups that can be processed in parallel. This quantity should not to be too small to allow the screening of the properties. These properties have to be measured on a sample which can be easily manipulated. The size of the classical sample is of 1mm thickness and 14mm diameter. The thickness of the sample is reduced for HTE to 0.5 up to 0.75 mm and the diameter to 7 mm. This allows a reduction of the quantity of powder of the half to produce the same number of samples.

To obtain a reliable measurement, the data of a minimum of three samples must be considered. As the upper and lower samples of the stack in the sintering boat are not used due to the diffusion with the sintering medium, five samples have to be produced per sintering. The diffusion of the lower sample with the sintering medium can be avoided with the use of a platinum foil. The lower sample is, in this case, used to analyse the microstructure.

As stated in sintering (see chapter IV.1.f), the sintering parameters are of importance for the properties of the material. They have to be screened in order to cover all combinations that may lead to the discovery of an adequate material. Four different sinterings are evaluated in a first step to screen a large panel and therefore guaranty

that all are parameters are ensured. To screen four sintering modus with five samples, twenty samples have to be produced. A sample weighs less than 1 g in case of PZT and roughly 1/2g for lead-free samples. Thus 20g of powder must be dosed for each new PZT composition and the quantity of powder can be reduced by 12 to 10g for lead-free samples.

During this work the powders were hand weight, as the automated powder dosing system was not sufficiently accurate. Moreover, processing parameters are decisive in the properties of the ceramic and the hand dosage allows keeping a certain flexibility which can be of great importance in the discovery of new materials. The dosing of eight compositions with six components takes approximately 3h.

During the hand dosage libraries of eight different compositions were processed. In a further step the powders have to be milled. This step takes place in a planetary milling machine which can accept a maximal of eight milling cups meaning that eight compositions were always handled in parallel.

b. Milling and drying

After the dosing the powders are milled in a planetary milling machine with 8 bowls containing 10-20g of powder. The planetary milling process is a high energy process, reducing the time that it takes to achieve the same or smaller particle size than in a milling banc. The planetary ball milling machine operates as described in the manual of the Fritsch Company: "The material is crushed and torn apart in eight grinding bowls by grinding balls. The grinding balls and the material in the grinding bowl are acted upon by the centrifugal forces due to the rotation of the grinding bowl about its own axis and due to the rotating supporting disc. The grinding bowl and the supporting disc rotate in opposite directions, so that the centrifugal forces alternately act in the same and opposite directions. This results in, as a frictional effect, the grinding balls running along the inner wall of the bowl, and as an impact effect, the balls impacting against the opposite wall of the grinding bowl. The impact effect is enhanced by the grinding balls impacting against one another. Loss-free grinding, even in the case of grinding of suspensions, is guaranteed by a hermetic seal between the grinding bowl and the cover"[122].

A typical grain size (d_{50}) after 18h on the milling banc is 0.9µm. After 3h in the planetary ball milling machine, a typical d_{50} is 0.5µm. The particle size of the powder is of great

importance to achieve a homogeneous material. The repartition of the particle size should be monomodal to avoid segregation during pressing.
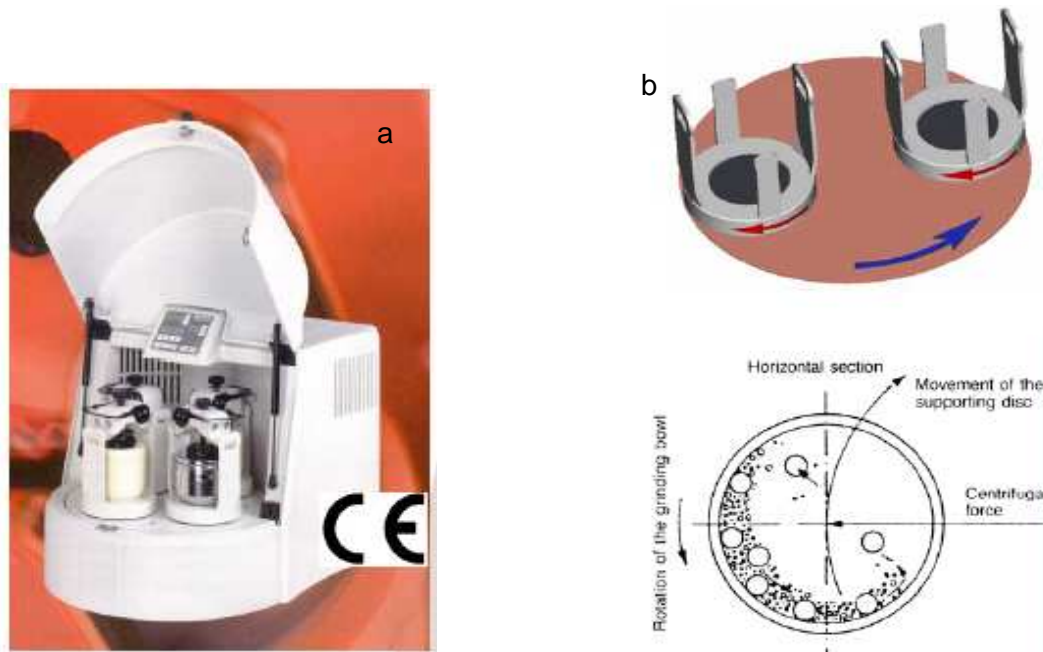

Fig. 14 a and b: Planetary ball milling machine and its operating principle

After milling the powders are dried in a freeze-dryer which allows the parallel drying of the 8 powders. The 8 slurries are poured in 8 steel plates and put together on a support. These are subsequently frozen at -40°C. After wards the frozen slurries are put on the freeze-dryer which is sealed with a bell. The pressure of the interior of the freeze-dryer is held at 0.02 mbar during 24h. This process presents the advantage of producing dry, non-agglomerated powders. Traditionally powders are poured in Petri cups and dried in a drying oven at some temperature, which creates bonding between the particles, agglomerating them and requiring further granulating and cleaning steps which are time consuming and decrease the quality of the powders.

The fundamental principle in freeze-drying is sublimation, the shift from a solid directly into a gas. Just as evaporation, sublimation occurs when a molecule gains enough energy to break free from the molecules around it. Water will sublime from a solid (ice) to a gas (vapor) when the molecules have enough energy to break free but the conditions aren't right for a liquid to form.
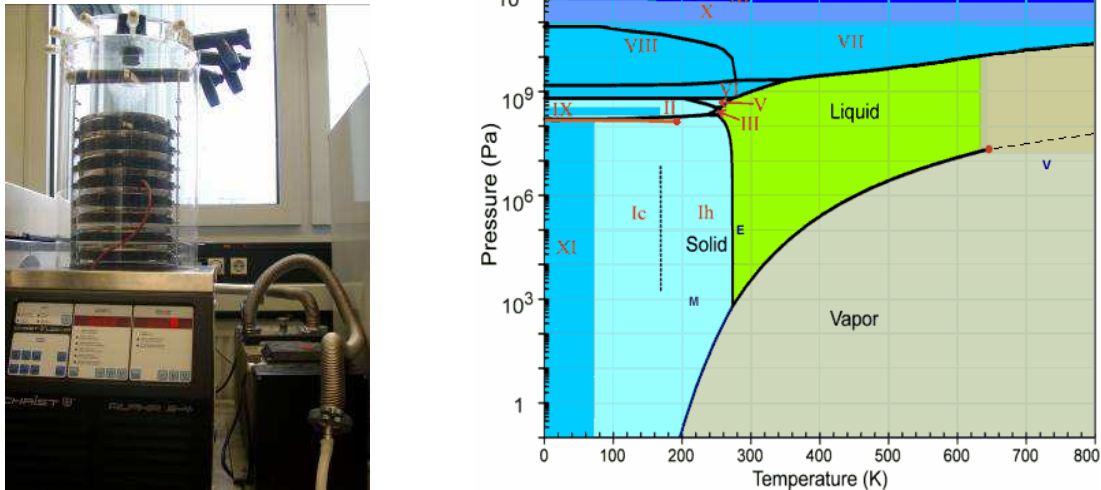
Fig. 15 a and b: Freeze-Dryer and water phase diagram [123]

There are two major factors that determine what phase (solid, liquid or gas) a substance will take: heat and atmospheric pressure. For a substance to take any particular phase, the temperature and pressure must be within a certain range. Without these conditions, that phase of the substance can't exist. The chart above shows the necessary pressure and temperature values of different phases of water. The material is frozen solid, which separates the water from everything around it, on a molecular level, even though the water is still present. Next, the machine turns on the vacuum pump to force air out of the chamber, lowering the atmospheric pressure below 0.06 mbar. The heating units apply a small amount of heat to the shelves, causing the ice to change phase. Since the pressure is so low, the ice turns directly into water vapour. The water vapour flows out of the freeze-drying chamber, past the freezing coil. The water vapour condenses onto the freezing coil in solid ice form. This continues for many hours while the material gradually dries out. After 24h the eight slurries are dried.

c. Pellets formation

The powders are then pressed into pellets. The traditional way to press the pellets (see IV.1.e) is too slow and the pressure achieved is not high enough to assure a good sample quality of reactively sintered samples (see IV.2.d) in any case and in particular and lead-free systems they can be difficult to sinter. An initial green density over 60% may overcome this kind of problems; to obtain it green samples must be isostatically pressed at 3000 bars. With this level of initial density the final density of sintered samples is comparable to that of those produced by the conventional processing. The dried powders fulfil a silicon mould were 20 holes are present. The silicon forms are 80

X 100 mm and holes of 10 mm diameter a performed each cm (see Fig. 16). A silicon mask is used on the bottom and on the top to seal the mould.
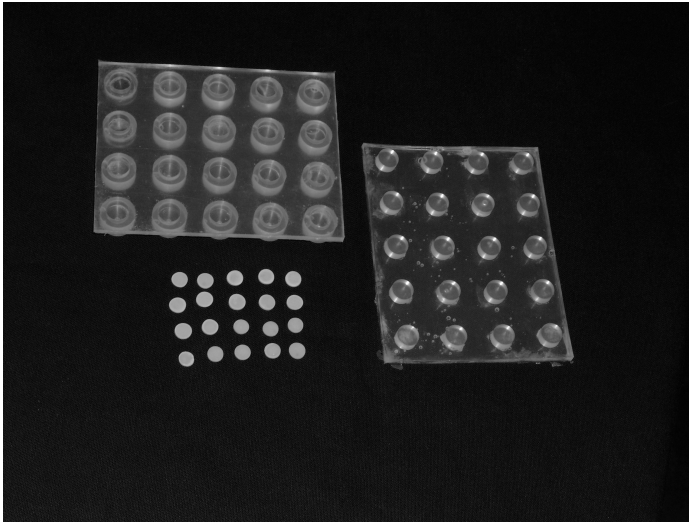

Fig. 16: Silicon mould for isostatic pressing

Eight moulds are filled in parallel and are pressed together. The isostatic pressing does only achieve a higher green density of the pellets but permits the parallel pressing of the different compositions simultaneously. Isostatic pressing allows a pressure 20 times higher than the pressure obtained by means of the uniaxial press. The pressing of 20 samples of 8 compositions as well as the cleaning of the moulds is carried out in 2 h.

d. Sintering

To save time a different preparation of the samples has to be found. The calcination process is very time consuming as the powders have to be milled and dried before and after calcination. There are some processes which alloy the calcination and the sintering to take place in one step. This preparation is called reactive sintering.

After the pressing of the powders into pellets the materials have to be sintered. As stated in section IV.1.a, 20 pellets are pressed for each composition and 5 are necessary for each sintering. The 8 compositions of the same library are sintered together. That means that for a library 4 sinterings are carried out. Five pellets are piled up on a platinum foil, and set on an alumina plate. The construction is sealed using an alumina boat.

The reactively sintered samples are generally not as dense as conventionally prepared samples. The density, however, affects the properties of the material drastically. In order to enhance densification and homogeneity an additional dwelling is realised at

the calcination temperature (generally between 700 and 850℃) for a couple of hours depending on the system (2 h for PZT and 5 h for KNN). Then the samples are heated up to the sintering temperature, between 1000 and 1200℃. The more important parameters are the dwelling temperature, time and sintering temperature. The selection of these parameters is fundamental to reach a high sample quality. The samples are cooled at a rate of 3 K/min up to room temperature.

The sintering is carried out during a period between 24 and 30 h.

The reactively sintered samples need a smaller particle size than the classically prepared ones as the sintering process requires more energy. A grain size of $d_{50} = 0.5$ µm can be achieved after 3 h of planetary milling. The grain size achieved after planetary ball milling is smaller than the grain size achieve after 18h on a milling bank thus making the planetary ball milling method more suitable for the reactive sintering. The reactive sintering is a satisfying process on PZT samples as part of the lead liquefies during the sintering, allowing a high densification of the ceramic.

e. Sample preparation

To characterise the materials the samples have to be polished to a plane surface, as to measure the dielectric properties the samples will be submitted to an electric field. If the surfaces are not planar and parallel the direction of the electric field deviates into different directions and the properties cannot be measured accurately. Additionally, during sintering chemical elements diffuse from the sintering atmosphere into the skin of the samples. Skimming it allows a more accurate measurement of the bulk properties of the material. The available equipment allows to polish one library of samples at the same time. This is a time consuming step, but it allows a better quality of the samples. The samples are glued with bee wax on a steel plate and are polished on one face. Afterwards the samples are turned over, glued and polished on the other face. The samples are polished to a thickness of 0.5 to 1 mm.

As the samples are porous the wax diffuses into the material. To remove the rest of the wax, the samples are heated at 550℃ for 1 h.
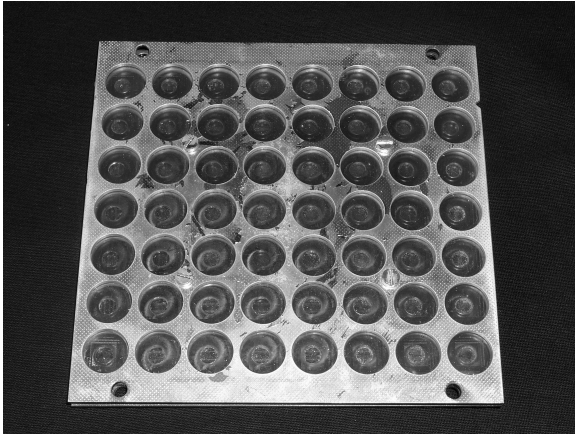
Fig. 17: Silicon mask for samples spattering

After the plane polishing silver electrodes must be applied to the surface. The contacting of the material takes place through sputtering of the ceramics. In the traditional preparation the samples are placed on plates with holes adapted to different diameters. In the case of the HTE preparation not all the diameters of the samples can be measured and placed in adequate plates, thus different compositions having different sintering behaviour and slight diameter variations appear. To adapt to these variations a silicon mask was developed (see Fig. 17). The silicon is elastic and adapts perfectly to small diameter variations. The silicon mask has small cavities of 7 mm diameter and 2mm depth. In one mask with a cavity diameter of 7mm, samples having a diameter between 7 and 7.5 mm can be placed. The silicon mask with the samples is placed in the sputtering machine and one face is sputtered. Then the samples are turned and the other face is sputtered. Two silicon masks are needed for one library. A silicon mask containing up to 56 samples. The sputtering of one library on two faces takes place during 1 h.

f.   Dielectric characterisation

As described before, many of the electrical parameters can be measured on a piezoelectric material to determine its properties. However one or more key properties have to be selected to test the new materials.

In the case of piezoelectric ceramics, the first property measured is the relative dielectric permittivity, ε_r. The measurement of the permittivity takes place manually. As permittivity cannot be measured directly measured, it is through the measurement of

the capacity C that ε_r is determined. Thus the diameter and the thickness of each sample are measured manually and the capacity is determined. This measurement is very quick; a library of 96 samples can be measured within 2 h.

The second important property for piezoelectric ceramic as actuators is the piezoelectric constant, d_{33}. As explain in the section 2.5, d_{33} is the strain of a sample subdued to an electrical field. As explained in the chapter I.5, the aim of this work is to find a candidate to replace PZT. One of the main applications of PZT for the industrial partners during this project was piezoelectric injectors where the large signal piezoelectric constant is a target property. Therefore, during this study, the large signal piezoelectric constant, here named d_{33}^*, was one of the target properties additionally to ε_r.

This constant is slightly different because the piezoelectric displacement is not linear with the voltage applied as schematically illustrated in Fig. 18. The piezoelectric displacement arrives to saturation and the large signal piezoelectric constant d_{33}^* is smaller than the small signal piezoelectric constant d_{33}. During this study much effort was dedicated to the construction of an automated d_{33}^* measuring equipment.
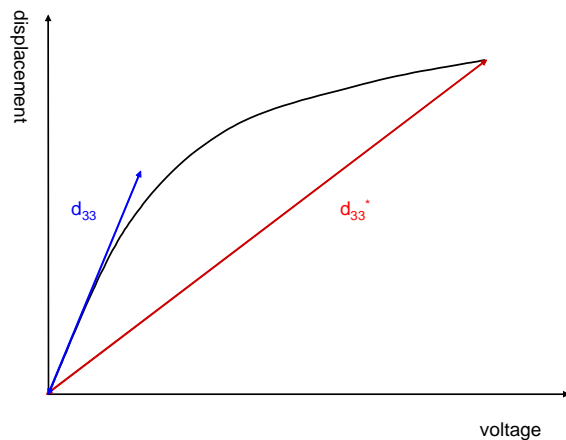

Fig. 18 : schematic piezoelectric displacement in function of voltage

To develop the automated d_{33}^* measuring equipment, three important points have been taken into account.

First, to measure properly the strain of the sample, two tips must hold it to avoid a false measurement of the displacement if the sample bends during measurement. If the sample is placed on a surface or if numerous tips hold the sample; the bending of the sample and the displacement can be measured at the same time. With this kind of method the d_{33}^* cannot be correctly evaluated. The placement between two tips allows

measuring strictly the strain of the sample. Fig. 19 shows a schematic representation of the measurement failure during d_{33}^* measurement if the sample is not held between two tips.
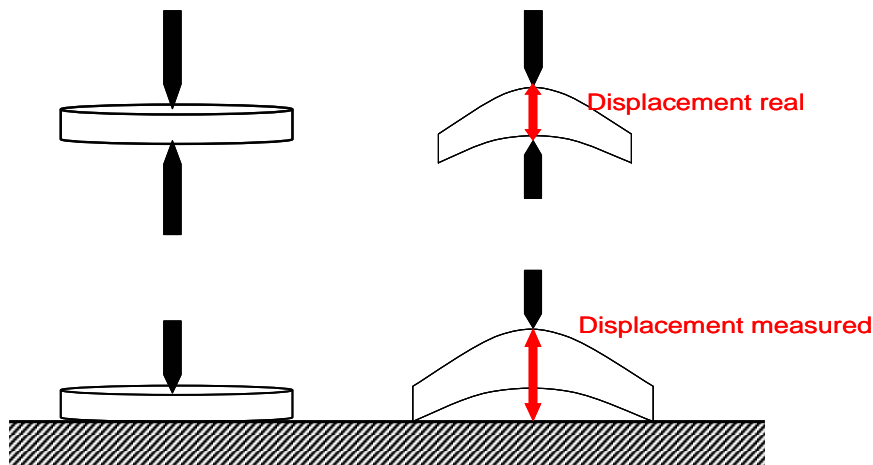

Fig. 19: bending of sample during d_{33}^* measurement

Secondly, the sample must be able to move freely between the two tips, which must be perfectly aligned. The tips must be on the same axe as the electrical field induced in the ceramic must be parallel to displacement. On the other hand the sample must be perpendicular to the field induced. The point impeaches the placement of the Z-axe on a XY plate, so the two tips have to be fixed on one axe and the only displacement allowed is on the Z-axe.

Finally,the sample must be free between the two tips to avoid any mechanical disturbances. The elongation measured is in the order of magnitude of the picometer therefore any external mechanical load on the sample can disturb the measurement and give a false result.

These three considerations have to be taken in account in the design of the test equipment.

The samples are placed on a plate with holes. Around the holes a cavity allows the precise positioning of the samples. The diameter of the cavities is 9 mm and the diameter of the holes is 6mm, which means that the samples must have a diameter between 6 and 9 mm. Plates contain 96 places to allow the simultaneous measurement of one library on one plate. The lower tip is mounted on a motorised plate (Z-axe motor). It passes through the hole and lifts the sample up. The tip displacement can be of a few centimetres. The upper tip is places within a few tenths of millimetre above the

surface of the samples. That means that the lower tip must lift the sample only a few tenths of millimetre until it contacts the upper tip. The displacement of the sample with the lower tip must be as short as possible to avoid sample deterioration. After this process takes place, the sample is held between the two tips and free of any mechanical disturbances.

The upper tip contains an inductive sensor that can measure the displacement of the sample with a high precision. The displacement is recorded with a millitron. During the lifting of the sample the Z-axe motor receives information of the millitron, stopping the raise of the downer tip when the displacement is reached. That means that the sample is lifted up to the reference point of the millitron. The measurement starts after the sample is finely adjusted by the vibration shaking of the lower tip.
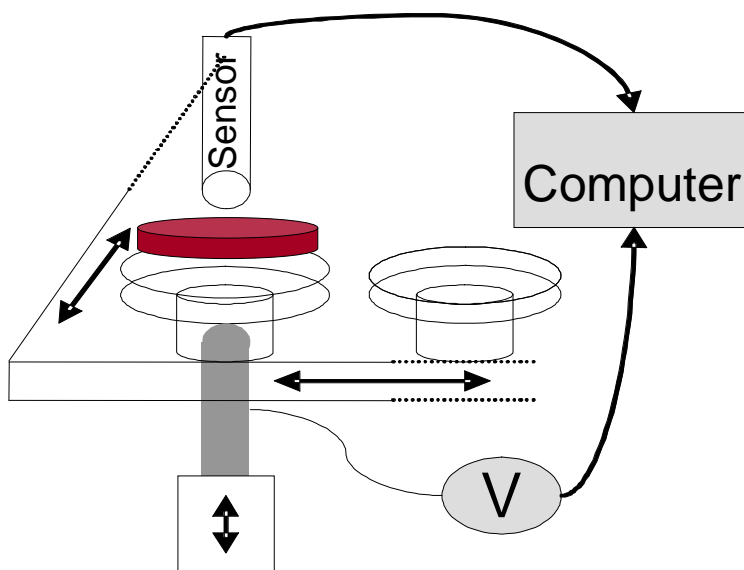

Fig. 20: schematic description of the d$_{33}$* measuring equipment

When the first sample is ready for measurement, the millitron stores the reference voltage given by its initial position. The voltage is given by a potentiometer that records simultaneously the voltage and the current that the sample receives. The sample is submitted to a high voltage to pole it. During the poling a displacement of the sample is produced. To avoid measuring the displacement during the poling 2 further measurements are carried out at the same voltage. The third measurement is taken into account to evaluate the performances of the material. Other measurements with a lower voltage can be carried out after the first cycle. The cycle of measurement should be entered for each library. Typically three ramps up to 2 kV/mm and two at 1 kV/mm are carried out. After the measurement of the sample the downer tip goes down and the plate drives to the next sample and a new cycle can begin again.

The software calculates the d_{33} values. In an old version, the difference between the upper and lower point were taken as the total displacement. In this version the rush of the curve is taken into the total displacement which can generate an error up to 20%. In the new version (used from 08/2006) the recorded curve is fitted and the rush of the curve is eliminated. The d_{33} values are calculated by using the expression (1.14):

$$d_{33} = \frac{d_{max} - d_{min}}{U * d} \tag{1.14}$$

d_{max} and d_{min} are respectively the maximal and minimal displacement of the sample, U the voltage per thickness unit and d the thickness of the sample.
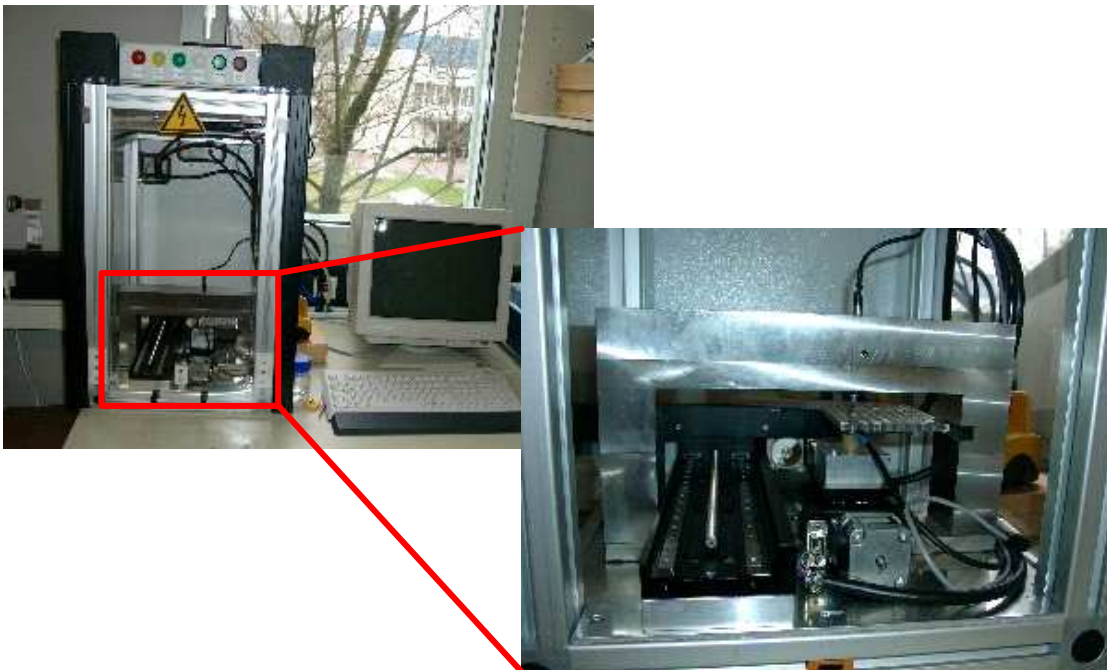

Fig. 21: Automated d_{33}^{*} measurement place
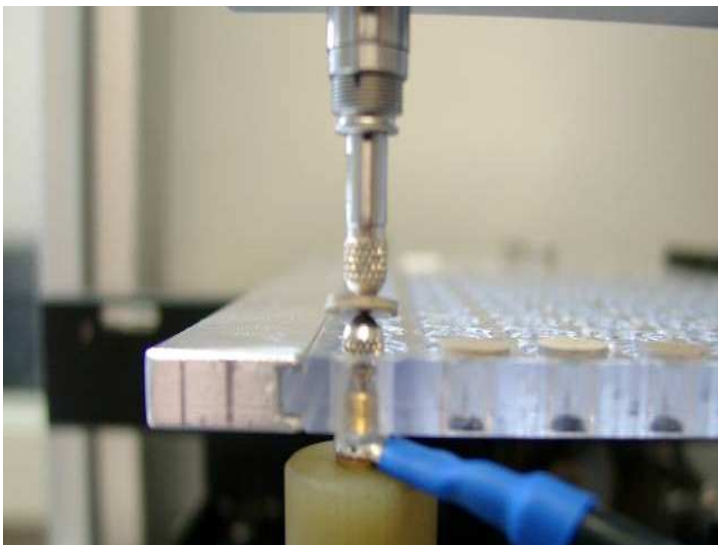

Fig. 22: two tips old a sample for the d_{33}^{*} measurement

With the values of the voltage and the displacement the software delivers automatically the d_{33}^{*}. The numerical results are saved in an excel table (see section 9.3.2) and the curves are saved as text file. For each sample and ramp the effective voltage, the voltage per thickness unit, the strain, the displacement, the d_{33} and the maximal current are saved in an excel table. The file is analysed afterwards with Spotfire (see section 9.3.2). Spotfire allows making clustering in the results. One of the must important values to take into account is the current. Even if samples having a high current are often conductive, the maximum allowed current should be calculated in order not to damage the sample.

For each library different parameters are evaluated together to determine the acceptable current. For some samples it is possible that the current decreases with the applied voltage. In this case only the current of the third measurement will be taken into account. For other samples, the current stays stable for each measurement. In this case the sample should be eliminated. Normally when the current is higher as 0.1 mA, the sample is eliminated.

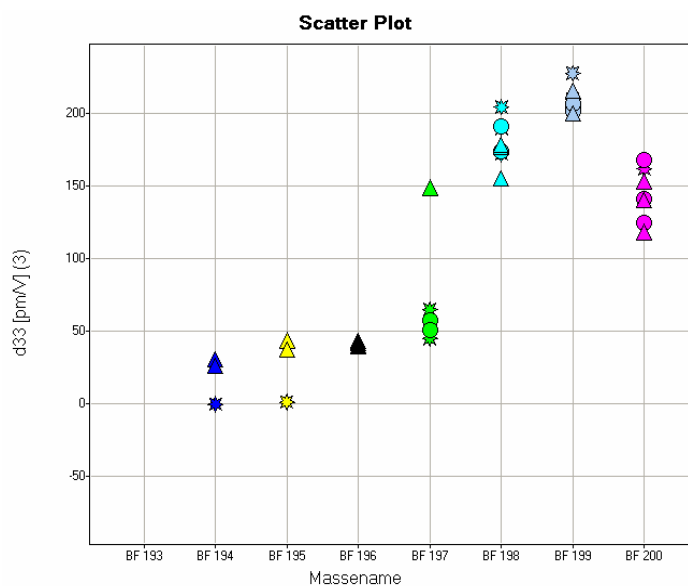**Fig. 23: Evaluation of the samples data with Spotfire**

The last property measured is the Curie temperature. For one composition the Curie temperature does not change with process parameters like sintering temperature and only one sample is necessary to record it. That is why no improvements were made in this direction as the throughput of the measurement is high enough (max. 10 samples per night).

The Curie temperature measuring apparatus consisted of 10 supports assembled together where an electrical contact is set up covered by alumina. The assembly is installed in a recipient and is warmed up with definite parameters. The capacities and temperatures are recorded and delivered in a text data. The analysis of the data takes approximately 30 min.

All the properties are recorded in an Excel table for each library. This table is loaded afterwards in an access-based database. The properties of the sample in this database are connected to the preparation of the samples.

3. Conclusion

HTE is a set of methods using automated sample preparation and characterisation. In this sense the preparation of the samples in this work cannot properly called HTE because it is more a parallelisation than a properly full automated method. However improvements inspired in the HTE method were adapted to accelerate the preparation. The preparation method described achieves a speeding up to four times in comparison with the classical method which is below the theoretical possibilities of HTE due to the a high level of human intervention required for the sample manufacture.

Bulk piezoelectric properties are fundamental for the definition of an adapted material for a given application. These properties can be evaluated only with samples having a high quality. The properties are strongly dependant on the phases present in the material as well as the density of the samples. High sample quality is difficult to achieve with a pure HTE approach. To obtain the high quality of the samples different preparation steps must be carried out. Within a library the results are comparable, and must be even further comparable between different libraries, meaning that meticulous sample processing is critical to obtain the required sample quality and homogeneity to carry out this work.

During the preparation of the powders and samples, manipulation can be complex to preserve the quality of the sample. This compromise between throughput and quality was critical for this work.
The measurement of the dielectric properties could be partly automated. Manipulation is needed between each step of the characterisation but different properties are necessary for a full characterisation of a sample. First the dielectric constant ε_r is

measured per hand because the diameter and the thickness of the sample must be known. The relatively short time needed to measure the geometry of each sample manually does not make it worth to set up an automated measurement system. After ε_r, d_{33}^* is automatically measured and finally the measurement of the Curie temperature is carried out. With the automated d_{33}^* measuring machine the characterisation of a library was carried out within 24 hours, thus 4 times faster than with the traditional methods.

Table 4 : comparison of traditional and HTE method

HTE Method		Time	Conventional method		Time
Dosage of 8x0.1 mole		2h	Dosage of one mole		0,5h
Grinding in planetary ball-milling machine		3h	First grinding and drying		36h
Drying in freeze dryer		24h	Calcination		10h
Moulding in isostatic press (160 samples)		2h	Second grinding and drying		36h
Reactive sintering		24h	Granulation		2h
			Moulding in uniaxial press (40 samples)		1h
			Sintering		24h

Table 4 compares both the HTE based method developed in this work and the traditional method. To prepare 8 new materials the time needed is about 55h with the HTE method and about 880h for the classical preparation. The theoretical acceleration is 16 times with the new way of preparation. Indeed due to the parallelisation of the processing in the classical method and a high degree of human intervention in the HTE-based method developed in this work the real improvement is about 4 times.

A real HTE characterisation could be implemented. Although the dielectric constant is measured manually, an automated process could be set up but is not justified as the improvement on the manual measurement is negligeable. The d_{33} measuring machine provides a real acceleration for the dielectric characterisation. Before the automated set-up was build it took 8 hours for a manipulator to measure all the d_{33} of a library. Now the automate needs 4 hours to characterise a library and the personal expense is only of 20 minutes. The information is delivered in an excel sheet form and can be directly imported into Spotfire. After selection only the data required for further

calculations is introduced into the database. The Curie temperature is then recorded as described before. The routine dielectric characterisation can be achieved within 24h for a library.

If no human intervention were needed a library could be produced and characterised within 10 days, with the present method it takes approximately 4 weeks. On the other hand the work can be parallelised, meaning that the real throughput is in average of one library each 3 weeks.

V. Tests on a Lead-Zircon-Titanate System

A number of improvements to accelerate the production of samples were investigated on PZT materials. As described in a previous chapter the preparation of the material is quite long due to multiple steps. One of the most time consuming steps is the calcination because the powder must be ground twice and dried. For the first tests the reactive sintering was tested on a PZT system. The reactive sintering is a simple and time saving processing method, where the oxide mixtures are directly calcined and sintered at high temperatures without undergoing a second milling after the calcination. The method has to be tested on a well known material and the data have to be compared. The material selected is a PZT, doped with 2 mol% of neodymium (Nd)[124]. The Nd is assumed to replace Pb in the perovskite structure[125]. However, due to the principle of electroneutrality, the Nd, which has a valence of 3 will create a disturbance in the material. Three possibilities exist: Zr or Ti will be reduced, O will be inserted in the lattice or Pb vacancies will be created. The Pb has a high vapour pressure therefore the creation of Pb vacancies will be favoured as explain in equation (1).

$$3Pb_A^{2+} + 2Nd^{3+} \rightarrow 2Nd_A^{3+} + \bullet_A + 3Pb^{2+} \uparrow \qquad\qquad (1)$$
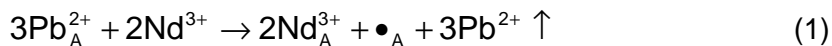
The A site vacancies are assumed to increase the mobility of ferroelectric grain boundaries and inhibit the grain growth[126]; however the concentration of Pb vacancies should not be too high to avoid negative effects on the dielectric properties[2]. As stated before the properties are optimal in the MPB. The MPB moves with the doping rate, the raw materials and the preparation method. The MPB should be reached adjusting the zirconium to titanium ratio.

The MPB of the PZT doped with 2% Nd is found around a ratio Zr :Ti = 0.48:0.52, but a slight stochiometry change is possible due to different parameters among the quality of the raw materials or the preparation method. In previous work[127] the influence of the Nd concentration, the ratio Zr:Ti as well as the sintering temperature was studied. This previous work will be use as a reference but, it has to be to taken into account that now

different precursors are available for the manufacture of PZT. To obtain a pure PZT through reactive sintering $(Zr,Ti)O_2$ proprietary precursors were used.

1. Reactive Sintering

The reactive sintering of PZT-based piezoelectric ceramics has been previously investigated[128]. However, it not nowadays a typical method to process PZT-based ceramics as the quality of the ceramics is lower than the quality of a ceramic produced by classical methods. In particular, PZT-based ceramics were difficult to process via this method, because large amount of PbO excess were needed to induce a liquid phase sintering and thus reducing the porosity of PZT.
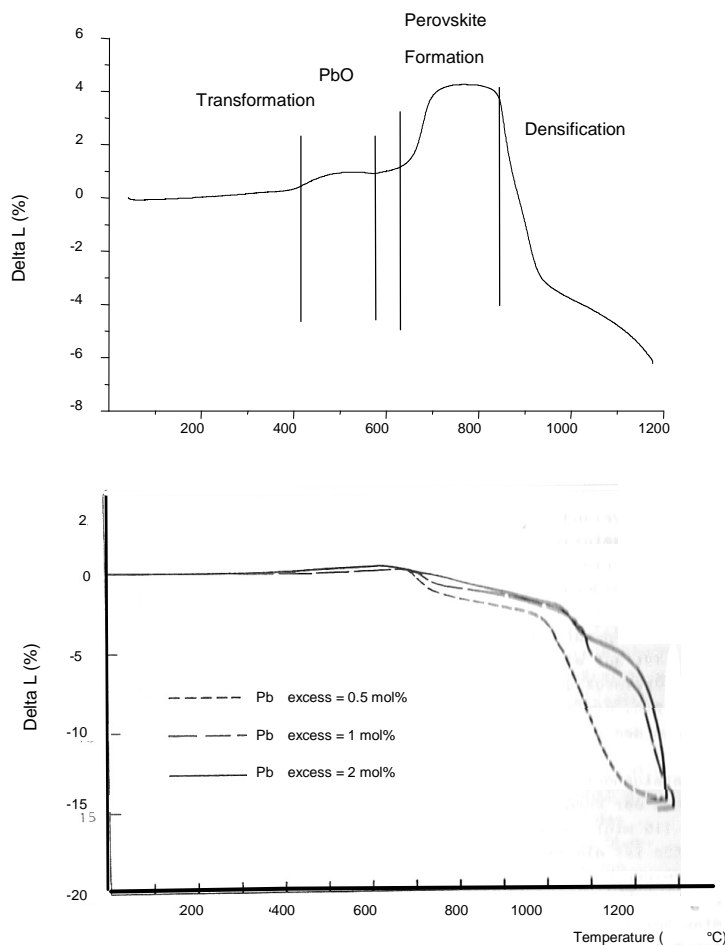

Fig. 24: Dilatometer curve of $(Pb_1Nd_{0.02})(Zr_{0.48}Ti_{0.52})O_3$ of a reactive sintered sample (a top) and a sample having suffered calcination (b, bottom)

Dilatometer measurements were carried out with an autoranging Keithley multimeter to investigate the sintering behaviour of PZT (see Fig. 24). The reactively sintered material shows a first anomaly between 400 and 550°C. This hump is the sign of the

transformation of PbO into Pb_3O_4[129]. The formation of Pb_3O_4 was also verified through XRD analysis (see

Fig. 25). The perovskite is formed between 750 and 900°C and the material densifies with a linear shrinkage of 11%. The material prepared with the classic methods, independently of its excess in Pb, shows a linear shrinkage of 15% as shown in Fig. 24 b. The samples prepared through HTE method have a lower density than the samples prepared through the classical route.

The densities of the samples were measured with a Micrometrics AccuPyc 1330 helium picnometer. The values of table 1 show that the densities of reactively sintered samples are 95% of the density of conventionally manufactured samples. A dwell at 850°C for 2 hours provides an enhancement of the densification and the density rises to 97% of the density of conventionally manufactured samples.

Vorstufe PZT:

Pb(Zr$_{0.52}$Ti$_{0.48}$)O$_3$, bis 500°C - File: 20050382_D8-SiLi_2.RAW - Anode: Cu - Creation: 05.01.2005 20:52:21
89-1947 (C) - Minium, syn - Pb$_3$O$_4$ - Y: 25%
77-1971 (C) - Massicot, syn - PbO - Y: 24%
85-1739 (A) - Litharge, syn - PbO - Y: 3%
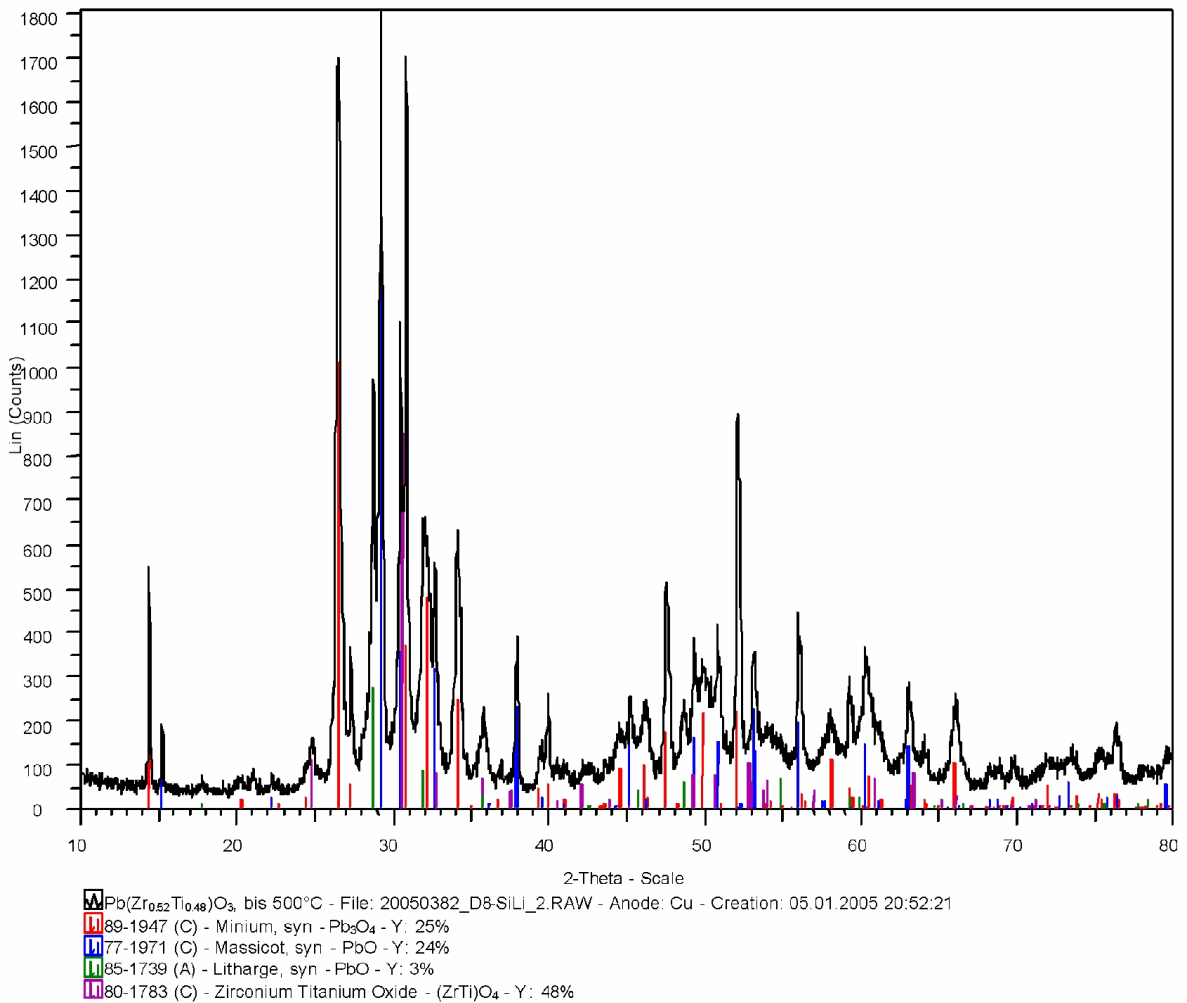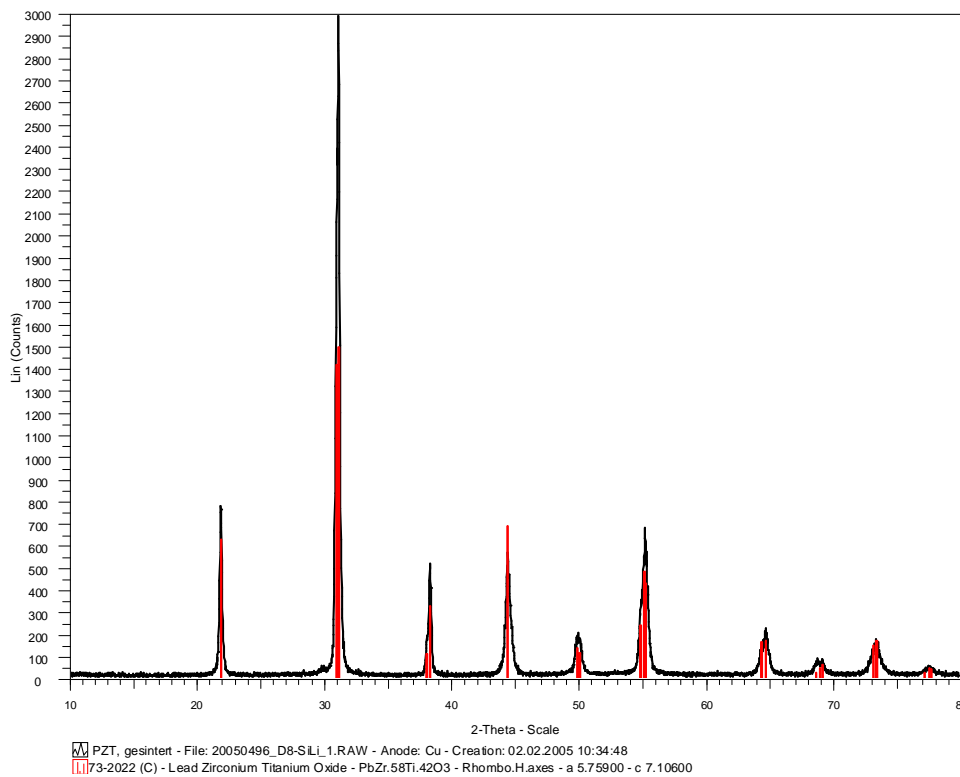80-1783 (C) - Zirconium Titanium Oxide - (ZrTi)O$_4$ - Y: 48%

Fig. 25: X-Ray diffraction pattern of a reactively sintered PZT at 500°C

Table 5 Density of different samples

Sample	Density [g/cm³]
Conventionally manufactured	7.7939
Reactively sintered	7.4697
Reactively sintered + dwell at 750°C for 2 hours	7.494 2
Reactively sintered + dwell at 850°C for 2 hours	7.527 3

To control the phase formation, an XRD pattern was carried out on samples after reactive sintering. As shown in Fig. 26 the material obtained shows a pure phase perovskite.

PZT, gesintert - File: 20050496_D8-SiLi_1.RAW - Anode: Cu - Creation: 02.02.2005 10:34:48
73-2022 (C) - Lead Zirconium Titanium Oxide - PbZr.58Ti.42O3 - Rhombo.H.axes - a 5.75900 - c 7.10600

Fig. 26: X-ray diffraction pattern of reactively sintered PZT with 2% Nd at 1200°C

2. Characterisation

The surfaces of polished and etched samples produced by reactive and conventional sintering were observed under a light microscope (Fig. 27 a and b). As shown in Fig. 27 the average grain size of the reactively sintered samples is 5µm and the grain size of the conventionally sintered samples is 3.5µm. The microstructure of the reactively sintered samples shows a closed porosity with large channels.

Samples were produced with different zirconium/titanium contents between 51 mol% and 55 mol% Zr with 0.5% increments. The dielectric values of the HTE samples with ε=923 and tan δ=2.3% for a zirconium content of 53 mol% were similar to the values of conventionally manufactured samples with ε=1042 and tan δ=1.4% [130]. The morphotropic phase boundary is clearly identified.

 shows the values of the relative dielectric constant before and after the poling for reactively sintered samples with a dwell at 800℃ for t wo hours. The same tendency is observable in each curve: a peak in the area of 53 mol% Zr. The MPB is clearly identifiable for the samples which contain between 52 and 53.5 mol% zirconium because the permittivity after poling is higher than the permittivity before poling. The results found with the reactively sintered samples are in accordance with the results found with the classical prepared samples as shown in
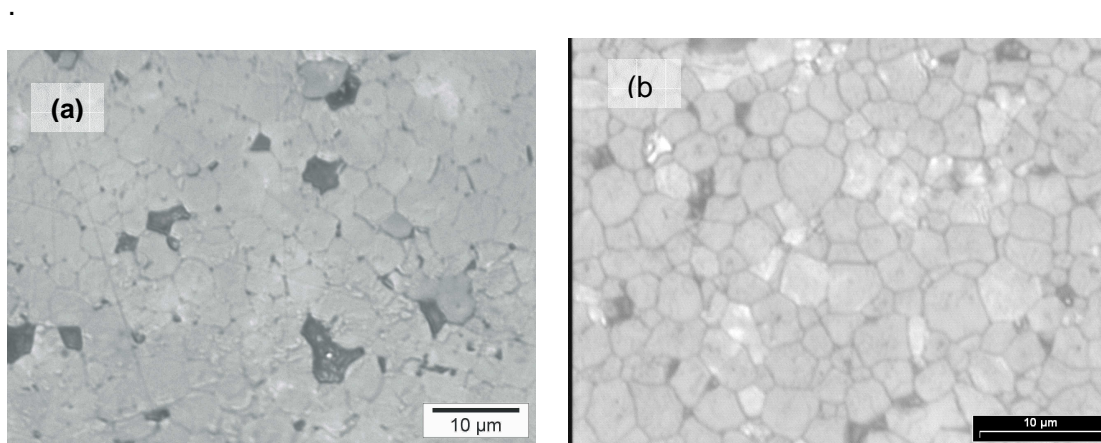
.

Fig. 27: Light microscope image f PZT reactively sintered (a) and conventionally sintered (b)

 shows the difference between the dielectric constant before and after poling for four different zirconium contents. The grey columns are the compositions with 3% Pb excess and the stroked out columns are those with 5% Pb excess. To investigate the effect of the calcination temperature during the reactive sintering of the samples, different oven programs have been used. First, the samples were heated up to 1250℃ at a rate of 2k/min, held for 2h and cooled down to room temperature. A second program was designed which consist of heat the samples up to 800℃ at 2K/min, maintain the temperature during 2h (which is the calcination temperature and time used during the classical preparation of this kind of PZT ceramics) and then heat the samples up to 1250℃ at 2K/min, held for 2h and fina lly cooled down at room

temperature. Two other programs consist of vary the temperature of the calcination, maintaining the oven temperature at 850℃ and 900℃ .

 shows the effect of the reactive sintering on the properties of the samples. The brighter colours show a reactive sintering without plateau at calcination temperature; the darker colours show a plateau at different calcination temperatures (the darker the colours are, the higher the plateau temperature is). This figure shows the importance of PbO excess during the processing of PZT materials as well as the maintaining time during the calcination step. PbO excess and control of the atmosphere are two important parameters for classic sintering of ceramics and particularly for PZT[131]. The PbO excess must be present to induce the liquid phase during sintering which allows higher densities to be reached. PbO vaporisation was controlled during sintering through the use of a firing boat which was saturated with a mix of PbO and ZrO_2 before. The optimal parameters found are an excess of 3 mol% of PbO and a plateau at 850℃ for 2 h. The optimal excess of PbO was shown not to be as high as in previous reports[132]. The plateau at 850℃ is optimal because calcination takes place between 700 and 875℃ and the plateau let more time to carry out the calcination. The temperature is chosen at the end of the calcination step when diffusion is fast but densification has not started. At lower temperatures (<800℃) the formation of the perovskite could not have been totally completed and higher temperatures showed no benefit either. As has been stated[133], the presence of PbO excess is crucial in achieving high density PZT. On the other hand, an unacceptably high PbO excess endangers correct densification due to the rapid formation of a liquid phase followed by a rapid particle rearrangement, and solution/precipitation induces an inhomogeneous microstructure with large pores. A PbO excess of 3 mol% leads to the optimum densification parameters.

Fig. 30 shows the piezoelectric coefficient d_{33} of samples with different preparation conditions for the same range of compositions. The bright grey line shows the results of the conventionally prepared samples. The dark grey and the black lines are the values of the reactively sintered samples; the black line represents values of samples with a dwell during the sintering at 900℃ for two hours. All the samples contained 3% PbO excess and were sintered at 1250℃ for two hours. The d_{33} values of the reactively sintered samples are lower than the values of the conventionally sintered samples. This is an expected result due to the low density of the samples; nevertheless the values are already close to the conventionally sintered ones and it should be noted that in the morphotropic phase boundary the values are somewhat higher (Zr content 0.53-0.535).
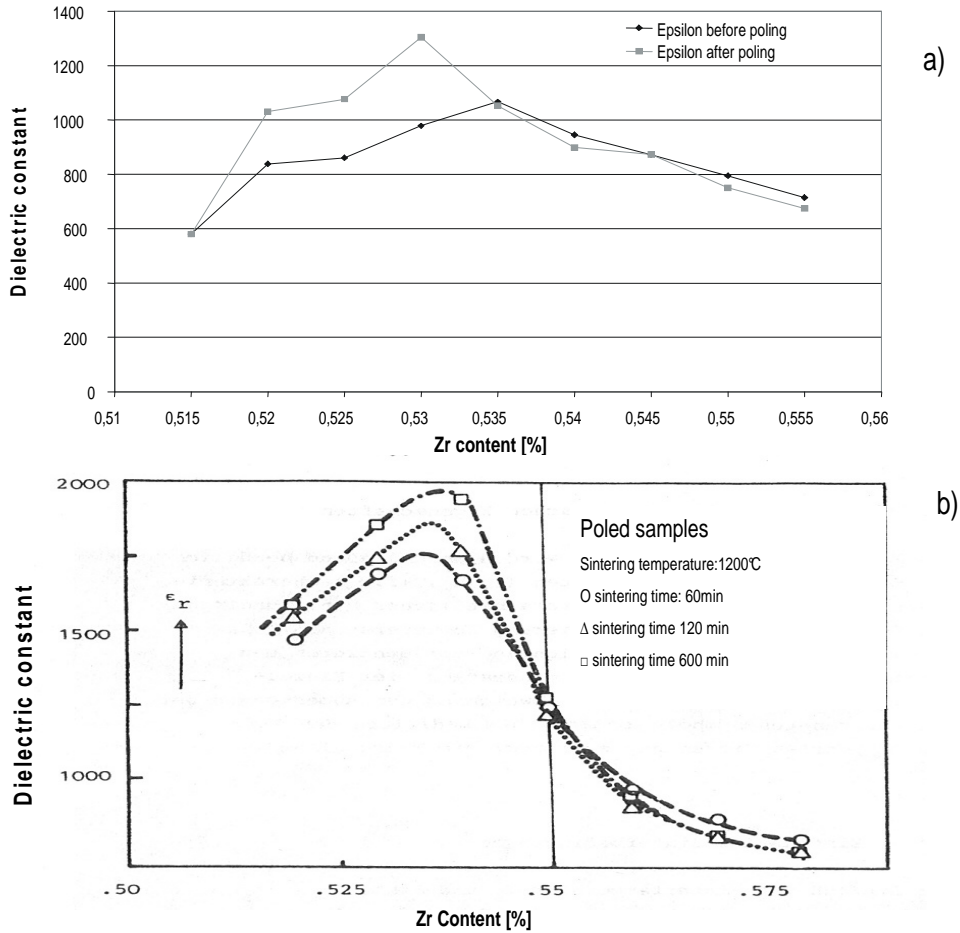
Fig. 28: Dielectric constants of reactive-sintered (a) and classically prepared (b) $Pb_1Nd_{0.02}(Zr_xTi_{1-x})O_3$ samples.
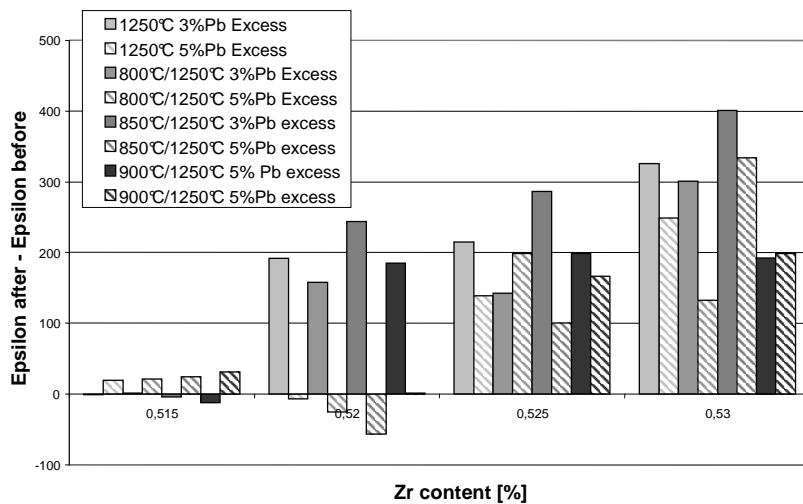

Fig. 29: Relative dielectric constant before and after poling of different PZT samples with zirconium content variation. The temperatures indicated are the plateau temperature/sintering temperature

The values of the samples having suffered a dwell at 900℃ are lower. This dwell, being in the densification zone, impairs the perovskite formation and the ceramic shrinks without having formed the perovskite.
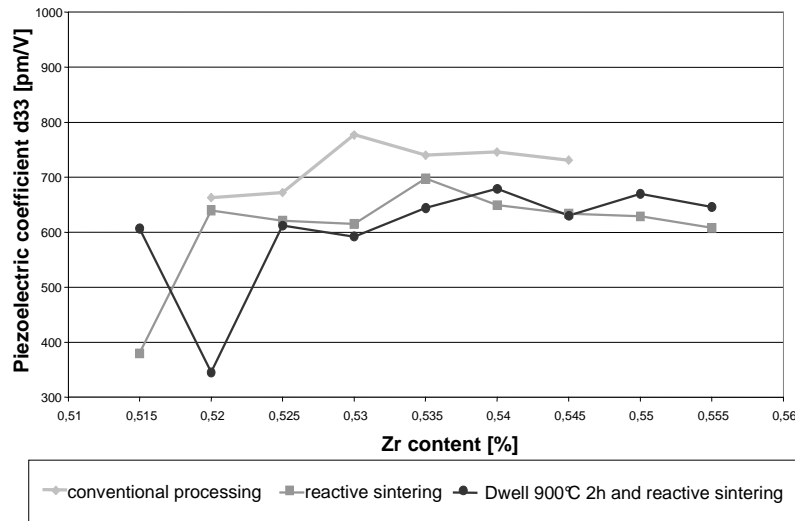

Fig. 30: Piezoelectric coefficient in poling direction (d_{33}) at 2kV/mm

3. Conclusion

A solid state synthesis and characterisation method for piezoelectric ceramics was established as described in chapter IV.2 and this method was first tested on a PZT system in chapter V.

This method achieved excellent results. The MPB is clearly observable through the values of the relative dielectric constant before and after the poling as well as the values of the piezoelectric coefficient d_{33}. For both measurements the values of the reactively sintered samples are almost as high as the values of the samples manufactured by conventional methods.

The remarkable results on a PZT system may be related to the quick formation of the perovskite structure and the high sinterability induced by the liquid phase formation during sintering. For different systems the method can be improved and used to develop any kind of piezoelectric material.

VI.   Test on a Lead-Free System

The high throughput experimentation method was proved on a PZT system and needs to be also validated on a lead-free system. The test on a lead-free system is carried out on a $(K_{0.5}Na_{0.5})NbO_3$ (KNN)-based system as recent studies on a (KNN)-based piezoelectric ceramic have demonstrate great improvements of the system performances[5].

1. Test system

The test system selected was developed by the company Toyota-Denso and has the formula: $[Li_x(K_yNa_{1-y})_{1-x}](Nb_{1-z-w}Ta_zSb_w)O_3$. A scientific publication[5] as well as a patent[134] came together in the second half of 2004 which reported the last improvement on the performance of KNN. In the patent a lot of variations have been tested and all the results are available which gave a good reference.

To test the method a few libraries were carried out with determined goals. As it was clarified before KNN has a MPB around K:Na=0.5:0.5[135,136]. The goal of one library was to find this MPB. A second library was carried out to establish the role of the two dopants lithium and antimony in the KNN composition.

2. Raw materials

Traditionally, to prepare KNN-based piezoelectric ceramics, sodium and potassium carbonates are used as raw materials. They are mixed, calcined, mixed again and sintered. During the calcination, the carbonates are transformed and a noticeable quantity of CO_2 is released. During the HTE process, the ceramics are reactively sintered and the use of carbonate can be difficult. If carbonates are used as raw materials for the reactive sintering, the amount of carbon and oxygen to be released

during the perovskite formation is too big to achieve dense ceramics (12% in weight) and according to the phase diagrams (see section 3.4.3) no liquid phase during the sintering is present. Therefore, the carbonates can definitively not be used and precursors were employed to perform the reactive sintering of KNN. The precursors chosen were $KNbO_3$, $NaNbO_3$ and $KTaO_3$. No precursor was used to incorporate lithium as the quantities are quite small and no commercial product was available.

3. Sintering

To test the reactive sintering on lead-free samples, dilatometer measurements were carried out (Fig. 31). The reactive sintering of the sample with carbonates shows 30% shrinkage whereas the sintering of a sample prepared from the same powder but calcinated shows 5% shrinkage. The reactively sintered sample prepared with oxides shows 1% shrinkage and the sample prepared from the same powders, but calcined, shows 2.5% shrinkage.

The difference of shrinkage between the samples prepared with carbonates can be explained by the release of CO_2 during the transformation of K_2CO_3, Na_2CO_3 and Li_2CO_3. In both reactive sintered samples a hump is visible between 500 and 850°C which is the sign of the perovskite formation. However, the hump of the reactively sintered sample prepared from oxides is not as high as those of sample prepared from carbonates as the precursors have a structure narrow to the structure of the KNN. The $NaNbO_3$ and $KNbO_3$ have both an orthorhombic perovskite structure at room temperature and undergo a series of transformations between 200 and 640°C [137]. Their lattice parameters are shows in Table 6. The $(K,Na)NbO_3$ has also an orthorhombic perovskite structure at room temperature with somewhat different lattice parameters and undergoes also a series of phase transformation[138]. The reactive sintering of KNN is also a mix of sintering and phase transformation of precursors, therefore the shrinkage is not as important for this sample as for the samples prepared from calcined powder.

To prove the quality of the method on KNN samples a high temperature X-ray analysis is carried out on different samples (Fig. 32). The analysis shows that the product of the reactive sintering with oxides is not a pure phase perovskite as it was in the case of PZT. This is a mix of perovskite (around 96%) and tungsten-bronze (around 4%). An improvement of the method has to be realised to obtain a pure phase perovskite.

Table 6: Lattice parameters of $NaNbO_3$, $KNbO_3$ and $(K,Na)NbO_3$

	$KNbO_3$[139]			$NaNbO_3$[140]			$(K, Na)NbO_3$[141]		
	orth	tetra	cub	orth	tetra	cub	orth	tetra	cub
A	5.689	3.986		5.598	5.531	-	5.671	4.015	-
B	3.969	-	4.02	15.523	-	3.952	3.945	-	3.99
C	5.725	4.142		5.505	3.974	-	5.645	3.97	-
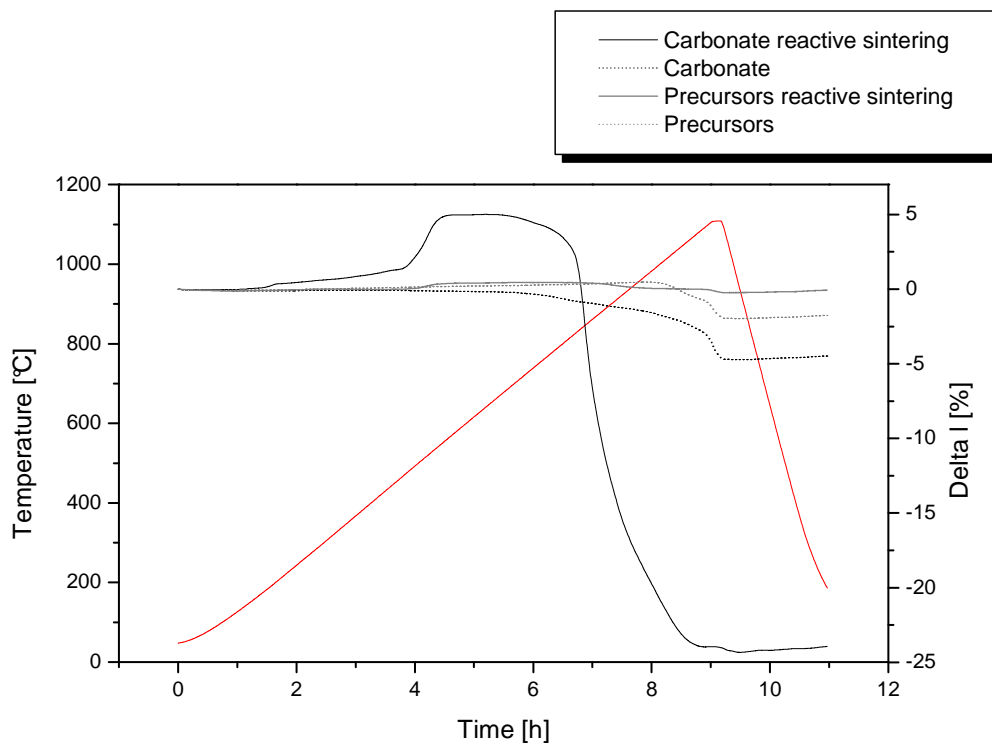
Fig. 31: Dilatometer measurement of [Li$_{.04}$(K$_{.47}$Na$_{.53}$)$_{.96}$](Nb$_{.84}$Ta$_{.1}$Sb$_{.04}$)O$_3$ processed differently

To obtain samples with a higher quality, the HTE preparation has to be closer to the classical preparation, thus an additional calcination was inserted in the workflow. The powders can be mixed and then a partial calcination could take place. The quality of the calcination will not be as good as if the powders were milled before. This step can improve the quality of the samples.
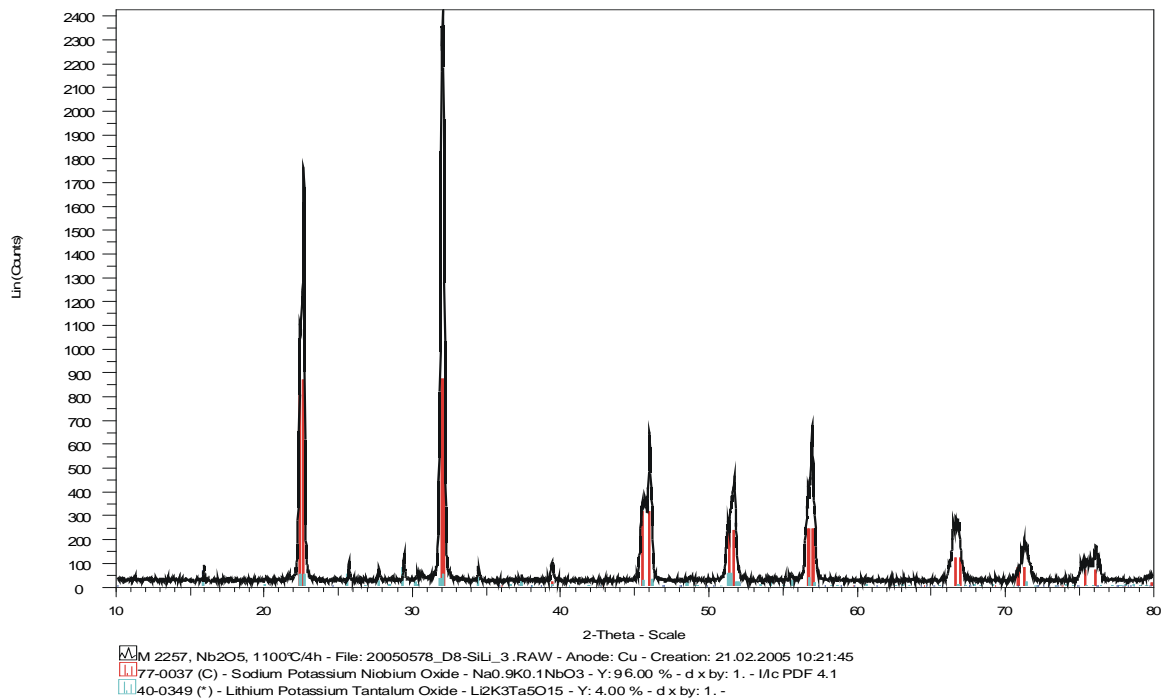
M 2257, Nb2O5, 1100°C/4h - File: 20050578_D8-SiLi_3 .RAW - Anode: Cu - Creation: 21.02.2005 10:21:45
77-0037 (C) - Sodium Potassium Niobium Oxide - Na0.9K0.1NbO3 - Y: 96.00 % - d x by: 1. - I/Ic PDF 4.1
40-0349 (*) - Lithium Potassium Tantalum Oxide - Li2K3Ta5O15 - Y: 4.00 % - d x by: 1. -

Fig. 32: X-ray diffraction pattern of a reactively sintered sample of $[Li_{.04}(K_{.47}Na_{.53})_{.96}](Nb_{.86}Ta_{.1}Sb_{.04})O_3$

The dosage of the powder takes place in a plastic cup which is adapted to the Speedmixer®. The Speedmixer® is a machine which homogenises the powder without milling. The plastic cup is put in a support which rotates like a centrifuge but the support possesses is own rotation system. The mixing of the powder is realised through the opposition of centrifugal forces of the central part and the centrifugal forces of the cup support. Fig. 33 illustrates the movement of a plastic cup in a Speedmixer®.
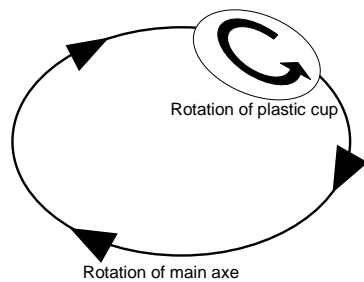

Fig. 33: schematic rotation of a cup in a Speedmixer

Alcohol is added in the mixing cup to improve the homogenisation of the powders. The alcohol does not solubilise the powders and can be quickly removed for the mixing cup by evaporation. The mixing in the Speedmixer is 1 m long for each powder. Thus the

mixing takes 8 m for all powders and the evaporation of the alcohol 1 h in a drying oven.

After the homogenisation the powders are calcined together in small crucibles. For KNN the calcination takes 5 h at temperature between 750 and 900°C. Once the calcination is finished, the powders are grinded in a planetary ball milling machine as previously described and the rest of the process follows, i.e. the powders are milled in parallel in a planetary ball milling machine for 3 h and dried in a freeze-dryer.

Typically the dosing of the powder is done in the morning, then the powders are mixed and dried in the afternoon and calcined overnight. The next day the powders are ready to be milled. The additional step takes 1 day more but allows to reach a higher quality of the samples. A good compromise between sample quality and throughput is here met. However this additional step does not disturb the throughput since the real throughput is lower than the theoretical one due to high level of human handling of the samples as stated in the section method.

To characterise the calcination step an X-ray analysis was obtained from three samples: a reactively sintered sample, a previously calcined and sintered sample and the calcined powders (without sintering) of the sample. It is shown that the sample having previously been calcined shows a pure phase perovskite (Fig. 34).
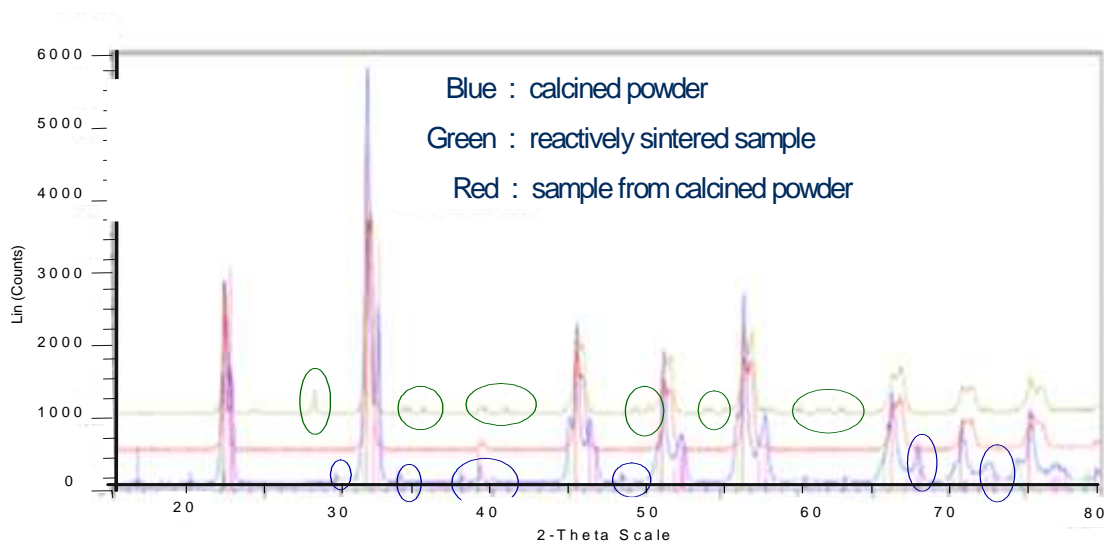

Fig. 34: X-ray diffraction pattern of [Li$_{.04}$(K$_{.47}$Na$_{.53}$)$_{.96}$](Nb$_{.86}$Ta$_{.1}$Sb$_{.04}$)O$_3$ samples having suffered different preparations

Furthermore to verify the phase formation during sintering high temperature X-ray analysis was carried out between room temperature and 1060°C on different samples

(from the Anadolu University, Turkey). Fig. 35a represents the pattern of a non calcined sample prepared from carbonates, Fig. 35b represents the pattern of a non calcined sample prepared from oxide precursors and finally Fig. 35c shows the reflexes of a calcined sample prepared from oxides.

The Fig. 35a shows clearly the transformation of the potassium and sodium carbonates and niobium oxide into KNN at temperatures from 570°C. The peaks for 2θ at 28 and 38° which are characteristic for sodium and potassium carbonates disappear and a peak at $2\theta=33°$ which is typical for a perovskite appears. The carbonates are presents up to 650°C and for temperatures above 650°C only the perovskite is present. At 900°C a new phase begins to appear recognisable for its peak at $2\theta=29°C$. This phase is unidentified but it stays present after cooling to room temperature.

The Fig. 35b represents the behaviour of a sample processed from precursors and reactively sintered. At room temperature near the perovskite structure of the niobates other peaks at $2\theta=23$, 29 and 33.5° reveal the presence of Li_2CO_3 and Ta_2O_5. These peaks disappear above 750°C, which is the calcination temperature, i.e. temperature at which the perovskite is formed. At 2θ between 45 and 46.5°, 51 and 52.5° and 56.5 and 58°, the reflexes of the potassium and sodium niobates are separated and as the temperature increases the peaks approach each other and finally fuse at 650°C. During the sintering the peaks of cubic KNN are more and more acute, after cooling at room temperature it seems that the ceramic has an orthorhombic structure identifiable by bright peaks at $2\theta=47$ and 52° (at $2\theta=47°$ reflexes of (200) (020) and (002) and at $2\theta=52°$(201), (210), (102), (012), (120) and (021)). Additionally to the perovskite, another unidentified phase was visible since the beginning of the heating at $2\theta=40°$ and reminded stable during the whole sintering and at room temperature.

The high temperature XRD profiles of the calcined sample prepared from precursors is similar to the profiles of the non-calcined one. However, the perovskite peaks are more intense and the intensity of the peaks of the external phases is diminished. Before calcination the powders are not intimately ground and are only mixed with the help of a Speedmixer®, therefore, the calcinations could not be finished as shown in Fig. 34. The near phases are present up to 1020°C but after cooling at room temperature the only phase present is a pure phase perovskite with two phases present: orthorhombic and tetragonal. In the literature[1] a new morphotropic phase boundary was discovered in the KNN system and this sample should have a composition in the MPB, therefore, the presence of both structures is in agreement with it.
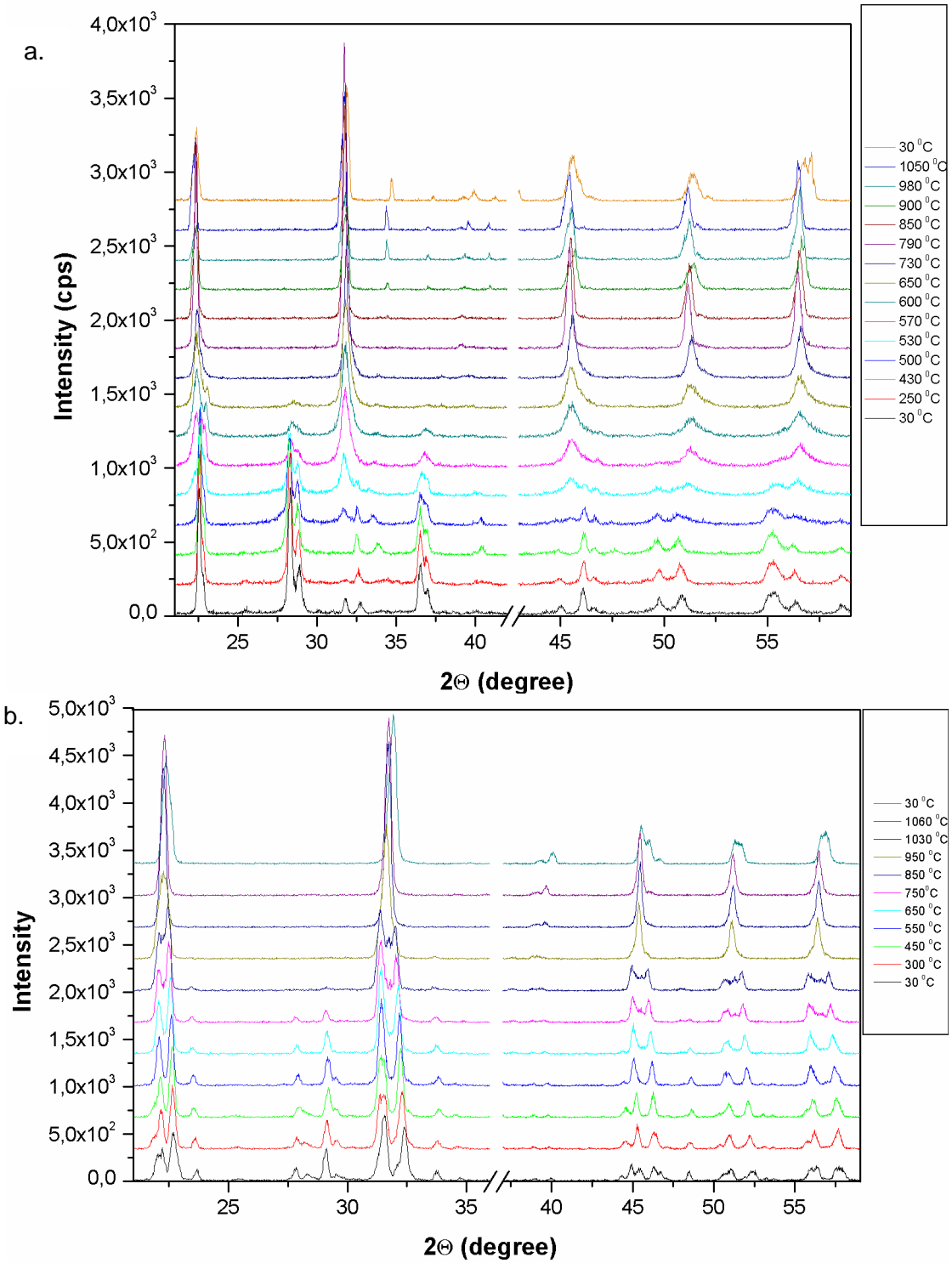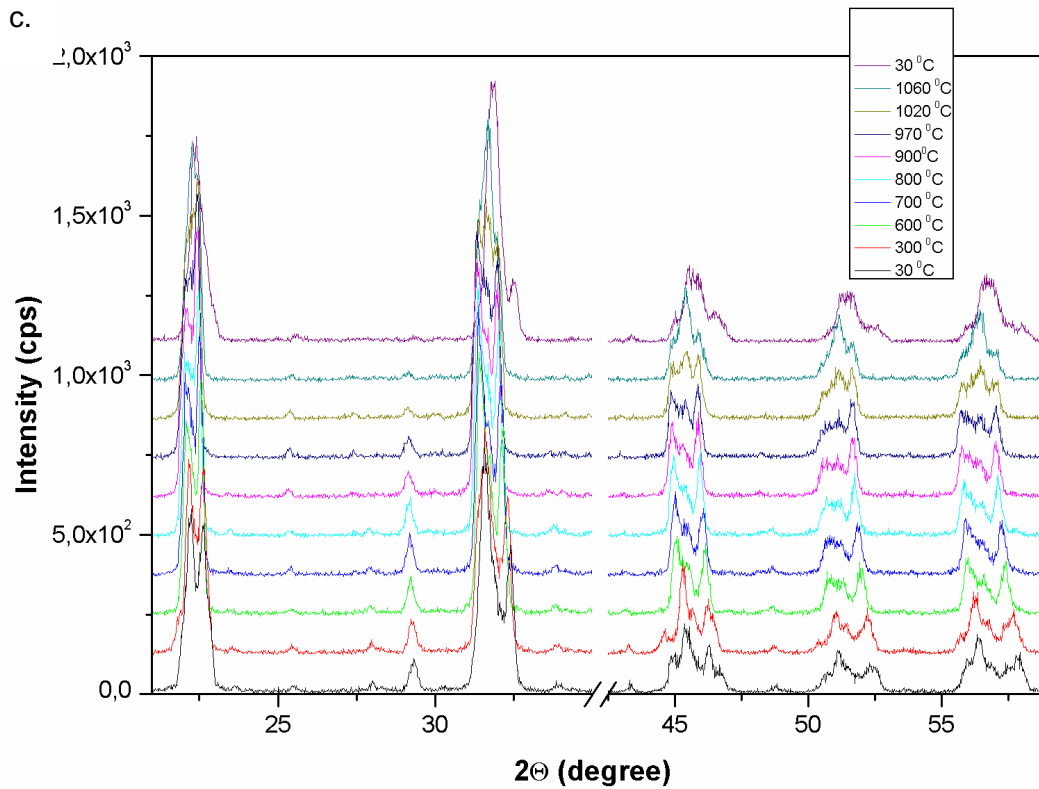
Fig. 35: high temperature XRD pattern of [Li$_{.04}$(K$_{.47}$Na$_{.53}$)$_{.96}$](Nb$_{.86}$Ta$_{.1}$Sb$_{.04}$)O$_3$

a. non calcined prepared from carbonates

b. non calcined prepared from oxides

c. calcined prepared from oxides

Only the ceramic processed from oxides having suffered calcination show the presence of a pure perovskite phase and furthermore, the presence of two structures, an orthorhombic and a tetragonal in accordance with the literature. Therefore this calcination process was implemented for KNN-based ceramics in the workflow of the HTE method developed.

4. Characterisation

As said in the previous section a few libraries were made to test the method on a lead-free system. The goal of the first library was to study the influence of a pre-calcination on the dielectric properties. The values of ε are presented in Fig. 36. No significant influence of the pre-calcination could be seen on the ε values. The KNN is certainly not such sensible as PZT is to impurity however the calcination will takes place as well. It is

difficult to estimate how sensible a material is to impurities. For further material developments the calcination step will always be done to ensure the chance to find a suitable material.
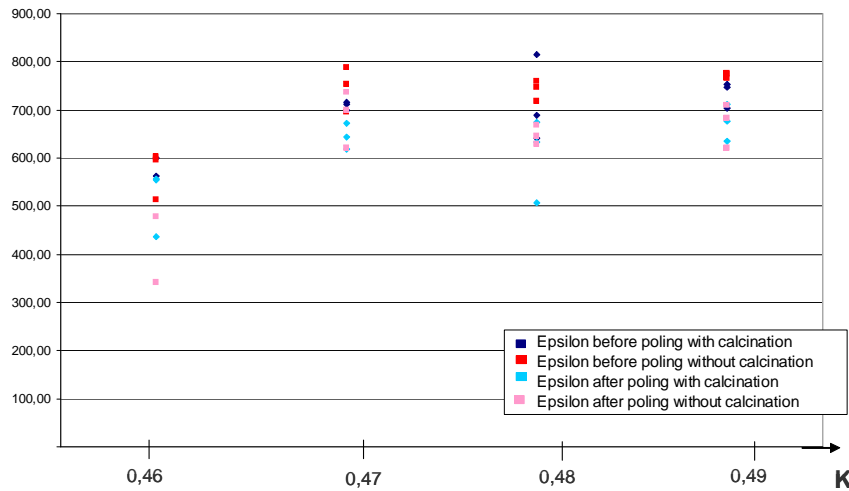

Fig. 36: epsilon before and after poling for samples with and without calcination

The aim of the next library was to find the MPB for a broad K/Na variation. A maximum is found around K:Na=0.45:0.55, where the MPB is normally positionned. It was found with a measurement called TkC (see Fig. 37). The TkC measurement is not a conventional one. To measure TkC ε is recorded at discrete temperatures between 20 and 80 ℃. At these temperatures ε varies linearly and the values of the slopes are recorded for each material. The Tkc is the slope of the ε curve around room temperature. If the material endures a phase transformation the ε doest not suffer a linear variation and it will give a significant change of the slope. This measurement is perfectly adapted to find the MPB as the boundary will be indicated with a peak or a deep in the value of the significant change of the slope. No measurements were available for samples containing 0.65 and 0.7 potassium as no measurable sample could be produced. Fig. 37 shows the change of slope around K/Na~0.8, i.e. K:Na=0.45:0.55, value in accordance with the values of the literature for the MPB of the Li, Ta and Sb modified KNN[5].

The second library was prepared to study the influence of lithium and antimony on the KNN doped with tantalum. Fig. 38 a, b and c show the results of the electric and piezoelectric measurements. The variation was not linear as both Li and Sb content were simultaneously changed. Eight compositions were selected where the ratio K/Na stays constant as well as the tantalum doping. Lithium and antimony were varied as followed: Li und Sb= 4, 8 and 12%. The effects of both dopings were evaluated.
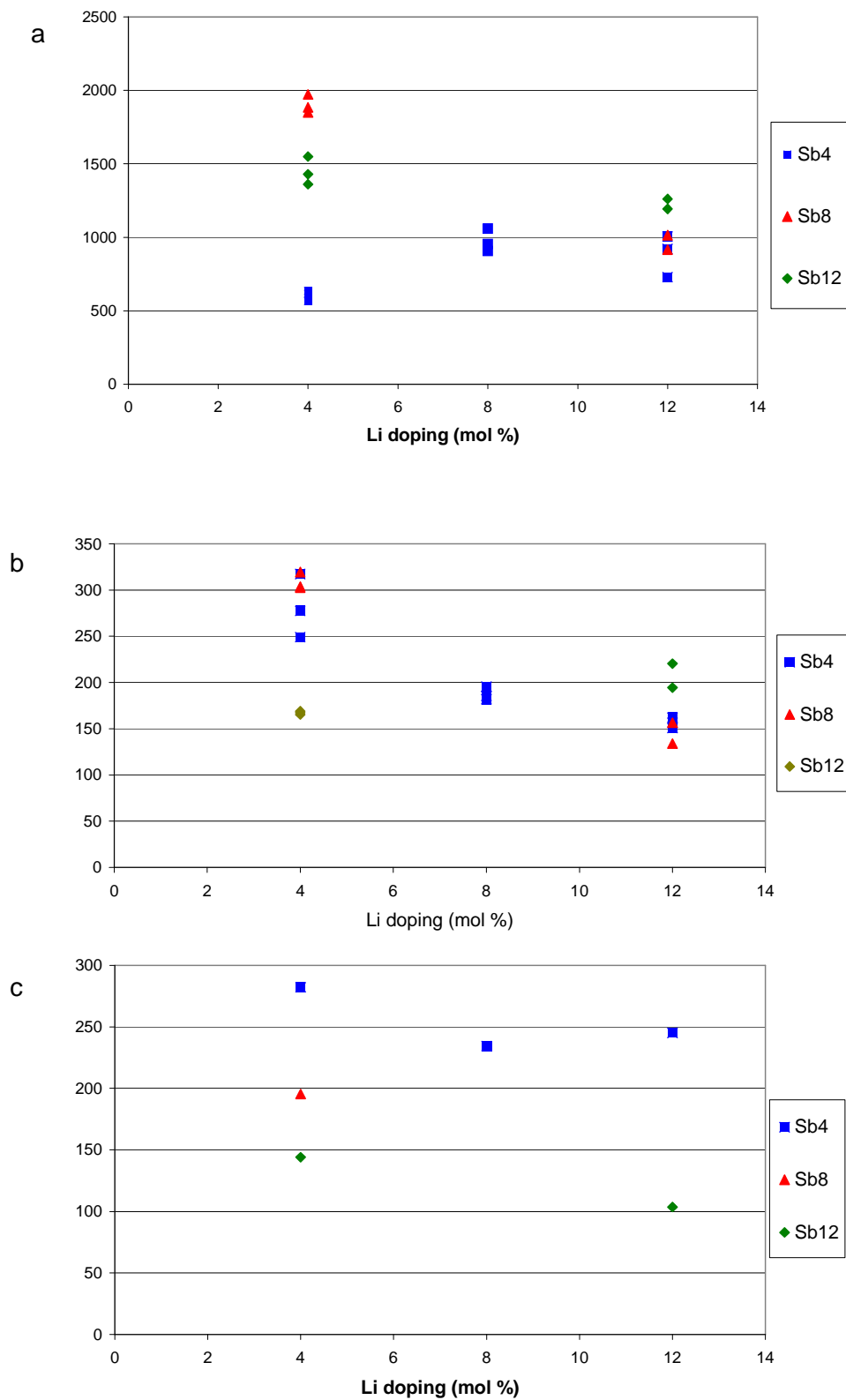
Fig. 37 a, b and c: dielectric measurement of $[Li_x(K_{.5}Na_{.5})_{1-x}](Nb_{.9-y}Ta_{.1}Sb_y)O_3$

The values of ε are optimal for 4% Li doping and 8% Sb doping, the increase of doping lowers the ε values. d_{33}^* is higher for 4% Li doping and 4 and 8% Sb doping. The increase in doping lowers the d_{33}^* values as the doping makes the MPB move. The highest d_{33}^* value reached is 300 pm/V which corresponds to the value cited in the references[1]. The Curie temperature is the highest for the sample having less doping as it is the case for PZT[142]. All the results are in accordance with the results given in the patent application[134].
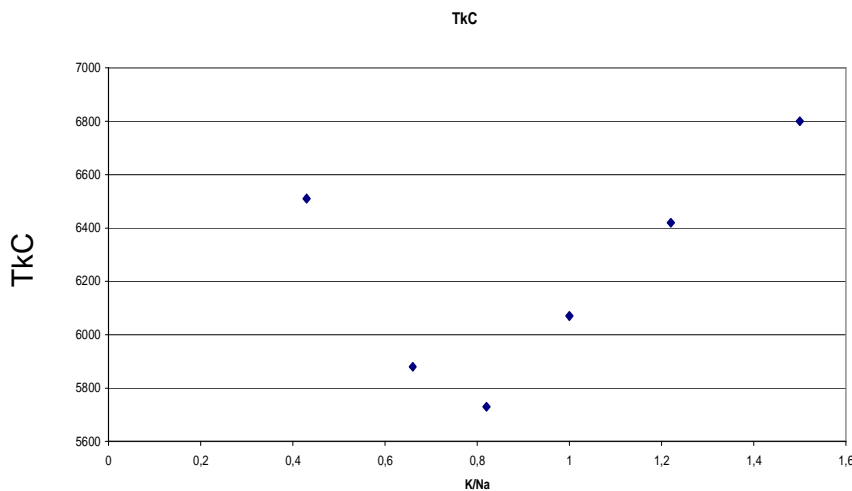

Fig. 38 : Tkc measurement for different K/Na variation

5. *Conclusion*

The developed preparation method was tested on a lead-free system. Some modifications had to be done as for example the use of specific precursors and the insertion of a new step in the workflow. The use of precursors was inevitable to obtain quickly high quality KNN samples despite a rapid preparation. Normally the use of precursors prevents a high flexibility in the compositions because they have a fixed stochiometry. The precursors employed in the case of KNN are generally stoichiometric $KNbO_3$ or $NaNbO_3$ which have the same stochiometry as the KNN therefore, the flexibility is guaranteed.

The calcination step helped to obtain pure phase perovskite samples. Nevertheless the KNN samples show a high stability despite the few disturbances due to external phases. However to reduce potential problems, the calcination step before sintering has been maintained during the rest of the studies as it is not very time consuming.

The MPB of a KNN-based system could be found through dielectric measurements. The dielectric values of the samples prepared with the HTE method were in accordance with those of the literature. The influence of doping elements like lithium and antimony could be clearly identified, they improve the ε and $d_{33}{}^{*}$ values but at the same time they lower the Curie temperature.

The method shows satisfying results on this KNN-based system and can now be used conventionally to discover new KNN-based compositions which are the most promising lead-free piezoelectric materials.

VII. New Potassium-Sodium-Niobate based Materials

1. Potassium-Sodium-Niobate doped with liquid phase inductive elements

a. Theory

One of the principal problems of KNN is its difficulty to densify due to high volatilisation of sodium and potassium at high temperatures[143]. To improve the densification, alternative sintering methods such as spark plasma sintering, hot pressing or hot isostatic pressing are often considered[144,145]. However it is of interest to sinter KNN under normal atmospheric conditions for industrial processing. Different routes can be used, among them, the addition of sintering aids is one of the most cost effective. One of the first elements used to induce a liquid phase sintering was the copper by Matsubara *et al.*[146]. The insertion of copper into KNN forms a copper potassium niobium compound $K_4CuNb_8O_{23}$ (KCN) and into Ta-doped KNN a copper potassium tantalum compound $K_{5.4}Cu_{1.3}Ta_{10}O_{29}$, (KCT) is generated. Both compounds act as a sintering aid and fill the pores into KNN thus, the material obtained is denser and the dielectric and piezoelectric properties are superior. Only a few copper is needed to obtain better values than those of KNN without sinter help (0.38 mol% of sintering aid KCT achieve an optimal density). The maximal d_{33} reported of KNN doped with KCT is 190 pm/V under an electrical field of 4 kV/mm.

b. Experimental (Part I)

A first library was realised with different copper contents (added as copper oxide) to evaluate the reproduction of the results reported by Matsubara *et al.*[154]. In another

library different cations (tungsten, germanium and gallium) were introduced together with copper to produce a co-doping.

c. Results (Part I)

As shown in Fig. 39 XRD analysis was performed on the copper-doped KNN. Traces of metallic copper are visible (light blue peaks).
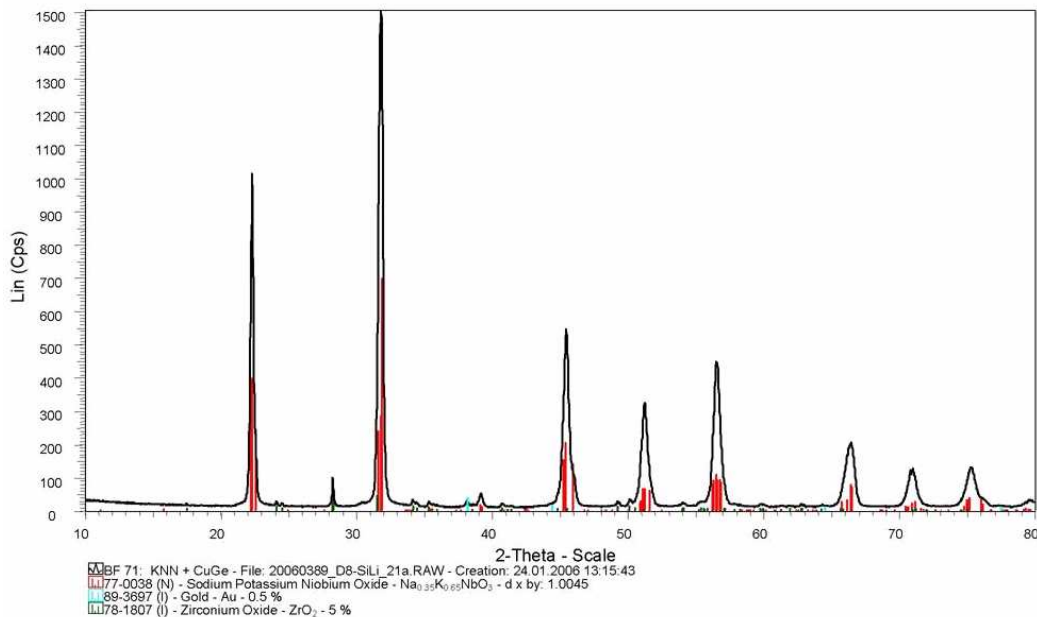

Fig. 39: XRD-Pattern of 0.95 (K$_{0.5}$Na$_{0.5}$) NbO$_3$ - 0.05 CuO

The results of the dielectric measurements and the piezoelectric coefficient d$_{33}^{*}$ of both libraries are visible in Fig. 40 and in Fig. 41. On these plots the copper content is diagrammed on the x-axis and the different colours represent different cations for the co-doping. The black points represent the values of the samples doped only with copper; the red, grey and green points represent respectively the values of the samples additionally doped with tungsten, germanium and gallium.

A microstructure examination and X-ray mapping were carried out on Cu-Ge-doped KNN (see Fig. 42). The mapping (figure on the right hand side) shows the distribution of the germanium in the ceramics. On the left-hand side figure, border of grains are easily recognisable (highlighted in white for more clarity), between the grains, the mapping shows the presence of the germanium. Therefore it seems that the germanium is not built into the ceramic, but is present between the grains, possibly forming a liquid phase sintering.
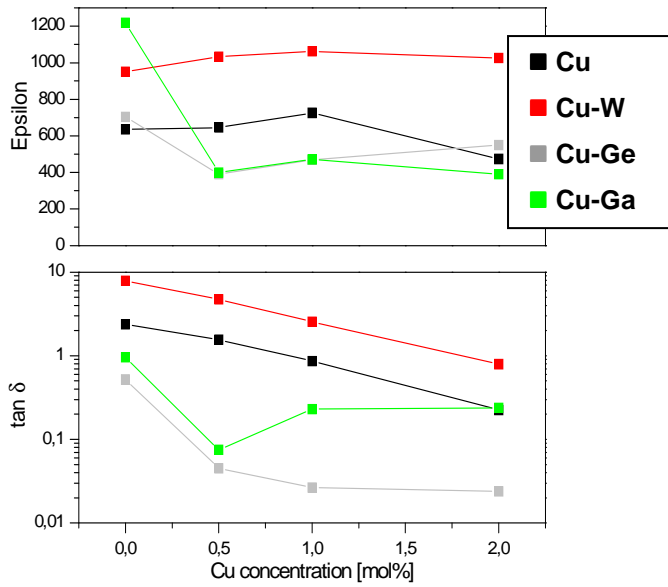
Fig. 40: dielectric properties of 1-x (K$_{0.5}$Na$_{0.5}$)Nb- x CuX samples with different doping (X=W, Ge or Ga)
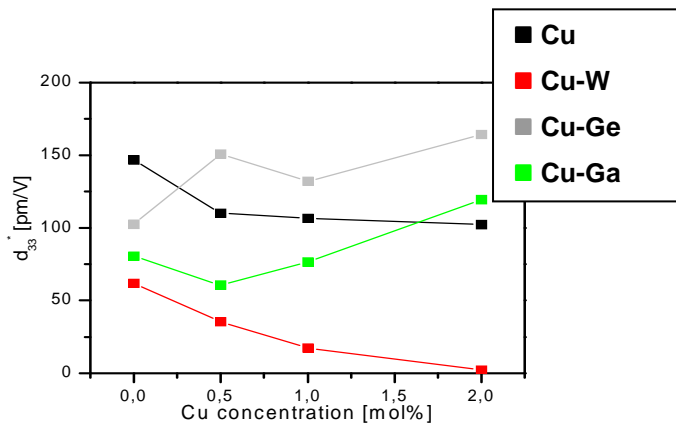

Fig. 41: d$_{33}$* of of 1-x (K$_{0.5}$Na$_{0.5}$)Nb- x CuX samples with different doping (X=W, Ge or Ga)
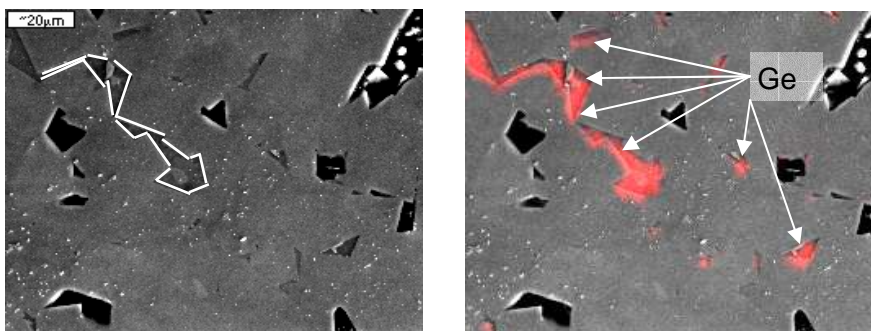

Fig. 42:   SEM micrograph of 0.98 (K$_{0.5}$Na$_{0.5}$) NbO$_3$- 0.02 (CuO-GeO2) and germanium distribution analysis

d. Discussion (Part I)

The dielectric losses of the KNN samples doped with copper oxide (CuO) are extremely high, which is often the sign of a high conductivity. Different hypothesis could explain it:

- Copper which will not form KCN is inserted in A-sites and is considered as a donor; in this case the conductivity can be caused by a deficiency in electrons to respect the stochiometry of the material

- Copper, which will not form KCN, is inserted in B-sites and is an acceptor, in this case the conductivity can be caused by an excess of electrons in the material respectively to the stochiometry

- KCN or KCT phases formed are conductive, a hypothesis which could explain why the amount of 0.38 mol% achieves optimal properties

To consider the insertion of an ion in the perovskite structure two aspects have to be considered: the size and the coordinate.

In a perovskite the A-sites are 12-coordinate and the B-site are 6-coordinate[11]. The copper is quite small to enter in an A-site and the higher coordination number makes it difficult to enter in an A-site therefore its insertion in a B-site seems to be more probable. The third hypothesis was also not considered as any traces of KCN or KCT could be detected by XRD analysis which proves that the amount of secondary phase was not significant enough.

To try to reduce the dielectric losses of the materials a co-doping was realised in the same manner as done with PZT[147]; i.e. an acceptor or donator ion is inserted in the structure. To compensate the insertion of an A-site acceptor is not possible as the A-site has a valence of one, then the compensation will be done in B-site with ions having a valence of four or less. The chosen ions are gallium, germanium and tungsten as their ionic radius fit the niobium radius. The conductivity of the copper doped samples lowers with the addition of these doping elements, i.e. the tan δ is lower. However, the effect of the germanium is more important than those of other elements as the

dielectric losses of the copper-germanium doped samples is low as it can be seen in
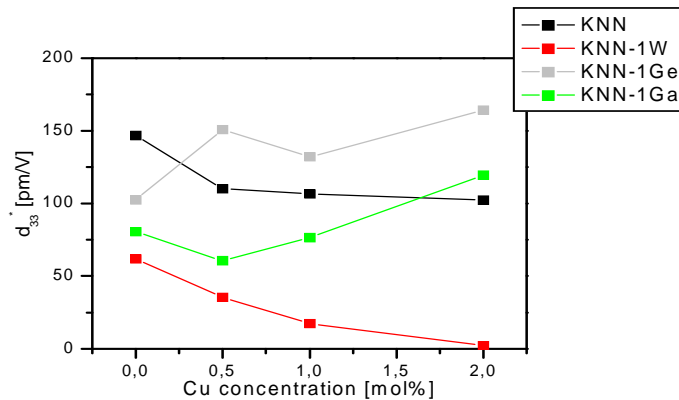

Fig. 41.

The d_{33}^* is improved as it can be properly measured due to the low level of current passing through the sample during the measurement. In further libraries an optimal copper and germanium content will be investigated as well as an optimal sodium to potassium ratio.

e. Experimental (Part II)

The d_{33}^* value can be improved with an adjustment of the Cu/Ge and K/Na ratios. First the optimal doping in Cu and Ge was searched then the ratio K/Na was investigated. The content in Cu and Ge was varied between 0 and 5% for the following formula $(K_{0.5}Na_{0.5})_{1-y}Cu_yNb_{1-x}Ge_xO_3$ as in Table 7.

Table 7: Doping rate of copper and germanium

Sample Nr	1	2	3	4	5	6	7	8
y	0.02	0	0.01	0.01	0.005	0	0	0
x	0	0.01	0.02	0.01	0	0.02	0.01	0.005

The further investigation on this material system concerns the K/Na ratio. The MPB of KNN can move with the addition of doping elements[148] and the adjustment of the Na/K ratio should provide better performances. However, since it is known that the MPB is situated around K/Na=0.5/0.5 the research zone is narrow and the sodium content was varied between 0.42 and 0.56 with 2% increment.

f. Results (Part II)
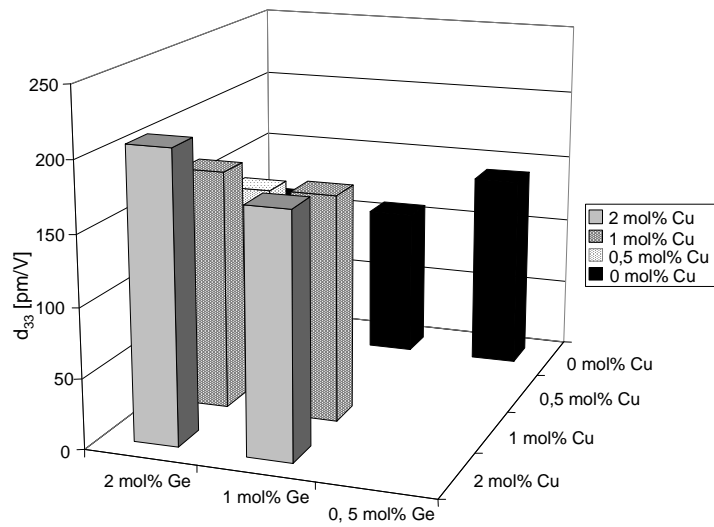
Fig. 43: d_{33}^{*} of $(K_{.5}Na_{.5})_{1-y}Cu_y Nb_{1-x}Ge_x O_3$

The values of the large piezoelectric signals of $(K_{0.5}Na_{0.5})_{1-y}Cu_yNb_{1-x}Ge_xO_3$ are
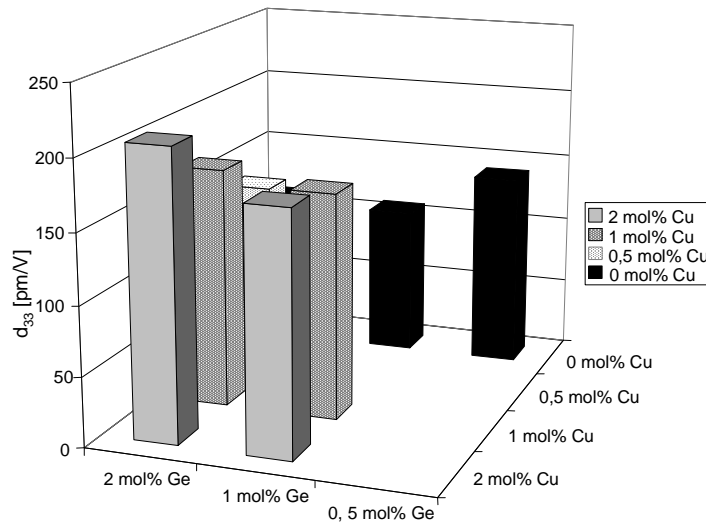
presented in

Fig. 43.

Fig. 44 shows the dielectric measurement for $(K_{0.5}Na_{0.5})_{0.98}Cu_{0.02}Nb_{0.98}Ge_{0.02}O_3$ having suffered 3 different sintering temperatures. The red lines show the sample sintered at 1050°C, the green ones at 1100°C and the blue ones at 1150°C.
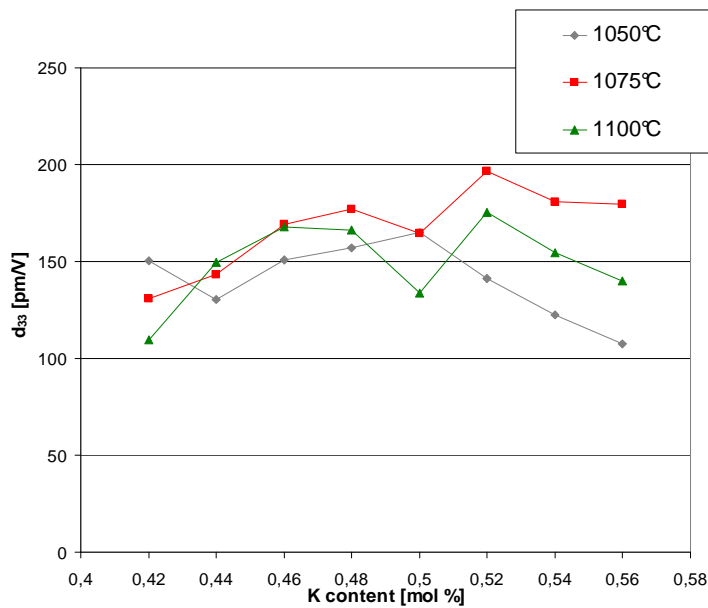
Fig. 44: dielectric and piezoelectric measurements of $(K_xNa_{1-x})_{.99}Cu_{.01} Nb_{.99}Ge_{.01} O_3$

g. Discussion (Part II)

It is though that copper and germanuim doping will not affect the place of the MPB because they are not built in the perovskite structure, therefore the optimum in copper and germanium doping can be searched independently of one another.

The first dielectric measurements carried out were surprising as the dielectric losses were high despite of the previous measurements where the losses were very low and the dielectric losses of this experimental series were independent of sintering temperature and composition. The difference between the sintering of the first library and this one was the sintering support employed (Pt-foil or Nb_2O_5-powder). The sintering on a Pt-foil was preferred since it acts as a diffusion barrier during sintering, however the samples sintered on the Pt-foil show high dielectric losses, therefore, it was though that the diffusion of niobium within the sample was the key processing parameter to achieve high quality samples. The tan δ of the sample sintered on the platinum foil reached values between 0.1 and 1 and with the Nb_2O_5-powder bed the values of tan δ drop to less than 0.03. Then d_{33}^* and ε_r can be properly measured. As shown in the doping with 2 mol% Cu and 2 mol% Ge gives the best results for this library with d_{33}^* reaching 200 pm/V. The values of d_{33}^* are lower than the values previously measured. This alteration can be attributed to a difficult processing of KNN.

h. Conclusion

The dielectric values measured on the samples from the second library were different to the values of the first library. Normally the higher the sintering temperature, the denser is the ceramic. In this case the values of the material sintered at higher temperature are lower than the values of the samples sintered at lower temperature. In the case of KNN too high temperatures damage the performance of the material due to the evaporation of sodium and/or potassium, resulting in an unstoichiometry of the material creating secondary phases which reduce the material performances.

Samples having a content in sodium around 52% and sintered at 1075°C show the highest values for d_{33}^* of almost 200 pm/V.

During the upscaling problems were met concerning the production of the samples and the properties measured during the HTE phase could not be reproduced. Therefore, a deeper investigation of the material will not be continued.

For the KNN system this investigation shows that the formation of a liquid phase sintering improves the performances (up to two times) but another strategy should be investigated to increase the performances to a level comparable to those of PZT.

2. KNN and Tungsten-Bronze

a. Theory

In a previous section the results of a composition patented by Toyota-Denso were used as material system to test this HTE processing route to KNN-based ceramics. Satisfying dielectric properties could be measured on samples having not a pure phase perovskite but a mix of 4% of tungsten-bronze and 96% of perovskite phases. The material showed the following properties: $\varepsilon_{r\ max}$ = 1247, tan δ = 0.02, $d_{33}^*{}_{max}$ = 400 pm/V and T_C = 281°C. These properties are better than those given in the patent application.

On the other hand a patent application from TDK Company was published[149] claiming that the properties of KNN doped with lithium, tantalum, zinc, magnesium and $BaNb_2O_6$ (member of the tungsten-bronze family) are definitively higher than those known up to now. They measured a d_{33} up to 436 pC/N for the following formula: 0,995

$(K_{.38}Na_{.57}Li_{.05})$ $(Nb_{.9}Ta_{.1})$ − 0,005 $BaNb_2O_6$ + 0,31 wt.% of KNN MnO +0,05 wt.% of KNN ZnO.

Seeing those two examples, it was thought that the addition of tungsten-bronze (TB) to KNN can improve its properties.

In order to screen the interaction between TB and KNN, three different TB were considered with different properties as shown in Table 8

SBN has a high ε_r and d_{33} whereas its Curie temperature is quite low, BNN has a high Curie temperature but low ε_r and d_{33}, and SCNN has medium values for all its properties.

Table 8: properties of different TB used

Formula	Abb.	ε Polycrystal	d_{33} Polycristal	ε Moncrystal	d_{33} Monocrystal	Tc ℃
$Sr_{.75}Ba_{.25}Nb_2O_6$	SBN	550		3000	670	56
$Ba_2NaNb_5O_{15}$	BNN	≈ 100		47	20	560
$Sr_{1.85}Ca_{0.15}NaNb_5O_{15}$	SCNN	≈ 1600	100	1740	270	270

b. Previous investigation

It has been shown in the last years that successful sodium-potassium niobate lead-free piezoelectric ceramics contain lithium and tantalum[150,151], therefore an investigation was carried out to find the optimal Li and Ta doping of a simple KNN which will be used as starting material for further TB doping.

i) Experimental

$KNbO_3$, $NaNbO_3$, $KTaO_3$ and Li_2CO_3 were dosed to obtain the following compositions: $[(K_{1-x}Na_x)_{0.96}Li_{0.04}](Nb_{0.96}Ta_{0.04})O_3$ with $0.5 \leq x \leq 0.57$. The doping of 4% $LiTaO_3$ was chosen according to the literature[152] which indicates that more than 4% $LiTaO_3$ induces a non perovskite phase near pure phase KNN. The K/Na ratio was varied to find a

suitable starting composition and ballast sintering was tried to impeach the volatilisation of the alkalis.

ii) Results

The microstructure was studied by means of SEM after polishing of the surface and thermal etching (see Fig. 45). The structure of KNN is easily recognizable with square grains and other grains showing an abnormal grain growth.
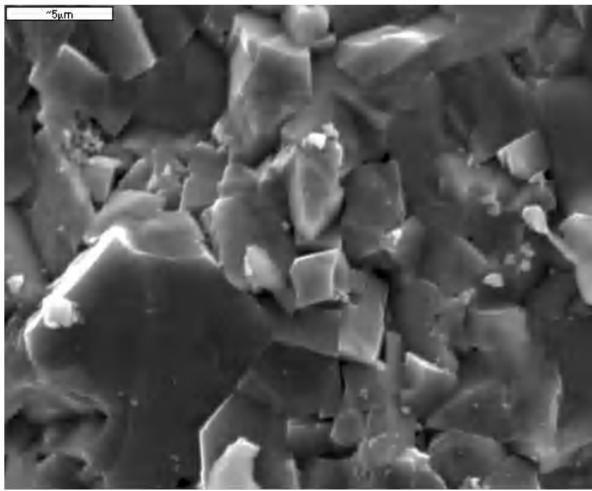

Fig. 45: microstructure of $(Li_{0.04}K_{0.47}Na_{0.53})(Nb_{0.96}Ta_{0.04})O_3$

The values of tan δ are shown in Fig. 46. The other dielectric values are not relevant as the dielectric losses are too high. Only the samples having a sodium rate between 52 and 55 mol% could be measured because the dielectric losses were not too high. The samples with a sodium rate below 52 mol% and above 55 mol% showed short circuit during the measurement of d_{33}^{*}.
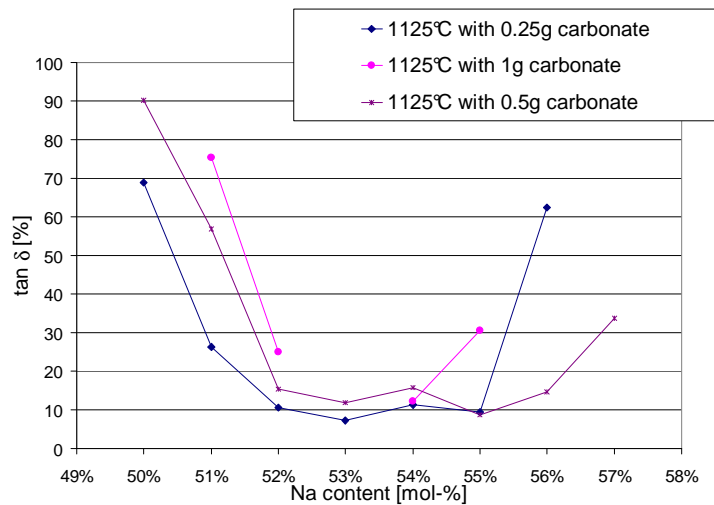
Fig. 46: tan δ of (K$_{1-x}$Na$_x$)$_{.96}$Li$_{.04}$ Nb$_{.96}$Ta$_{.04}$ O$_3$

iii) Discussion

Lithium and tantalum are both inserted in the KNN structure as their sizes and properties are similar to the sizes and properties of sodium, potassium and niobium and so they affect the place of the MPB on a phase composition diagram[153]. The presence of the MPB was detected for 4 mol% LiTaO$_3$ in the literature but for a K/Na ratio of 0.5/0.5. For this library it could be observed that the losses were lower in the region of 52 to 54 mol% sodium for all sintering processing which indicates a better stability of the samples. The change of optimal composition range can be attributed to the use of sodium and potassium precursors on one hand but also to the preparation mode on the other hand. Second phases may be present in the raw materials which impacts the properties of the material employed and the accelerated preparation mode does not lead to a pure phase perovskite material.

The most favourable sintering is carried out with 0.25g of sodium-, potassium- and lithium-carbonate in the sintering boat. The addition of these carbonates allows the saturation of the sintering atmosphere in the boat and so the evaporation of sodium, potassium and lithium is reduced. On the other hand too high amounts of these carbonates disturb the stoichiometry of the samples leading to the creation of external phases. So the dielectric losses of the samples sintered with 1g carbonates in the boat were too high and it did not allow the proper measurement of the rest of the properties. The samples sintered with 0.5g carbonates present higher losses than the samples sintered with 0.25g carbonates.

c. Strontium-Calcium-Sodium-Niobate

Ceramics from the system (1-x) $Sr_2NaNb_5O_{15}$-x $Ca_2NaNb_5O_{15}$ (SCNNx) were investigated as lead-free piezoelectric ceramics due to their interesting properties. The properties of SCNN15 as polycrystalline material were already investigated by Xie *et al.* and they measured superior properties for d_{33} and ε[154].

i) Experimental

The SCNN15 was prepared from Sr-, Ca-, Na_2- CO_3 and Nb_2O_5 powders. The powders were grinded together 18h in a PVC cup with alcohol as cooling medium, dried and used as a precursor for a binary library. The doping of LKNNT with SCNN15 was as follows: 0.5, 1, 1.5, 2, 2.5, 3, 4 and 5 mol%.

ii) Results

The first measured property is ε_r (see Fig. 47). The dielectric constant varies not linearly with the SCNN15 content. With the increasing of the doping level the values first decrease and then increase from 1.5 mol% doping.
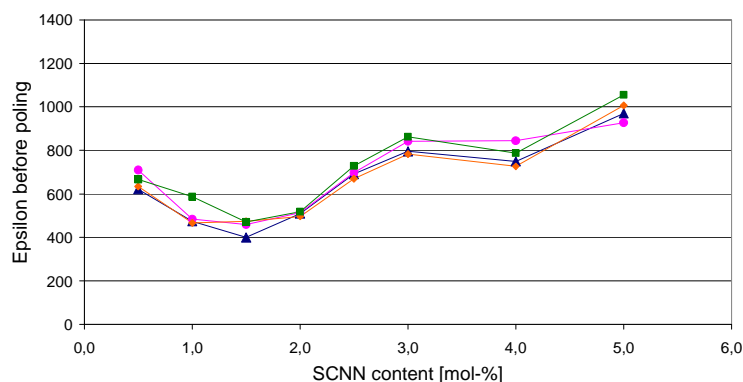
Fig. 47: Epsilon before poling for 1-X [Li$_{.04}$(Na$_{.53}$K$_{.47}$)$_{.96}$](Nb$_{.96}$Ta$_{.04}$)O$_3$-X Sr$_{1.85}$Ca$_{.15}$NaNb$_5$O$_{15}$

The measurement of d_{33} is shown in Fig. 48. Between 0.5 and 4 mol% SCNN15 doping the tendency is the same for ε_r and d_{33}^* but for the sample doped with 4 and 5 mol% SCNN15 the value of ε increases whereas the value of d_{33}^* decreases.
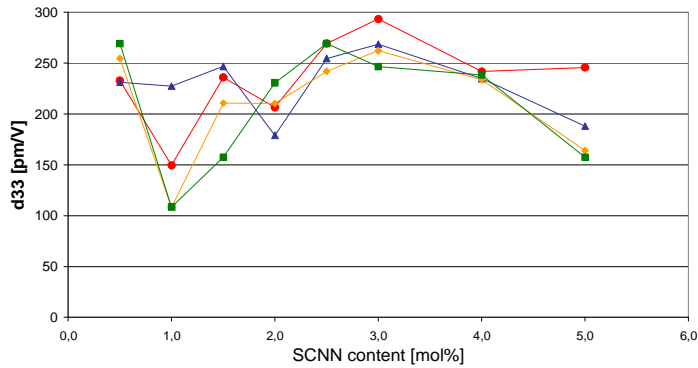

Fig. 48: d_{33}^* at 2kV/mm of 1-X [Li$_{.04}$(Na$_{.53}$K$_{.47}$)$_{.96}$](Nb$_{.96}$Ta$_{.04}$)O$_3$-X Sr$_{1.85}$Ca$_{.15}$NaNb$_5$O$_{15}$

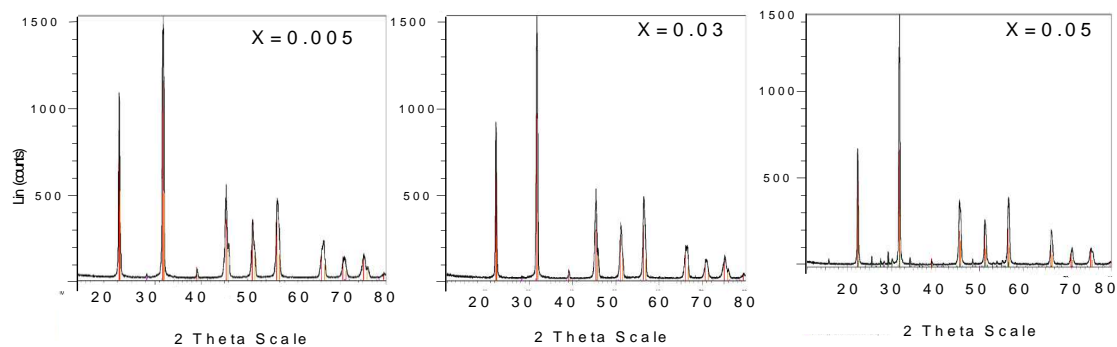To investigate the phases present in the samples XRD analysis was carried out (see Fig. 49).

Fig. 49: X-ray pattern of 1-x [(K$_{0.47}$Na$_{0.53}$)$_{0.96}$Li$_{0.04}$](Nb$_{0.96}$Ta$_{0.04}$)O$_3$ - x Sr$_{1.85}$Ca$_{0.15}$NaNb$_5$O$_{15}$

Fig. 50 shows micrograph of samples doped with different concentration of SCNN15 and the evolution of the main crystallite size is reported in
Fig. 51. It is easy to see from the Fig. 50 the influence of the doping, the shape and size of grains of different samples being rather different the one to the others. With 0.5 mol% SCNN doping the microstructure remains almost the same as without doping, the main crystallite size decreases up to 2mol% SCNN, reaches a maximum for 3 mol% SCNN and then decreases again. The curve of the main crystallite size is comparable to the curve of d_{33}^*.

The last property to be routinely measured is the Curie temperature (Fig. 53). The sample 0.995 [Li$_{0.04}$ (Na$_{0.53}$K$_{0.47}$)$_{0.96}$](Nb$_{0.96}$Ta$_{0.04}$)O$_3$-0.005 Sr$_{0.85}$Ca$_{0.15}$NaNb$_5$O$_{15}$, whose

measurement is represented by the black line shows a peak around 280°C which can be associated to the Curie temperature. For samples containing higher doping the behaviour is quite different: the samples containing 1 and 3 mol% SCNN15 show two little peaks and the samples containing 4 and 5 mol% do not show any peak.
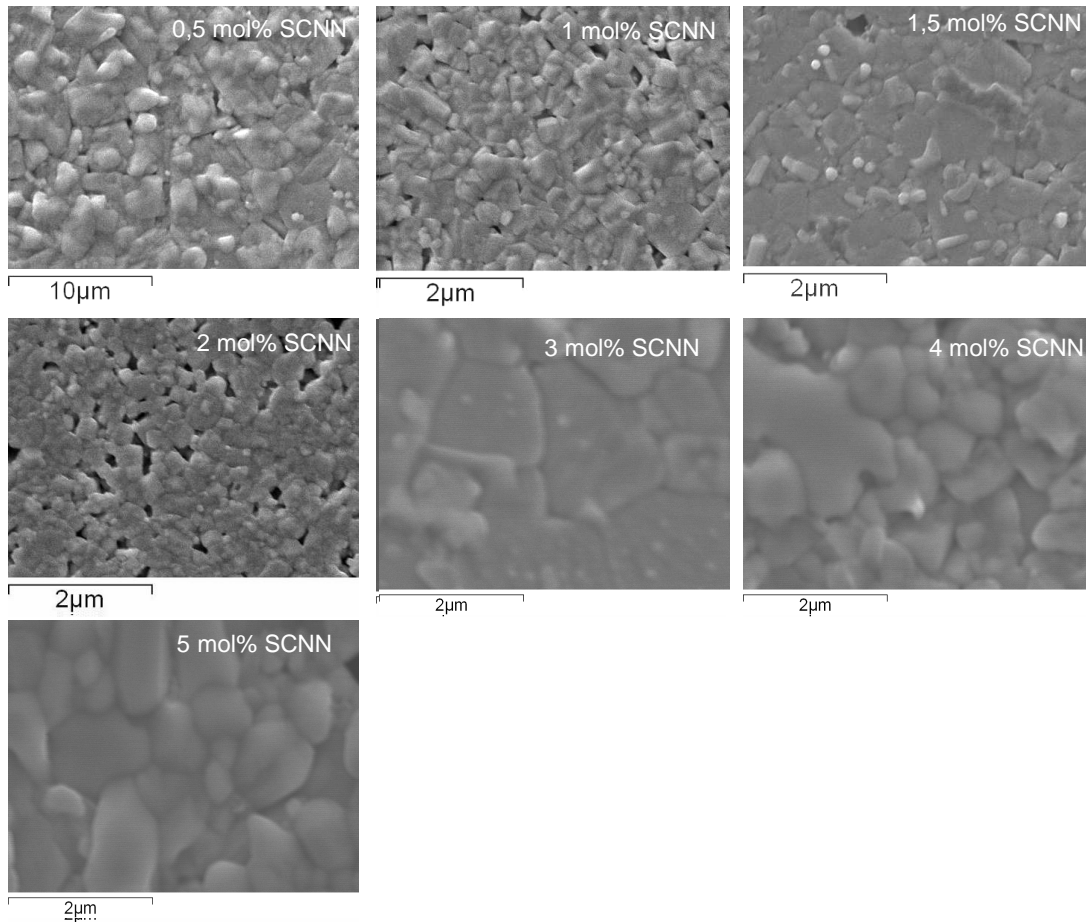
Fig. 50: microstructrure evolution of 1-x [Li$_{.04}$(Na$_{.53}$K$_{.47}$)$_{.96}$](Nb$_{.96}$Ta$_{.04}$)O$_3$-X Sr$_{1.85}$Ca$_{.15}$NaNb$_5$O$_{15}$
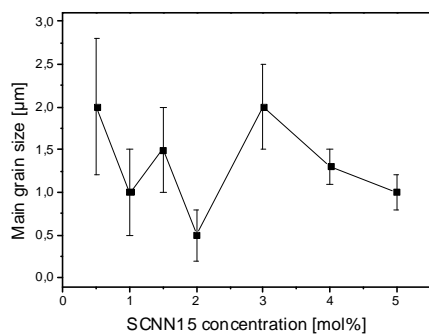
Fig. 51: Main crystallite diameter in dependence of SCNN15 concentration

To investigate the phase transformations high temperature XRD was carried out on one sample having the composition $0.97 [Li_{0.04}(Na_{0.53}K_{0.47})_{0.96}](Nb_{0.96}Ta_{0.04})O_3$-$0.03 Sr_{0.85}Ca_{0.15}NaNb_5O_{15}$.

Fig. 52 displays a general overview of the reflexes obtained between room temperature and 400℃; Fig. 54 shows the repartition of the peaks intensity for 2θ between 44.5 and 46.5° which are the reflex of (002) in function of the temperature during heating and cooling.
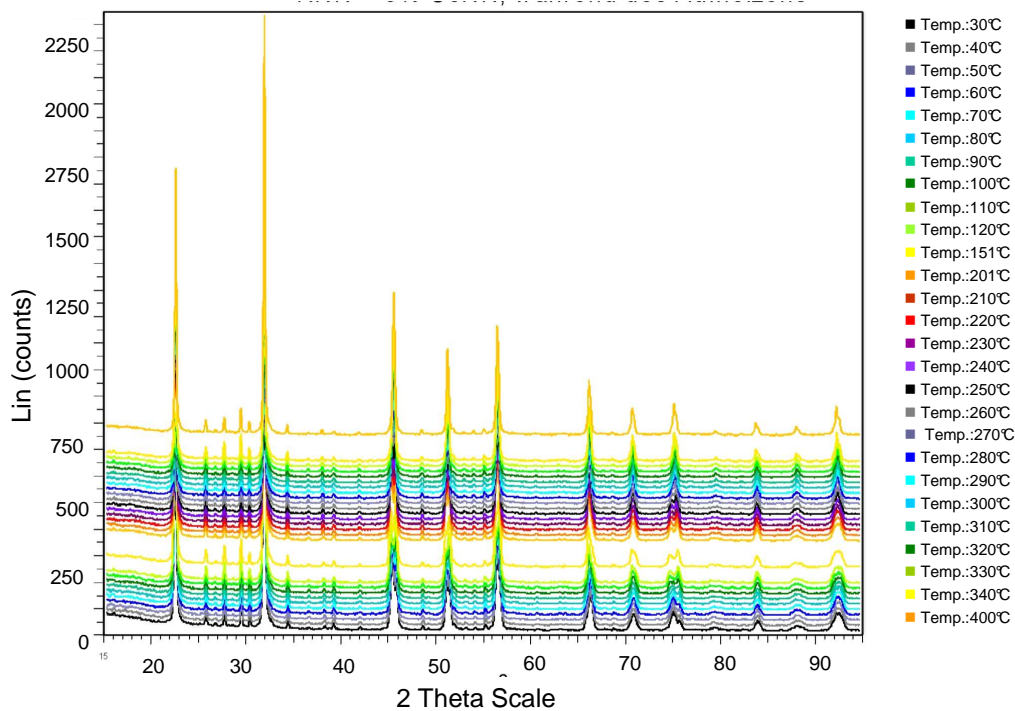
Fig. 52: X-ray pattern of 0.97 [Li$_{.04}$(Na$_{.53}$K$_{.47}$)$_{.96}$](Nb$_{.96}$Ta$_{.04}$)O$_3$-0.03 Sr$_{.85}$Ca$_{.15}$NaNb$_5$O$_{15}$ during heating up to 400℃
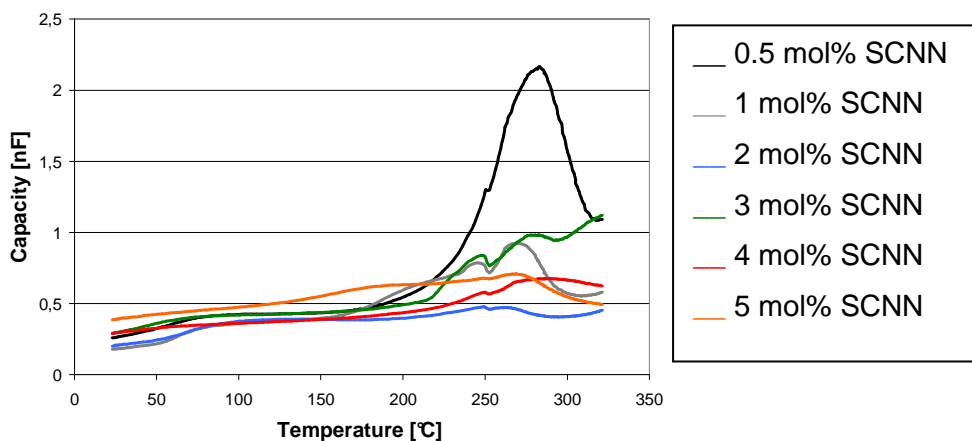
Fig. 53: capacitance vs. temperature of 1-x [Li$_{.04}$(Na$_{.53}$K$_{.47}$)$_{.96}$](Nb$_{.96}$Ta$_{.04}$)O$_3$-X Sr$_{.85}$Ca$_{.15}$NaNb$_5$O$_{15}$
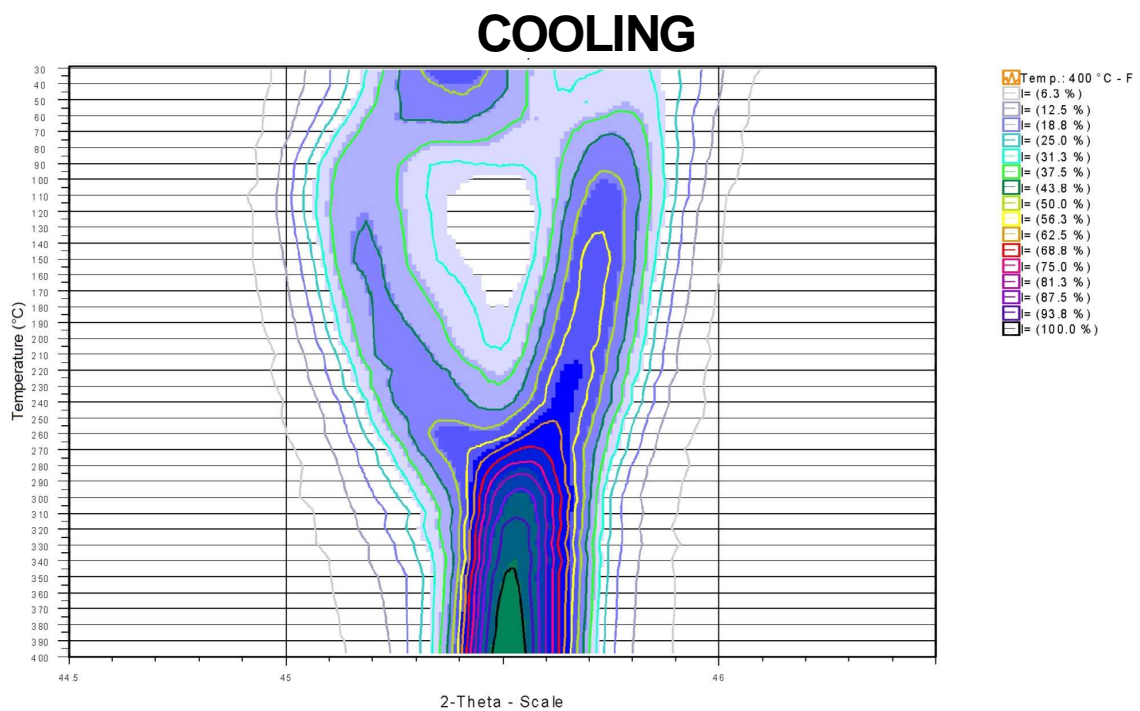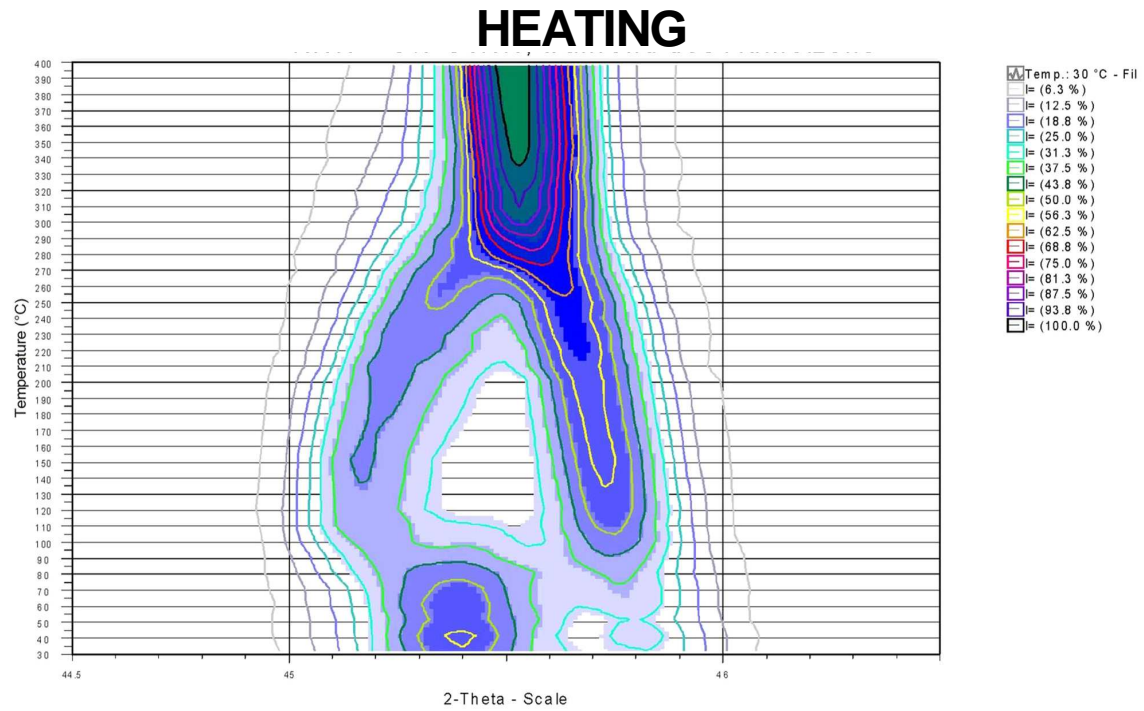
Fig. 54: high temperature diagram of XRD-reflexes at 2θ=44.5-46.5 for 0.97 [Li$_{.04}$(Na$_{.53}$K$_{.47}$)$_{.96}$](Nb$_{.96}$Ta$_{.04}$)O$_3$-0.03 Sr$_{.85}$Ca$_{.15}$NaNb$_5$O$_{15}$ during heating and cooling of the sample

A DSC measurement was carried out on the calcined sample and on the sintered sample (see Fig. 55) to complete the high temperature XRD patterns.
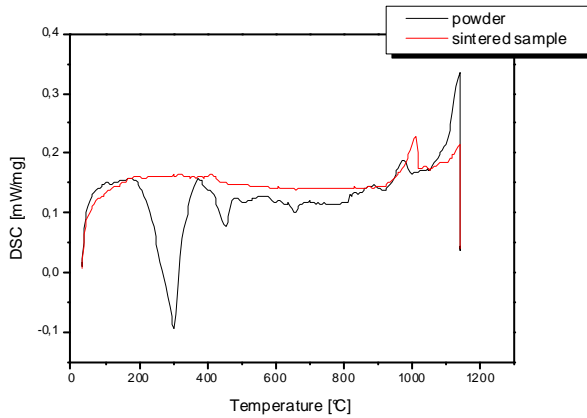
Fig. 55: differential scanning calorimetry of 0.97 [(K$_{0.47}$Na$_{0.53}$)$_{0.96}$Li$_{0.04}$](Nb$_{0.96}$Ta$_{0.04}$)O$_3$ - 0.03 Sr$_{1.85}$Ca$_{0.15}$NaNb$_5$O$_{15}$

The black line represents the DSC curve of the powder after calcinations and the red line represents the DSC curve of a sintered sample. In this diagram an endothermic peak is visible around 300°C which is the signal of the Curie point. No other endo-other exothermic peak is visible for inferior temperatures.

d. Barium-Sodium-Niobate

The BNN is also a TB characterised by the occupancy of all A-sites whereas the C-sites are empty in the formula [(A1)$_2$(A2)$_4$C$_4$][(B1)$_2$(B2)$_8$]O$_{30}$. BNN is widely used as singe crystal as electro-optic and acousto-optic material and for optical frequency converters or generators[155].

i) Experimental

The BNN starting powder was conventionally prepared from BaCO$_3$, Na$_2$CO$_3$ and Nb$_2$O$_5$. A binary library was carried out mixing LKNNT and BNN.

The preparation of precursors allows the weighting of only two powders instead of 8 (KNbO$_3$, NaNbO$_3$, KTaO$_3$, BaCO$_3$, Na$_2$CO$_3$, K$_2$CO$_3$ and Nb$_2$O$_5$) thus accelerating the

preparation time. After the weighing of both powders, the binary library was handled as described in the section "method".

The library prepared included different levels of BNN doping into LKNNT: 0.5, 1, 1.5, 2, 2.5, 3, 4 and 5%.

ii) Results

The results for the measurement of the relative dielectric constant are shown in Fig. 56 and the piezoelectric constants are displayed in Fig. 57.
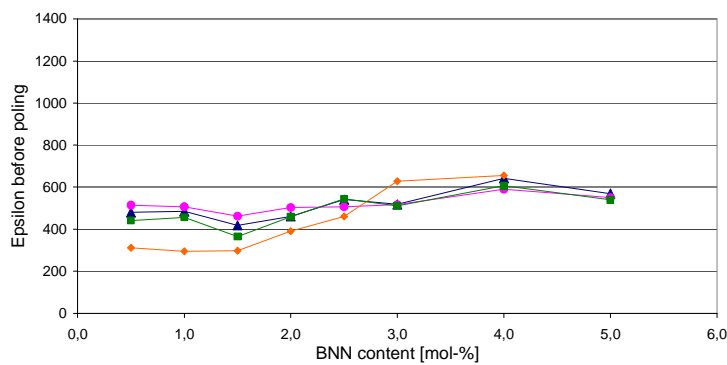
Fig. 56: Epsilon before poling of 1-X [Li$_{.04}$(Na$_{.53}$K$_{.47}$)$_{.96}$](Nb$_{.96}$Ta$_{.04}$)O$_3$-X Ba$_2$NaNb$_5$O$_{15}$
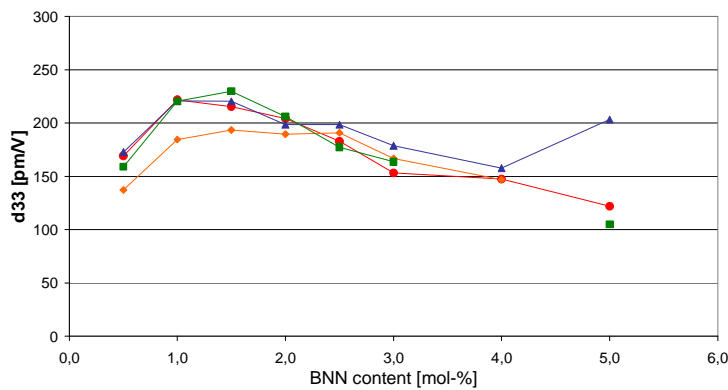
Fig. 57: d$_{33}$* at 2kV/mm of 1-X [Li$_{.04}$(Na$_{.53}$K$_{.47}$)$_{.96}$](Nb$_{.96}$Ta$_{.04}$)O$_3$-X Ba$_2$NaNb$_5$O$_{15}$
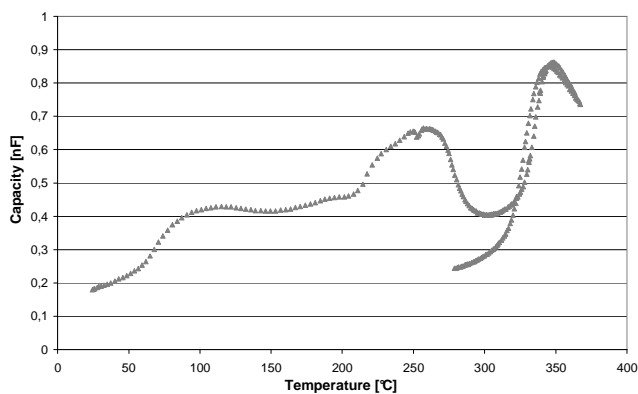
Fig. 58: capacitance vs. temperature for 98.5 $[Li_{0.04}(Na_{0.53}K_{0.47})_{0.96}](Nb_{0.96}Ta_{0.04})O_3$-1.5 $Ba_2NaNb_5O_{15}$

The study of the Curie temperature is focussed on a sample containing 1.5% of BNN, because this composition shows the best dielectric and piezoelectric properties. On the other hand, the behaviour of all samples during the measurement of the capacitance in function of the temperature was comparable.

The hysteresis effect between heating and cooling during the Curie temperature measurement was investigated by measuring the Curie temperature again on the same sample different laps of time after the first measurement (see Fig. 59).
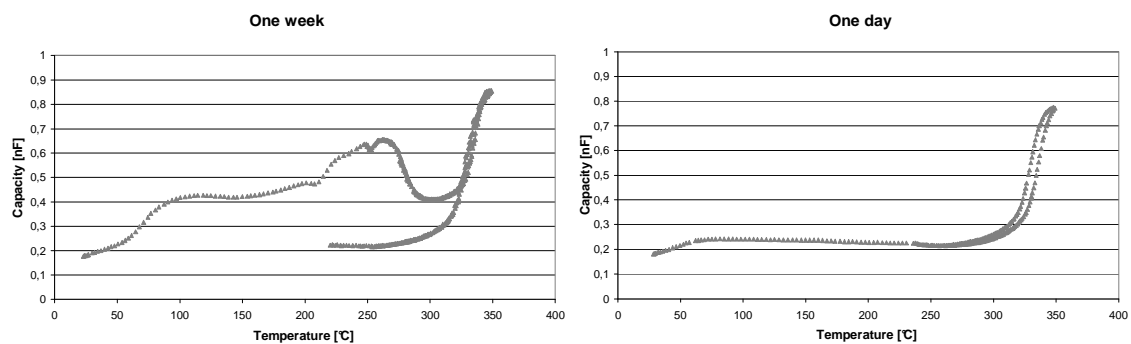
Fig. 59: capacitance vs. temperature for 98.5 $[Li_{0.04}(Na_{0.53}K_{0.47})_{0.96}](Nb_{0.96}Ta_{0.04})O_3$-1.5 $Ba_2NaNb_5O_{15}$ different period after the first measurement
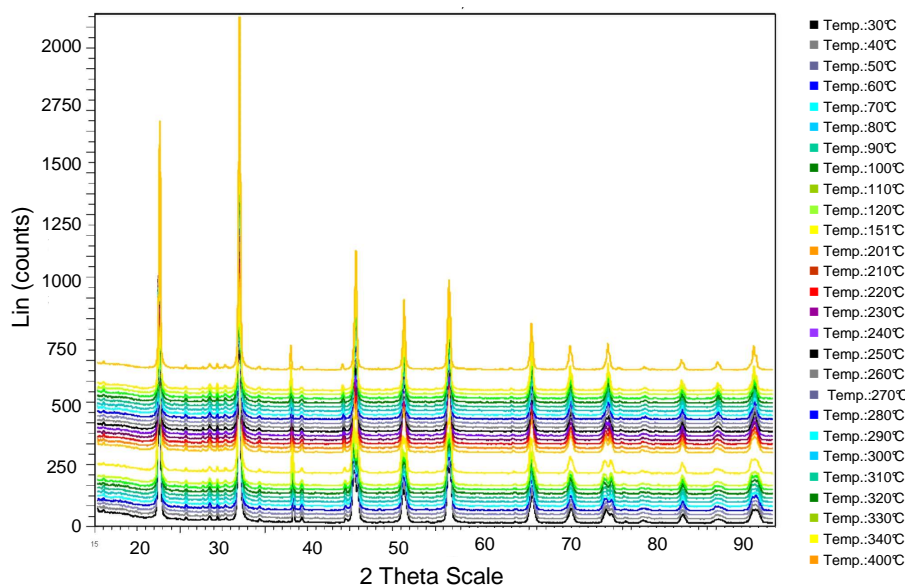
Fig. 60: high temperature X-ray pattern of 98.5 [Li$_{.04}$(Na$_{.53}$K$_{.47}$)$_{.96}$](Nb$_{.96}$Ta$_{.04}$)O$_3$-1.5 Ba$_2$NaNb$_5$O$_{15}$ between room temperature and 400°C

The investigation of the phase transformation in function of the temperature was carried out by high temperature XRD (up to 400°C) as it can be seen in Fig. 60. Fig. 61 shows the repartition of the peaks between 44.5°< 2θ < 46.5°.

Fig. 61 displays a repartition of the peaks between 2θ=44.5 and 46.5° in function of the temperature.
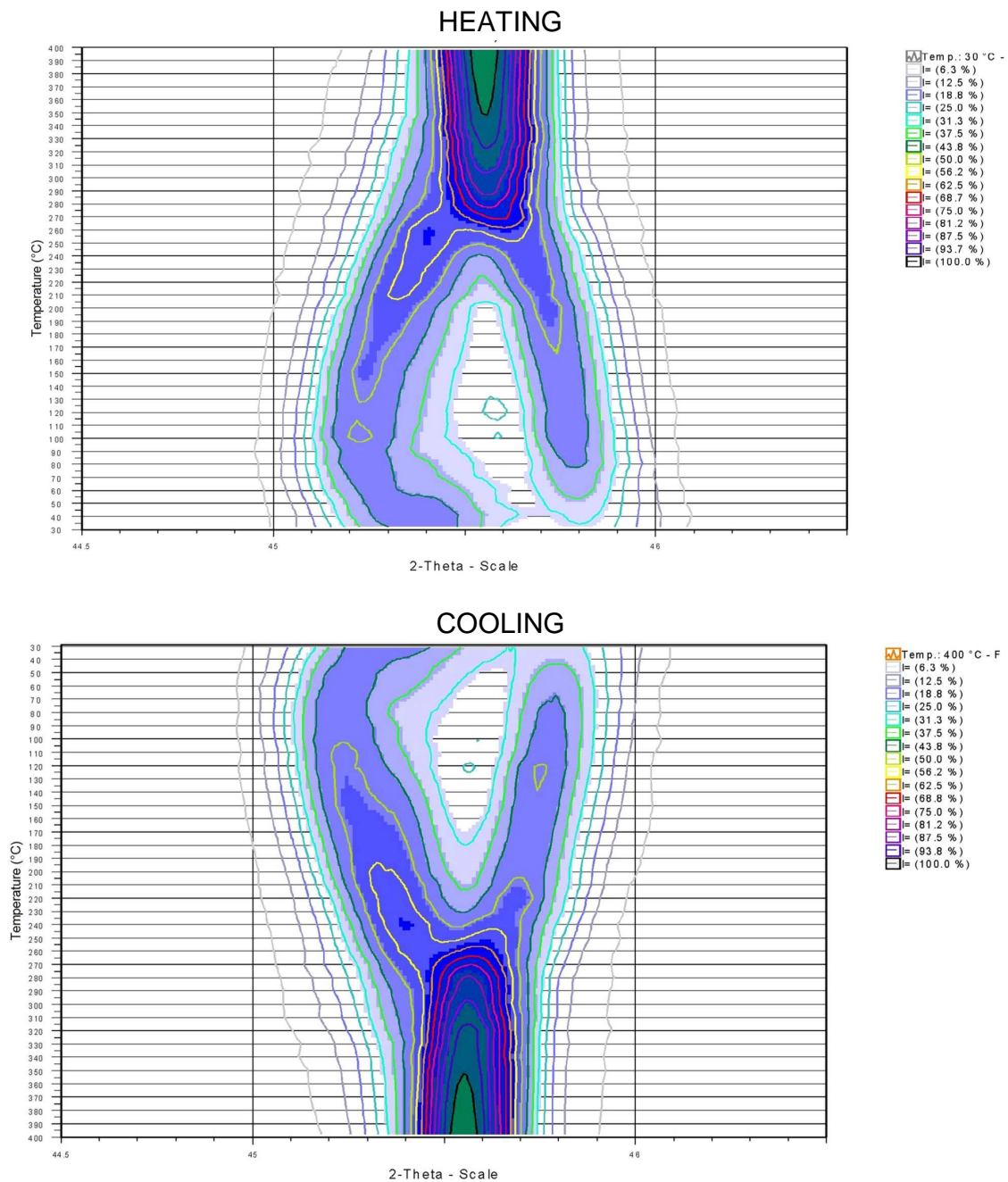
Fig. 61: high temperature diagram of XRD-reflexes at 2θ=44.5-46.5 for 98.5 [Li$_{.04}$(Na$_{.53}$K$_{.47}$)$_{.96}$](Nb$_{.96}$Ta$_{.04}$)O$_3$-1.5 Ba$_2$NaNb$_5$O$_{15}$ during heating and cooling of the sample

e. Strontium-Barium-Niobate

SBN has also a TB structure where out of six possible A-sites occupied only five are occupied by alkaline-earth ions, which is called partially filled TB[156]. Pure SBN has been used into pyro-electric, electro-optic, piezoelectric and photo-refractive devices

and its properties have been improved by producing single crystals or oriented ceramics through template grain growth[157].

i) Experimental

The SBN precursor was also conventionally prepared from Sr-, $BaCO_3$ and Nb_2O_5 in the same manner as described before and was used with LKNNT powder to prepare a binary library. The library is also similar to the previous one, with 8 different doping level of LKNNT with SBN: 0.5, 1, 1.5, 2, 2.5, 3, 4 and 5 mol %.

ii) Results

The relative dielectric constants are displayed in Fig. 62.
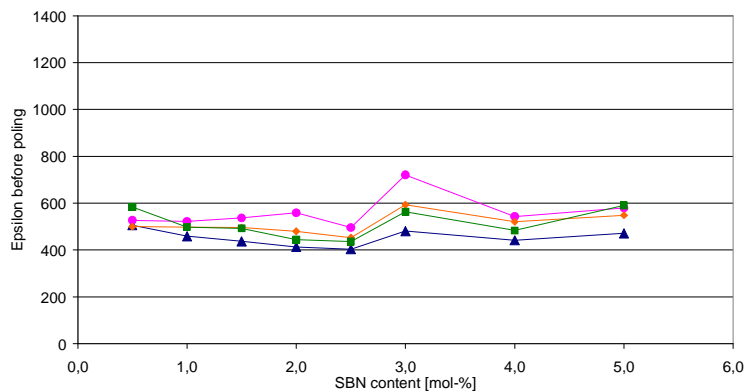
Fig. 62: Epsilon before poling for 1-X [Li$_{.04}$(Na$_{.53}$K$_{.47}$)$_{.96}$](Nb$_{.96}$Ta$_{.04}$)O$_3$-X Sr$_{.75}$Ba$_{.25}$Nb$_2$O$_6$

In this library the dielectric constant does not vary with the doping content. Except for 3% SBN were a slight peak can be detected for all sintering parameters. The Fig. 63 shows the measurement of $d_{33}{}^*$.
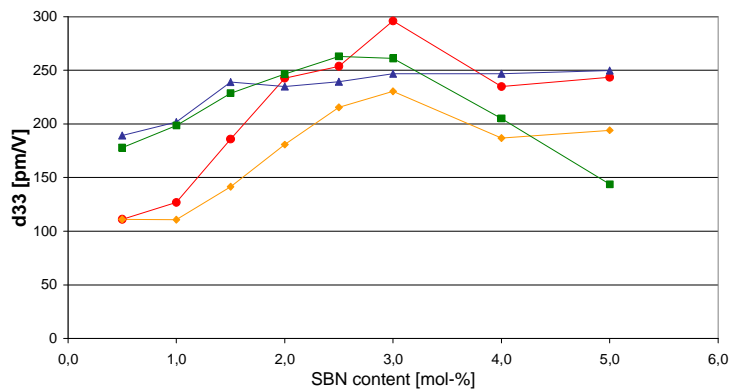
Fig. 63: d$_{33}$ at 2kV/mm of 1-X [Li$_{.04}$(Na$_{.53}$K$_{.47}$)$_{.96}$](Nb$_{.96}$Ta$_{.04}$)O$_3$-X Sr$_{.75}$Ba$_{.25}$Nb$_2$O$_6$

For this library the measurement of the Curie temperature was also obtained and shows also a non typical tendency (see Fig. 64). A first hump is present around 220°C, a second around 260°C. Then the values of ε_r decrease to 300°C and increase again. No values where measurable above 340°C because the equipment to measure the Curie temperature could not achieve those temperatures.
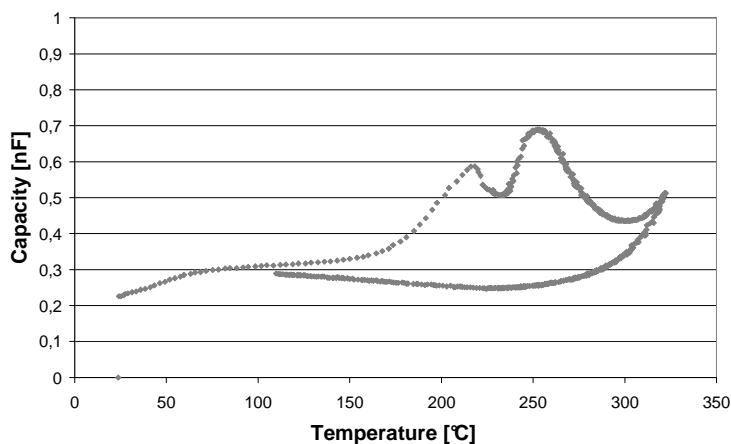
Fig. 64: capacity vs. temperature for 97 [Li$_{.04}$(K$_{.47}$Na$_{.53}$)$_{.96}$](Nb$_{.96}$Ta$_{.04}$)O$_3$-3 Sr$_{.75}$Ba$_{.25}$Nb$_2$O$_6$

f. Discussion

Due to stoichiometric considerations the addition of TB can probably provoke A-site vacancies in the perovskite. As stated in a previous chapter, the general formula of a TB is [(A1)$_2$(A2)$_4$C$_4$][(B1)$_2$(B2)$_8$]O$_{30}$ and for the TB selected the A-sites are earth alkali, C-sites (when occupied) sodium and B-sites niobium. The ions occupying the A- and C-sites in the TB can be inserted into the A-sites of the perovskite as the ionic radie are similar. The ions of the A-sites of TB are earth alkali and they have a valence of two whereas the alkali ions of the perovskite have a valance of one. Therefore, if an earth

alkali is inserted into an A-site of a KNN perovskite, it creates disturbances because the electro-neutrality is not respected. The addition of more positive or less negative ions induces A-site vacancies[158] and the earth-alkali elements introduced must create A-site vacancies. The Kröger-Vink notation which treats the point defect in analogy to atoms and molecules in chemical reaction equations can be employed to describe it.

It was found that only A-site vacancies in the KNN improve the performances[159] but do not induce the desired top performances as describe above.

i) Strontium-Calcium-Sodium-Niobate doped Lithium-Sodium-Potassium-Tantalum-Niobate

The Kröger-Vonck notation for SCNN15-doped LKNNT is:

$$(1-x)A_A + 2xEA_A^{\bullet} + xNa_A + 2xV_A^{'} + 1 - xB_B + 5xB_B + (3+15)O_O$$

where A represents the alkali elements (K, Na, Li) in the perovskite, EA represents the earth alkali elements (Sr and Ca) and B the elements of the B-site (Nb and Ta).

Between 0.5 and 4 mol% SCNN15 doping, the tendency is the same for ε_r and d_{33}^{*} but for the sample doped with 4 and 5 mol% SCNN15 the value of ε_r increases whereas the value of d_{33}^{*} decreases. This is probably due to the competition between SCNN15 and KNN. SCNN15 has high ε_r value which influences the ε_r values of the two-phases ceramic and then high ε_r values are achieved, whereas the quantity of SCNN15 is not sufficiently important to produce also improvements on the d_{33}^{*} values.

As it can be seen in Fig. 49 the phase composition of KNN evolves with the doping level. For doping content of 0.5 and 3 mol% the material presents a pure phase perovskite but for other doping level an additional unidentified phase is visible. The materials presenting a pure phase perovskite also show the highest piezoelectric coefficient d_{33}^{*}.

The measurement of the Curie temperature shows a particular behaviour of the samples: some curves possess two or more peaks during heating and are flat during cooling. The non-doped KNN shows a peak at 200°C which is the orthorhombic to tetragonal phase transformation[160] but for the doped-samples no peak is visible in this area of temperature; which means that the orthorhombic-tetragonal phase transformation has been shifted to lower temperatures or it does not exist anymore.

As it can be seen in Fig. 53, the Curie temperature of the sample containing 3 mol% SCNN15 seems to be above 320℃, maximal temperature a t which the measurement was done. The peak at 270℃ is present which can be assimil ated to the Curie temperature of SCNN15 but the first peak around 240℃ can not be identified. Therefore high temperature XRD were carried out (see

Fig. 52). In this diagram we can clearly see that at room temperature the structure of the material is monoclinic or orthorhombic (the X-ray does not allow differentiating both structures), then at 90℃ a tetragonal structure begi ns to appear. The tetragonal structure is stable up to 270℃. However, for this com position in Fig. 53 the curve of the capacity in function of the temperature seems to continue increasing after the phase transformation into a cubic structure. The peaks around 250℃ could not be explained by a phase transformation therefore, external phenomena must be the cause of this anomaly. Possible reasons are the presence of water in the sample or the presence of a secondary phase which cannot be detected by XRD. Differential scanning calorimetry of this sample shown in Fig. 55 does not allow discerning a phase transformation as the temperature interval between both peaks was too low. In this diagram an endothermic peak is visible around 300℃ which is the si gnal of the Curie point. No other endo- other exothermic peak is visible for inferior temperatures, therefore the hypothesis of a phase transformation about 240℃ cannot be validated. Water release during heating would have been noticed in the DSC measurement. During DSC measurement the sample sintered is different to the bulk samples produced, i.e. its surface in contact to air is smaller and the mechanisms of water absorption and release should be different. Thus, if nothing appears during DSC measurement that does not mean that the hump shown at 240℃ during the Curie t emperature measurement was not water release. Due to lack of powders of the compositions investigated this phenomena could not be deeper explored.

ii) Barium-Sodium-Niobate doped Lithium-Sodium-Potassium-Tantalum-Niobate

The Kröger-Vinck notation for BNN is the same as for SCNN15 as the formula is the same, i.e. $EA_2NaNb_5O_{15}$ where only barium is the earth alkaline present. The values of ε_r are almost the same as the values of non-doped LKNNT. The doping has no real

influence on the values of ε_r. The values of $d_{33}{}^*$ are improved in comparison with the values of non-doped LKNNT and reach 230 pm/V for a sample doped with 1.5 mol% of BNN, sintered at 1100°C for 1 hour with a maintain of 2 hours at 750°C. The values of tan δ are also better than those of the sample from the section b, as the values stay stable between 0.04 and 0.07. The last measured property is the Curie temperature. In the Fig. 58 different peaks are observable that are not the Curie temperature. The two peaks could be interpreted as phase transformations. The Curie temperature is situated at 350°C but the peaks at 100 and 250°C are not yet identified.

It is known that the pure KNN endures an orthorhombic-tetragonal phase transformation at about 200°C [161] (T_{O-T}). In the case of KNN doped with tantalum, the Curie temperature lowers as well as the transition temperature. For 10% tantalum doping, T_{O-T} lowers from 200 to 160°C and the Curie temperature decreases from 400°C to 350°C [162]. For LT-doped KNN, it is known[13] that the Curie temperature is shifted to 320°C and T_{O-T} is shifted around 100°C for KNN doped with 4% LT. Therefore in this material the first peak around 100°C could be identified to an orthorhombic-tetragonal phase transformation as the presence of water was excluded during the DSC measurements.

For the second peak, it is remarkable that during the cooling the curve of the plot is flat instead of rising at temperatures around the Curie temperature like the heating curve. This kind of phase transformation seems to have a hysteresis. Therefore the capacity vs. the temperature was measured one week after and one day after as seen in Fig. 59. One day after the first measurement the profile of the curve is different with a disappearance of the peak at 250°C, whereas the peak attributed to the orthorhombic-tetragonal transformation always exists but with a lower intensity. One week after the first measurement both peaks are present with the same intensity. XRD analyses were performed on a sample to identify the phases at least one week after this measurement.

High temperature XRD was also carried out on a sample having the composition 98.5 $Li_{0.04}(Na_{0.53}K_{0.47})_{0.96}](Nb_{0.96}Ta_{0.04})O_3$ - 1.5 $Ba_2NaNb_5O_{15}$ between room temperature and 400°C to try to find a second phase transformation ; the X-ray pattern are shown in Fig. 60 and Fig. 61. On these figures it can be seen that a tetragonal structure appears at 60°C and stays stable up to 340°C, temperature at which only the cubic structure is visible. No phase transformation in the region of 250°C is visible. As well as for the other sample (KNN-based ceramic with SCNN15 doped) complementary analysis method as differential scanning calorimetry could not reveal more information as it was the case for SCNN15-doped KNN. However, it is to note that the anomaly for BNN-

doped LKNNT appears in the same temperature region as for SCNN15-doped LKNNT, hence, the research will be focused on one doping system to try to find an explanation and this will be applied on the second doping system to verify the results found on one system.

iii) Strontium-Barium-Niobate doped Lithium-Sodium-Potassium-Tantalum-Niobate

The A-site vacancies concentration is different with SBN as with the two other tungsten-bronzes because of its different composition. For KNN-based ceramics doped with SBN the Kröger-Vink notation is the following:

$$(1-x)A_A + xEA_A^{\bullet} + xV_A^{'} + (1-x)B_B + 2xB_B + (3+6)O_O$$
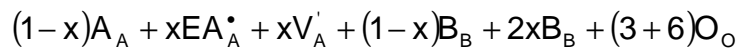
In this library the effect of the TB doping seems to be maximal for 3 mol% SBN where the values of d_{33}^{*} reach 300 pm/V for samples being sintered 1h at 1150°C with a dwell for 2h at 750°C and with 0.5g Na-, K- and Li$_2$CO$_3$ in the sintering boat. In this library the values of the dielectric losses are also low (around 5%) which validate the results.

For this composition the high temperature behaviour is comparable to 0.985 LKNNT-0.015 BNN and 0.97 LKNNT-0.03 SCNN. The Curie temperature seems to be higher than 350°C but the apparatus could not achieve higher temperatures. No more analysis was performed on this library as the behaviour is so similar to the other ones. The doping of KNN with LiTaO$_3$ and Sr$_{0.75}$Ba$_{0.25}$Nb$_2$O$_6$ gives interesting results which should be later pursued.

iv) General discussion

For each atom of earth alkali added one A-site vacancy is created, i.e. for each mol of SCNN15 or BNN added two moles of A-sites vacancies are created and for each mol of SBN added one mole of A-sites vacancies is created. In PZT the introduction of A-site vacancies induced by the doping with cation having a valence of three and a large radius (rare earth or bismuth fpr example) modifies the electric and piezoelectric properties depending on the cation employed and its concentration[163,164].

A maximum of average crystallite size was observed for 3 mol% SCNN15 which also corresponds to 6 mol% A-site vacancies. None of the samples observed showed abnormal grain growth contrarily to LKNNT samples. The abnormal grain growth was systematically studied by Drofenik *et al.* on semiconductive BaTiO$_3$[165]. According to their theory the driving force for the abnormal grain growth is the stored free surface energy of fine grains, which is released during abnormal grain growth. This surface energy is consumed in oxygen release and donor-dopant incorporation. The abnormal grain growth observed for LKNNT composition can be explained by the same theory. During sintering the evaporation of lithium, sodium and potassium induced oxygen vacancies, in the same way oxygen vacancies are naturally present into PZT due to lead evaporation during sintering[166]. These oxygen vacancies provoke abnormal grain growth in LKNNT ceramics.

Recently Tashiro *et al.* observed that abnormal grain growth occurs in Sr-doped KNN for low dopant level (between 1 and 4 mol% Sr content) and they related it to dopant-donor incorporation[167]. In the Tb-doped LKNNT, despite the possible creation of A-site vacancies no abnormal grain growth could be observed. Another explanation is that the charge compensation occurs by decreasing the number of oxygen vacancies present in the original LKNNT which shows abnormal grain growth. With the decrease of oxygen vacancies the densification can be superior if, as in PZT ceramics, the oxygen vacancies are the slowest moving species and they control the densification rate according to Kington and Atkin[168,169]. Higher densification means also higher electric and piezoelectric properties, which explains the superior properties of TB-doped LKNNT. Moreover in PZT the domain wall pinning does not occur since the donor doping suppresses the formation of oxygen vacancies. It is supposed that the poling of donor-doped PZT is in this way promoted[170].

3. Conclusion

Different doping was successfully applied to KNN-based ceramics to improve the performances of this material. Two different strategies were assessed to enhance the performances: the addition of a liquid phase sintering to reach high density and therefore, higher dielectric and piezoelectric properties and the addition of elements which can be introduced in the perovskite structure inducing different effects.

The piezoelectric properties of air-sintered non-modified KNN could be enhanced trough the formation of a liquid phase sintering containing copper and germanium. The literature describes the doping of KNN with a small quantity of copper inducing a liquid phase sintering of KCN or KCT which improve the density. During the reproduction of the results we found that high amounts of copper induce also high conductivity into the material. To try to control this conductivity, crystal defects were created by the addition of a second doping element. Among them the germanium showed the most interesting properties by reducing the dielectric losses and improving the piezoelectric coefficient. The presence of a liquid phase could be identified through microstructure analysis and the presence of germanium was proven with energy dispersive X-ray analysis.

The addition of tungsten-bronze based compositions improved the dielectric and piezoelectric properties of LT-doped KNN. For two chosen TB the values of d_{33}^{*} almost approached 300 pm/V. The doping with TB induced anomaly for almost doped samples during the Curie temperature measurement. This anomaly could not be explained with the method employed, therefore, a deeper investigation of this composition should be carried out. The improvement of the piezoelectric properties induced could not be clearly explained at the moment. The creation of A-site vacancies induced by the introduction of earth alkaline elements and at the same the decrease of oxygen vacancies play an important role and their effects are positive on the dielectric and piezoelectric properties of KNN-based ceramics. The maximum d_{33}^{*} for samples having TB doping was measured for samples doped with 3 mol% SBN and SCNN15. Moreover samples doped with SCNN15 showed another maximum for 0.5 mol% doping. The effects of the dopants employed in addition to strontium (calcium or barium) are also not clarified and more investigations would be necessary. First the attention will be focused on the doping with SCNN15 for two reasons: the creation of vacancies is more effective in comparison to SBN, for one mol SCNN15 added two mol A-site vacancies are created and in the measurement of d_{33}^{*} in dependence of the doping content, two peaks are visible.

VIII. Optimisation of Lead-Free Compositions

The HTE process set-up allows the optimisation of a composition space as the process is rather close to a classical processing. The previous chapter was focussed on the discovery of new lead-free piezoelectric ceramics and now this part will focus on the further development of one of the most promising compositions. The best results were measured on [(K,Na)NbO$_3$ - LiTaO$_3$ – Sr$_{1,85}$Ca$_{0,15}$NaNb$_5$O$_{15}$]-based ceramics, therefore, it is in this composition area that improvements should be made.

The exact composition on which the best results were obtained was exactly 0.93 (K$_{0,47}$Na$_{0,53}$)NbO$_3$ – 0.04 Li TaO$_3$ - 0.03 Sr$_{1,85}$Ca$_{0,15}$NaNb$_5$O$_{15}$. The first investigation was to find out the optimal LiTaO$_3$ doping as well as an alternative processing route.

1. *First Experimental Series: Optimal LiTaO3 Doping*

The LT-doping of KNN was found in the literature to be optimal for 4 mol%[171] and it was on this basis that further doping with Sr$_{1,85}$Ca$_{0,15}$NaNb$_5$O$_{15}$ (SCNN15) was made, but now, in order to optimise the interactions (if there are) of both doping, their contents should be adjusted. In parallel a different processing of the powder was carried out to understand the influence of each compound on the final composition.

a. Experimental

Three powders were simultaneously prepared:

(K$_{0,47}$Na$_{0,53}$)NbO$_3$ from KN and NN

LT from Li$_2$CO$_3$ and Ta$_2$O$_5$

SCNN15 from SrCO$_3$, CaCO$_3$, Na$_2$CO$_3$ and Nb$_2$O$_5$

These powders were ground for 24h on a milling banc with alcohol as cooling medium, dried and sieved. Half of each powder were independently calcined at temperature allowing the formation of the desired compound (i.e. 750°C, 5h for $(K_{0.47}Na_{0.53})NbO_3$[172]; 1150°C, 2h for SCNN15 [173] and 800°C, 2h for LiTaO$_3$[174]) and both calcined and non-calcined powders were used as starting materials for this experimental series.

The variation consisted in holding the SCNN15 content at 3 mol% and varying the content in LiTaO$_3$ between 0 and 7 mol% for both calcined and non-calcined powders as described in Fig. 65. The first series with the non-calcined powders is represented with the number 1 and the series with the calcined powders is represented by the number 2. In these experimental series, two compositions are the same as a composition found in chapter VII.2.c (the compositions with 4 mol% LiTaO$_3$ which contain 3 mol% SCNN15) in order to have a reference between different experimental series.
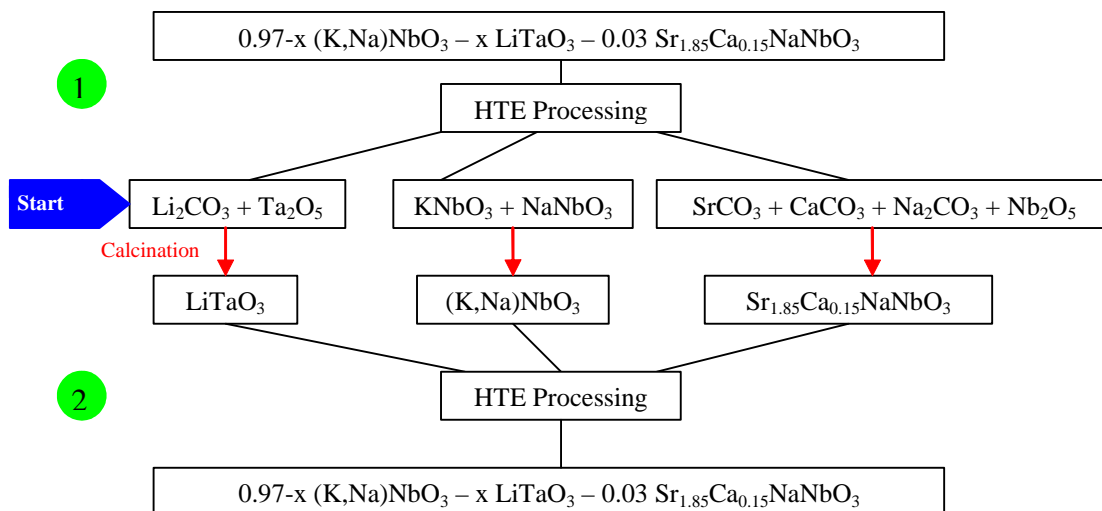
Fig. 65: First experimental series

b. Results Reactive Sintering

The relative dielectric constant and dielectric losses obtained for the library processed with non-calcined powders are shown in Fig. 66 and the piezoelectric constant in Fig. 67.

The relative dielectric constant and the dielectric losses show unexpected values. The ε_r-values of samples sintered at the lowest temperature are lower than for the samples sintered at temperatures above 1125°C. For low LT co ntent (0 and 1 mol%) the values

of ε_r are inconsistent. For higher doping levels only the sintering temperature shows an influence. The dielectric losses are dramatically high in comparison to the first library. The $d_{33}{}^*$-values show a maximum for 6 mol% LT at 200 pm/V.
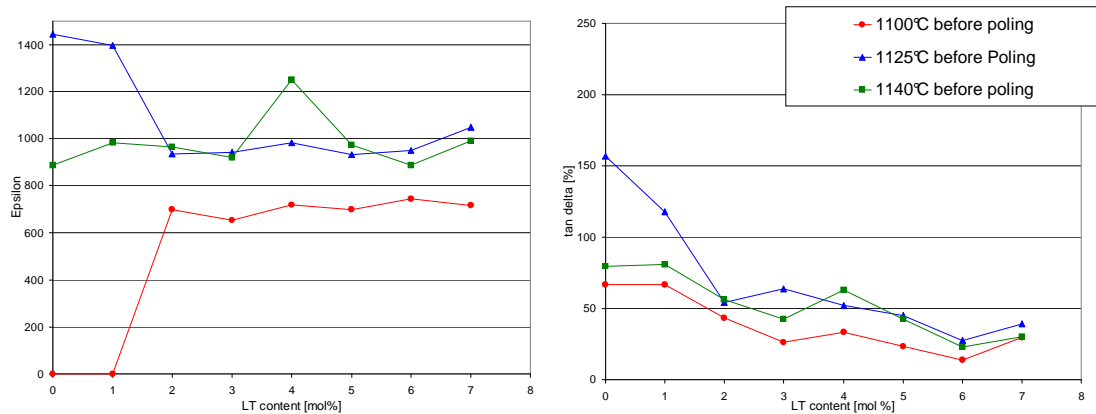
Fig. 66: ε_r and tan δ of 0.97-x (K,Na)NbO$_3$ - xLiTaO$_3$ - 0.03 Sr$_{1.85}$Ca$_{0.15}$NaNb$_5$O$_{15}$
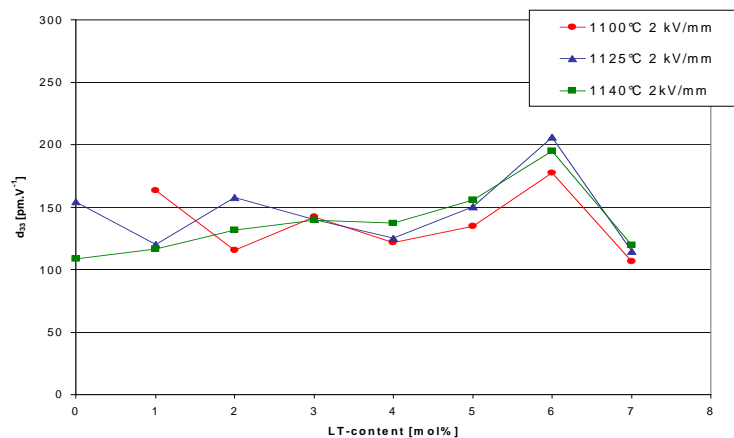
Fig. 67: $d_{33}{}^*$ of 0.97-x (K,Na)NbO$_3$ - xLiTaO$_3$ - 0.03 Sr$_{1.85}$Ca$_{0.15}$NaNb$_5$O$_{15}$

c. Results Influence of Precalcination

The results of the dielectric constant and piezoelectric constants are shown in Fig. 68 and Fig. 69.

The relative dielectric constant and the dielectric losses show different values to those of the previous part of this experimental series. The ε_r-values of the samples are independent of the sintering temperature. For 4 mol% LT content the values of ε_r as well as tan δ are significantly lower than for other doping levels. For doping content higher than 4 mol% LT, the values of the dielectric losses stay low. The $d_{33}{}^*$-values are

not strongly affected by the doping level but a maximum for 4 mol% LT up to 200 pm/V is observable.
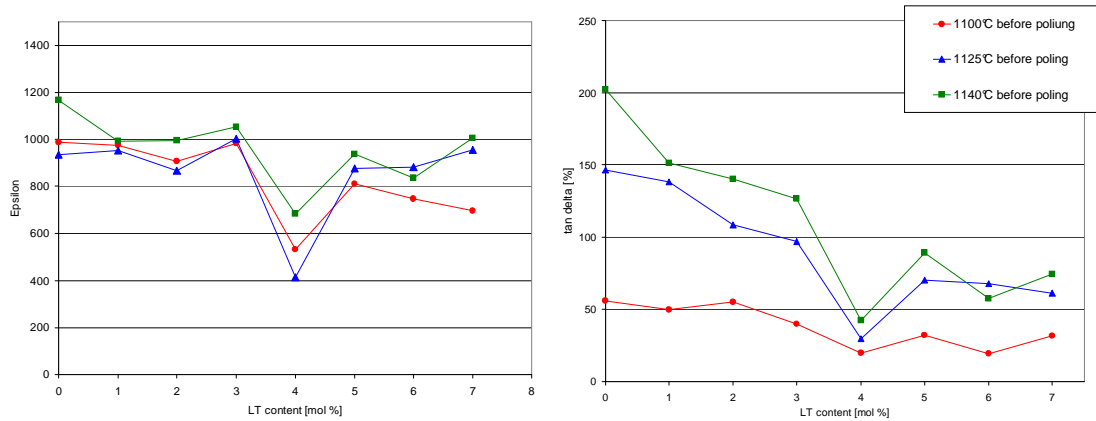
Fig. 68: relative dielectric constant and dielectric losses of 0.97-x (K$_{0.47}$Na$_{0.53}$)NbO$_3$ - x LiTaO$_3$ - 0.03 Sr$_{1.85}$Ca$_{0.15}$NaNb$_5$O$_{15}$ dependant on the firing temperature
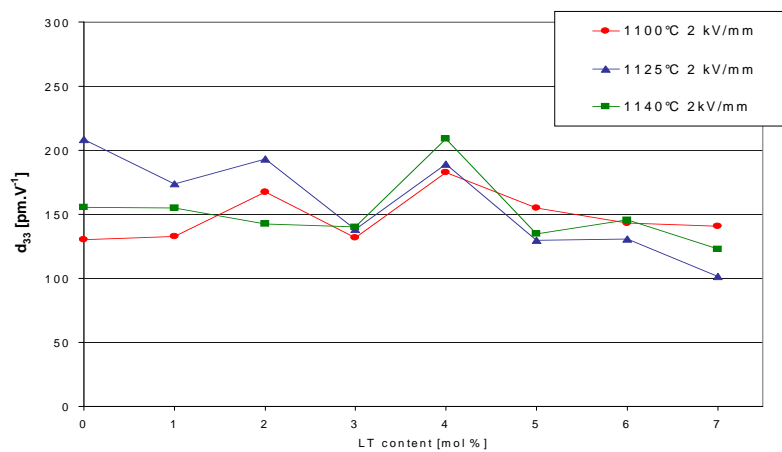
Fig. 69: d$_{33}$* of 0.97-x (K$_{0.47}$Na$_{0.53}$)NbO$_3$ - x LiTaO$_3$ - 0.03 Sr$_{1.85}$Ca$_{0.15}$NaNb$_5$O$_{15}$ depending on the firing temperature

d. Discussion

The lowest dielectric losses of the library with the samples produced from non-calcined powders were measured for the samples containing 6 mol% LT, but the value attain was of 0.2 which is clearly higher than the value of the sample measured in the first library (see Chap. 7.2). This can be related to the low density of the samples.

The theoretical density of KNN is approximately 4.5 g/cm³ and the average density measured of the samples of this library was only 3.7 g/cm³ which is almost 80% of the

theoretical density. The density was not high enough to allow a measurement reflecting the real properties of the materials. Nevertheless, a tendency in this library could be identified. The d_{33}^* values of the samples containing 6 mol% LT are higher than the other ones, meaning that this doping level should be better for this composition space. However, d_{33}^* values measured are lower than those expected, especially for the samples doped with 4 mol% LT as the value of 290 pm/V was previously measured on a sample having this composition.

The results of the relative dielectric constant are more consistent for the library prepared from the calcined powders than for the library with the non-calcined powders because a tendency could be observed: ε_r is around 1000 at concentration below 4 mol% SCNN15 doping, then a peak of low ε_r for 4 mol% SCNN15 is observed and finally ε_r remains around 900 for higher doping levels. On the other hand the dielectric losses are even higher than for the library prepared from non-calcined powders. The lowest dielectric losses measured for the samples containing 4 mol% calcined LT were only of 0.25. The average density of the samples from the library prepared from calcined powders was 3.52 g/cm³ whereas the average density of the samples from the library prepared from non-calcined samples was 3.7 g/cm³. The lack of density of the samples can explain also in this case the high values of the dielectric losses. The values of d_{33}^* are as low as those recorded for the library where the samples were produced from non-calcined powders, but the peak maximum is not located at the same LT content. In this case the optimal d_{33} values are recorded for 4 mol% LT.

A piezoelectric constant of 200 pm/V could be measured for one composition in both libraries, however this maximum was not observed for the same composition: for the library where the different powders were non-calcined a maximal of d_{33}^* was observed for 6 mol% LT and for the library where all compounds where individually calcined the composition with 4 mol% LT shows the maximal piezoelectric coefficient.

The interactions between the perovskite and the tungsten-bronze could not be totally understood but these libraries give indication of the orientation of further experiments: in order to produce samples with higher density and therefore lower dielectric losses, no previous separate calcination of the compounds should be carried out. Therefore, the doping with 6 mol% LT presents the best dielectric and piezoelectric properties for this mode of preparation.

In the first library prepared for doping of LKNNT with SCNN15, the content of LT chosen was 4 mol% as a MPB for the system KNN/LT at this doping level has been observed by Zhen et al.[175]. However as it is the case for PZT, the MPB can move with the incorporation of dopants in the cell[176]. The doping of KNN with earth-alkalis like strontium and calcium makes the MPB move as they are built in the perovskite cell. Therefore the content in LT for 3 mol% SCNN15-doped KNN is optimal for 6 mol%.

From this library the main conclusion is that 6 mol% LT into 0.97 $(K_{0.47}Na_{0.53})NbO_3$ - 0.03 SCNN15 shows the best properties. But the results are troubling as the composition used as reference between two libraries does not provide the same properties. Different reasons could cause these results:

- Different preparation (before $(K,Na,Li)(Nb,Ta)O_3$ were ground together and in this case KNN and LT are separately ground).

- Use of different starting materials.

- Drastic reproducibility problems of KNN-based piezoelectric ceramics[177].

During the first phase, i.e. the development of new lead-free piezoelectric ceramics, a different batch of powder was used for KN as well as for NN. This was known and attention was paid to compensate the slight stoichiometry variations but other parameters may influence the piezoelectric properties of the samples.

From this point on, the work will be focussed on the precursors and their influence on the properties of KNN-based piezoelectric ceramics.

2. Second Experimental Series: Influence of Precursors

a. Different Precursors

As it has been observed in the previous experimental series the influence of the precursors is important for the properties of the piezoelectric KNN-based ceramics, in this second experimental series one composition was selected which was produced with different precursors to observe correlations between raw materials compositions and electric properties. In a first part, different sources for potassium, sodium, niobium and tantalum were tested and in a second part various potassium niobates having different stoichiometry were employed to determine their influence on the piezoelectric properties. The final stoichiometry of the materials produced is always the same

(0.93 $(K_{0.47}Na_{0.53})NbO_3$ - 0.03 SCNN15 – 0.04 LT) and, the stoichiometry variations due to different stoichiometry of the starting materials were compensated using carbonates.

i) Experimental

The raw materials used to produce the first series were 3 different potassium- and sodium-niobate, tantalum- and niobium-pentoxide, sodium- and potassium-carbonate. Table 9 gives the composition of the starting materials employed for each composition (enumerated from 1 to 8). The composition of the precursors employed was determined by the results of X-ray fluorescence spectroscopy given by the manufacturer. To describe the precursors the nomenclature employed refers always to the niobium and tantalum being 1 (as they are non-volatile elements, it can be though that their content remains constant in the ceramic) and the number written is the content of alkali in reference to those elements. For example K:Nb=1.014 means that the stoichiometry of this precursor is $K_{1.014}Nb_1O_{3+\delta}$; the compensation of this precursor is made with the addition of niobium oxide to achieve the stoichiometry $KNbO_3$. For precursors having a deficit in sodium or potassium, this is compensated by the addition of sodium or potassium carbonate. In the precursors, niobium and tantalum were selected as references as they are not as volatile as the alkali elements. The composition selected was 0.93 $(K_{0.47}Na_{0.53})NbO_3$ – 0.04 $LiTaO_3$ - 0.03 SCNN15 where SCNN 15 was already prepared without calcination.

Table 9: starting materials and their composition

1	Carbonate
2	K:Nb=1, Na:Nb=1.021, K:Ta=0.934
3	K:Nb=1.014, Na:Nb=0.9934, K:Ta=0.934
4	Ta_2O_5, K:Nb=1.014, Na:Nb=0.9934
5	K:Nb=1.027, Na:Nb=0.996, K:Ta=0.934
6	Ta_2O_5, K:Nb=1.027, Na:Nb=0.996
7	K:Nb=1.014, Na:Nb=0.996, K:Ta=0.934
8	K:Nb=1.027, Na:Nb=0.9934, K:Ta=0.934

The composition number 1 was produced with carbonates in order to have a reference; the other combinations of starting materials were arbitrarily selected, considering the 8 compositions per series and the starting materials available. The analysis of this series was more detailed than the other ones as the key parameter for an optimal processing are investigated.

ii) Results

First dilatometer measurements on non-calcined powders allow the observation of the calcination and sintering behaviour of different materials; the two parameters considered are the sintering starting temperature and the sintering rate. Fig. 70 shows the densification behaviour and the densification rate for compositions 1 and 3 of table 9. The difference of sintering behaviour between the samples produced with carbonates as raw materials and the samples produced with precursors was investigated and subsequently the difference between the raw materials was analysed.
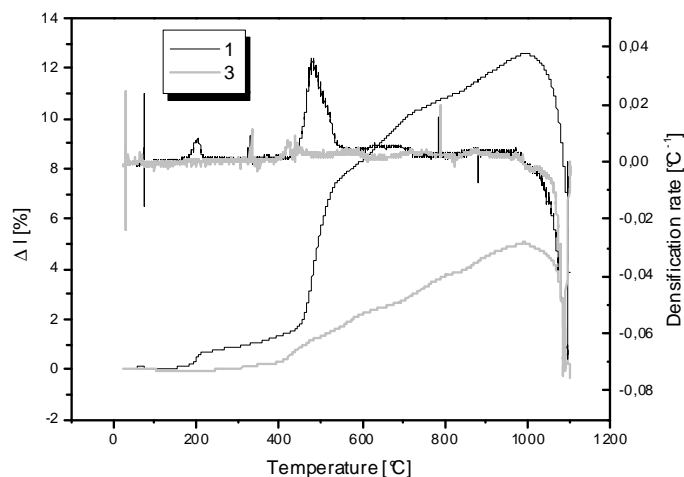
Fig. 70: Densification behaviour of two samples having the composition 1 and 3 of table 9

The sintering behaviour of all samples is shown in Fig. 71. The sintering begins around 1000°C for all samples.

Fig. 71: Sintering behaviour of 0.93 ($K_{0.47}Na_{0.53}$)NbO$_3$ − 0.04 LiTaO$_3$ - 0.03 SCNN15 prepared with different precursors

In addition to dilatometer measurements, X-ray analysis of the calcined powders were carried out to prove the phase formation in the samples. The composition of the calcined powders can have an influence on the sintering behaviour of the ceramics, so the detection of second phases, which can have benefits on the sintering is essential to control and understand the interactions between the different elements.

The results of the X-ray analysis of powders, calcined at 750°C for 5 hours, are given in Table 10.

The dielectric measurements of the samples are shown in Fig. 72; the different colours presented different sintering processes.

Fig. 72: dielectric constant and losses of 0.93 ($K_{0.47}Na_{0.53}$)NbO$_3$ − 0.04 LiTaO$_3$ - 0.03 SCNN15 prepared with different precursors

To complete the dielectric measurement the piezoelectric coefficients d_{33}^* are measured as shown in Fig. 73.
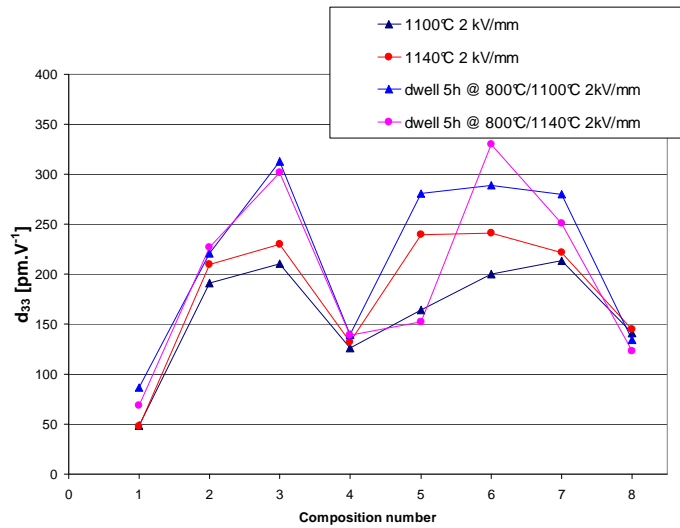
Fig. 73: d_{33}^* of 0.93 $(K_{0.47}Na_{0.53})NbO_3$ − 0.04 $LiTaO_3$ - 0.03 SCNN15 prepared with different precursors

Table 10: phase composition of calcined powders in vol. %

Sample	KN	NN	TB	(K,Na)NbO3
1	44,7	33,1	7,6	14,6
2	41,9	36,8	6,2	15,1
3	44,8	32	6	17,2
4	43,1	38,2	5,5	13,2
5	41,7	37,6	5,8	14,9
6	39,4	39,7	6,5	14,4
7	40	38,5	5,4	16,1
8	42,5	35,7	5,2	16,6

The samples from the composition 2 of table 9 have a d_{33}^* of around 200 pm/V independently of their sintering parameter. The highest d_{33}^* values were recorded for the samples from the compositions 3, 6 and 7. The piezoelectric coefficients measured were partly higher than those previously measured with values higher than 300 pm/V.

b. SodiumNiobate

i) **Experimental**

Eight lots of NN were prepared by the supplier with different stoichiometry (~20g each). The eight stoichiometries available for Na:Nb were: 0.934, 0.9964, 1.0198, 1.0266, 1.0369, 1.0379, 1.04154 and 1.0443, i.e. for 2 samples potassium was in deficit and for the 6 others potassium was in excess. The other raw materials used were KT (K:Ta=0.934:1), KN (K:Nb=1.014:1), Nb_2O_5 and Li_2CO_3.

ii) **Results**

As well as for the other experimental series first a dilatometer measurement of all samples was carried out (see Fig. 74).
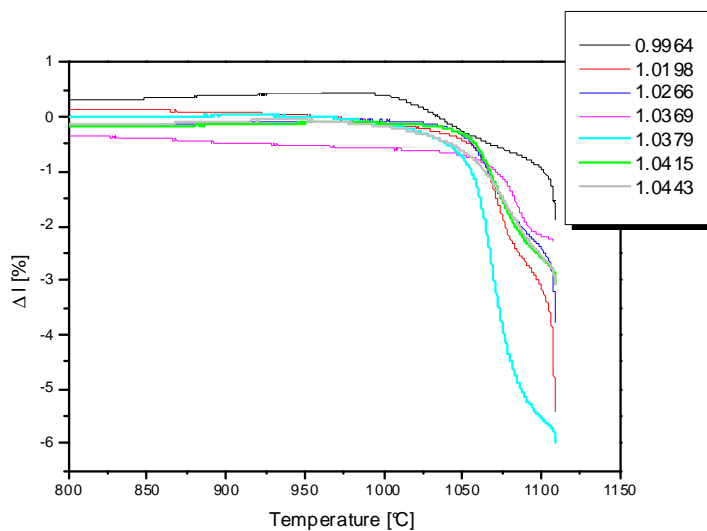
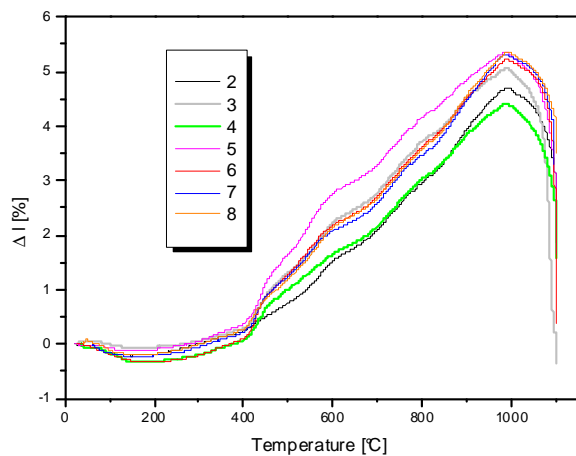**Fig. 74: sintering behaviour of 0.93 ($K_{0.47}Na_{0.53}$)NbO$_3$ - 0.04 LiTaO$_3$ - 0.03 SCNN15 prepared with different NaNbO$_3$**

The influence of the dwell to enhance the formation of the perovskite was also analysed. Three different sintering programmes were carried out:
- maintain 5h at 800℃, sintering 1h at 1140℃
- maintain 2h at 800℃, sintering 1h at 1140℃
- sintering 1h at 1140℃

Fig. 75 shows the dielectric properties of the samples prepared with different NaNbO$_3$ precursors as a function of the potassium excess in these precursors with different sintering programs.
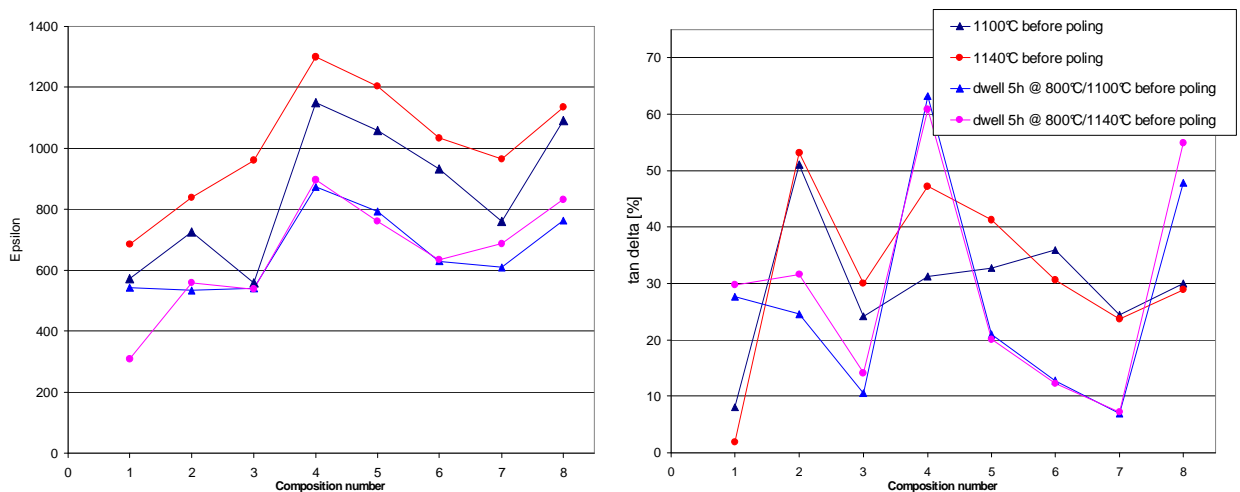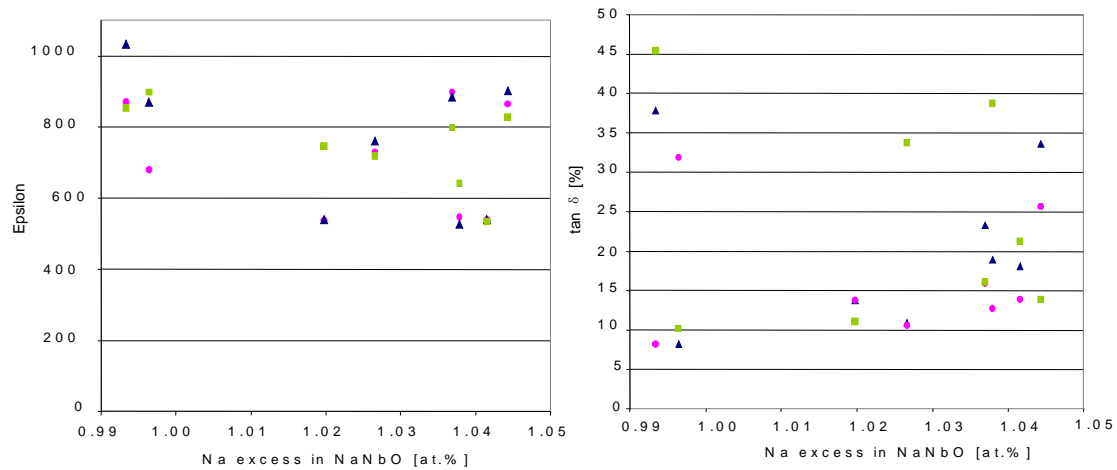
Fig. 75: dielectric contant and losses of 0.93 (K$_{0.47}$Na$_{0.53}$)NbO$_3$ - 0.04 LiTaO$_3$ - 0.03 SCNN15 prepared with different NaNbO$_3$ precursors

The piezoelectric constant should complement the overview on the material properties in relation to the stoichiometry of the potassium niobate employed in the preparation. These are shown in Fig. 76 in function of the potassium excess used.
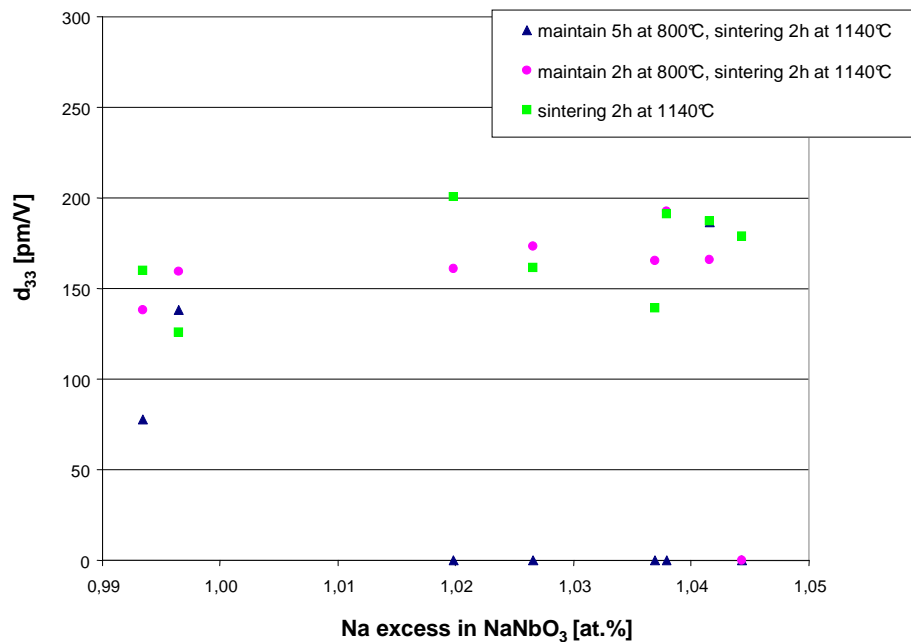
Fig. 76: d$_{33}$* of 0.93 (K$_{0.47}$Na$_{0.53}$)NbO$_3$ − 0.04 LiTaO$_3$ - 0.03 SCNN15 prepared with different NaNbO$_3$ precursors

c. Discussion

During the dilatometer measurements of samples from the library of the first part, i.e. in the library where the samples were prepared with different sources for potassium, sodium, niobium and tantalum (see 8.2.1), a first hump is visible at 200°C for the carbonate-based ceramic; this can be attributed to the beginning of the decarboxylation of the carbonates. Then the densification rate increased around 450°C. That can be attributed to the perovskite formation. The precursor-based ceramic (number 3, in grey) shows an almost linear expansion up to 1000°C which mea ns that this ceramics shows a flat densification rate. The formation of the perovskite for the precursor-based ceramic can not be easily detected by dilatometer measurement as the main precursors employed (NN and KN) have the same crystal structure as the final compound (perovskite) and the parameters of their unit cells are close (See section 3.4.3).

The dilatometer curves of all the samples shown in Fig. 71 are quite similar to those in Part 7.2 and the sintering of all ceramics begins around 1000°C. It can be observed that the samples having the compositions 3 and 6 have a higher densification rate than the other samples.

The phase compositions of the calcined samples are similar as shown in table 10. The contents in potassium and sodium niobate are higher than expected. The perovskite transformation of potassium and sodium niobate is quasi undetectable through dilatometer measurement on the calcined samples, therefore it was thought that their content would be rather low in comparison to KNN. It can be observed that the tungsten bronze structure is already formed at low temperatures although in the literature the calcination of SCNN15 is reported to be effective only at high temperature[178]. This is also surprising as in the previous series no presence of tungsten-bronze was detected in the sintered ceramic.

The values of the dielectric constant and losses are scattered for both measurements and highly dependent on the sintering temperature and the sintering program. The samples sintered at 1140°C for 1 hour show the highest relative dielectric constant. The samples sintered at 1100°C for 1 hour show lower r elative dielectric constants and the samples sintered with a dwell show the lowest dielectric constant. Regarding the dielectric losses, they are dependent on the composition as well as on the sintering temperature. For almost all the samples the dielectric losses of samples sintered with a dwell are lower than the dielectric losses of samples sintered without. The

compositions 3 and 6 from table 9, which showed the fastest sintering rate in Fig. 71, show also the lowest dielectric losses with samples of the composition 7. Samples from the compositions 2, 4 and 8 from table 9 show the highest dielectric losses and samples from the compositions 4 and 8 from table 9 the highest relative dielectric constant. Often samples having high dielectric losses show low electric resistance and for those compositions it is difficult to dissociate the contribution to the relative permittivity from the elevated conductivity and the intrinsic property of the material.

As for the other properties the piezoelectric coefficient of the samples is highly dependent on the sintering temperature. This was not the case in the previous series (see chapter 8.1). The lowest values were measured on the samples of the compositions 1, 4 and 8 from table 9. The composition 1 is carbonate-based, and it is assumed that the samples are porous due to the evaporation of CO_2 during the preparation. Therefore the piezoelectric coefficient remains low; the samples 4 and 8 show the highest dielectric losses and among the highest relative dielectric permittivity.

The second part of this experimental series focussed on the stoichiometry of the sodium niobate. The sample processed with NN having a deficit in potassium begins to sinter at lower temperature (around 1000°C) but the densification rate is rather low. The samples prepared with NN with an excess in potassium begin to sinter at higher temperatures (around 1050°C) but with a high sinteri ng rate and among them the sample prepared the NN with 3.79 mol.% potassium excess shows the quickest sintering rate.

The values for both, relative dielectric constant and dielectric losses, were scattered and independent of the sintering program. The interpretation of the differences between the two precursor families (those having potassium excess and deficit) is not clear as few precursors with potassium deficit were available and so no statistic could be established.

The samples prepared with NN containing potassium excess have a slightly higher d_{33}^* and a dwell at 800°C is not suitable to improve the p iezoelectric properties. The majority of the samples having suffered a long maintain previous to the sintering (5h) were not measurable at 2 kV/mm due to short-circuits.

All the piezoelectric and dielectric results of the first part of this experimental series are summarised in Fig. 77, showing the dependence of the piezoelectric coefficient, the relative dielectric permittivity with the stoichiometry of the potassium and sodium niobate. The other precursors are not summarised in this figure as the potassium and

sodium niobate are the main components and the addition of other parameters would complicate the visualisation.
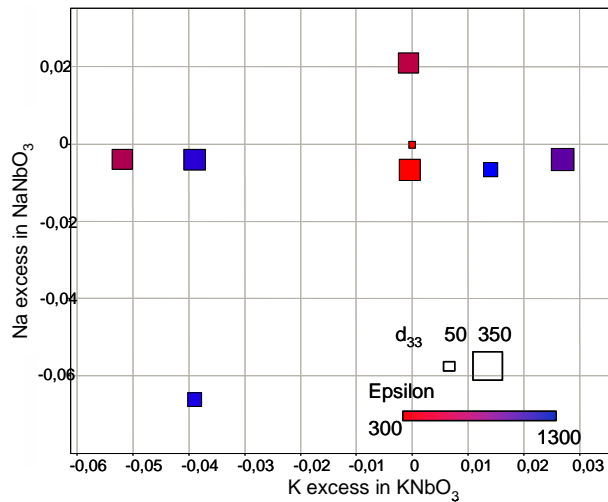
Fig. 77: dependence of electric properties of 0.93 ($K_{0.47}Na_{0.53}$)NbO$_3$ − 0.04 LiTaO$_3$ - 0.03 SCNN15 prepared with different precursors sintered at 1140°C

The dependence of the properties on the stoichiometry of the starting materials cannot be directly seen with this experimental series, therefore parameters must be handled separately. Thus in the next series which is the second part of this experimental series, different batches of NN will be tested, the other raw materials being constant.

The best properties were obtained in the second part of this experimental series for the samples processed with the NN having 1.98 mol% sodium excess, sintered at 1140°C without maintain; moreover, the relative dielectric constant of this sample is 750 and the losses are rather low (0.12). With this second experimental series high d_{33}^* values as well as low tan δ could be reproduced but correlations between the raw materials employed, the preparation, the sintering and the properties are difficult to identify at this state of the research. It has been observed that the use of NN with a slight potassium excess provides better properties of the material. A slight potassium excess into NN can have two influences on the material:

- compensate the evaporation of sodium during firing and achieve optimal equilibrium in the material

- secondary phases induced by the potassium excess can favour the sintering of the materials

Moreover no maintain should be carried out during the sintering since the desired properties decline. A dwell increases the sintering time and the probabilities of alkali

evaporation are also increased. So a dwell for this area of material compositions does not contribute to the improvement of the material.

More parameters, such as the stoichiometry of the alkali elements in the material play an essential role and will be thereafter analysed in the third experimental series.

3. Third Experimental Series: Evaluation Non-Stoichiometry

a. Experimental

It has been reported in the literature that for PZT a part of the lead evaporates during sintering, therefore, during the preparation a small lead excess is employed to compensate the evaporation[179]. For KNN-based materials the low vapour pressure of potassium and sodium can create a non-stoichiometry in the material resulting in formation of undesired secondary phases as it is the case for KN, consequently, as for PZT small excess of potassium and sodium was studied. At the same time the literature describes that a slight stoichiometric deficit in alkali elements into KNN favours the sintering[180]. A bright variation in potassium and sodium excess was studied during this experimental series and different powder combinations were also experimented to see the influence of their composition on the properties. For these libraries no sodium niobate with sodium excess was available as determined in the previous experimental series, consequently the libraries were processed with those present in laboratory, i.e. two powders with 0.4 and 0.7 mol% sodium deficit, named respectively $NN_{-0.4}$ and $NN_{-0.7}$ and the deficit was compensated with potassium carbonate.

The compositions studied were 0.97 $[(K_{0.47}Na_{0.53})_{0.94-x}Li_{0.06}]$ $(Nb_{0.94}Ta_{0.06})O_3$ − 0.03 SCNN15 with -0.04 ≤ x ≤ 0.03, i.e. a deficit of 3 mol% sodium and potassium up to an excess of 4 mol% were processed. The powders available were two potassium niobate, one with 1.4 mol% potassium excess ($KN_{1.4}$) and one with 2.7 mol% excess ($KN_{2.7}$) and the two sodium niobate described above. Four combinations were possible with these four powders:

KN$_{1.4}$/NN$_{-0.7}$

KN$_{2.7}$/NN$_{-0.4}$

KN$_{1.4}$/NN$_{-0.4}$

KN$_{2.7}$/NN$_{-0.7}$

The four combinations lead to four libraries with identical compositions prepared with the four different precursor sets. The compositions of these libraries are shown in Table **11**.

Table 11: compositions of the libraries of the experimental series

Nr.	x	Composition 0.97 [(K$_{0.47}$Na$_{0.53}$)$_{0.94-x}$Li$_{0.06}$] (Nb$_{0.94}$Ta$_{0.06}$)O$_3$ – 0.03 SCNN15
1	+0.03	0.97 [(K$_{0.47}$Na$_{0.53}$)$_{0.91}$Li$_{0.06}$] (Nb$_{0.94}$Ta$_{0.06}$)O$_3$ – 0.03 SCNN15
2	+0.02	0.97 [(K$_{0.47}$Na$_{0.53}$)$_{0.92}$Li$_{0.06}$] (Nb$_{0.94}$Ta$_{0.06}$)O$_3$ – 0.03 SCNN15
3	+0.01	0.97 [(K$_{0.47}$Na$_{0.53}$)$_{0.93}$Li$_{0.06}$] (Nb$_{0.94}$Ta$_{0.06}$)O$_3$ – 0.03 SCNN15
4	0	0.97 [(K$_{0.47}$Na$_{0.53}$)$_{0.94}$Li$_{0.06}$] (Nb$_{0.94}$Ta$_{0.06}$)O$_3$ – 0.03 SCNN15
5	-0.01	0.97 [(K$_{0.47}$Na$_{0.53}$)$_{0.95}$Li$_{0.06}$] (Nb$_{0.94}$Ta$_{0.06}$)O$_3$ – 0.03 SCNN15
6	-0.02	0.97 [(K$_{0.47}$Na$_{0.53}$)$_{0.96}$Li$_{0.06}$] (Nb$_{0.94}$Ta$_{0.06}$)O$_3$ – 0.03 SCNN15
7	-0.03	0.97 [(K$_{0.47}$Na$_{0.53}$)$_{0.97}$Li$_{0.06}$] (Nb$_{0.94}$Ta$_{0.06}$)O$_3$ – 0.03 SCNN15
8	-0.04	0.97 [(K$_{0.47}$Na$_{0.53}$)$_{0.98}$Li$_{0.06}$] (Nb$_{0.94}$Ta$_{0.06}$)O$_3$ – 0.03 SCNN15

b. Results

The relative dielectric constants and the dielectric losses of the four libraries are represented in Fig. 78 (library prepared with the combination KN$_{1.4}$/NN$_{-0.7}$), Fig. 79 (library prepared with the combination KN$_{2.7}$/NN$_{-0.4}$), Fig. 80 (library prepared with the combination KN$_{1.4}$/NN$_{-0.4}$) and Fig. 81 (library prepared with the combination KN$_{2.7}$/NN$_{-0.7}$).
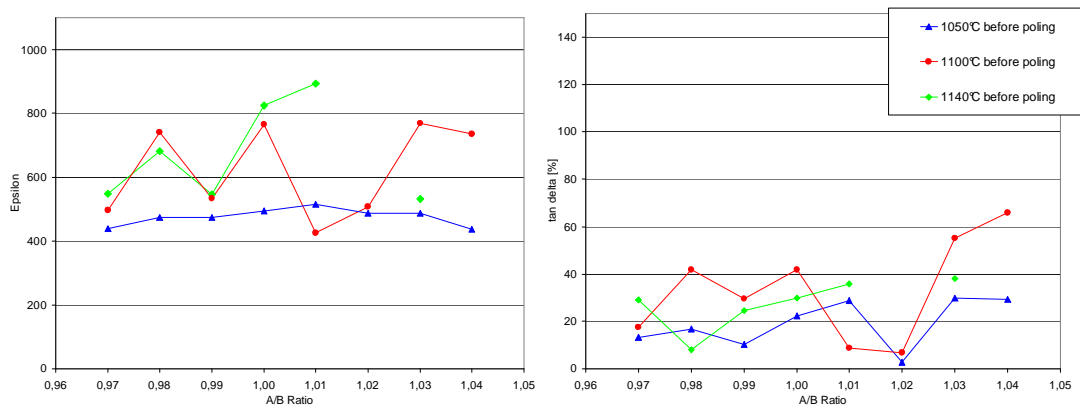
Fig. 78: relative dielectric constant and dielectric losses of 0.97 [(K$_{0.47}$Na$_{0.53}$)$_{0.94-x}$Li$_{0.06}$] (Nb$_{0.94}$Ta$_{0.06}$)O$_3$ – 0.03 SCNN15 prepared with KN$_{1.4}$ and NN$_{-0.7}$
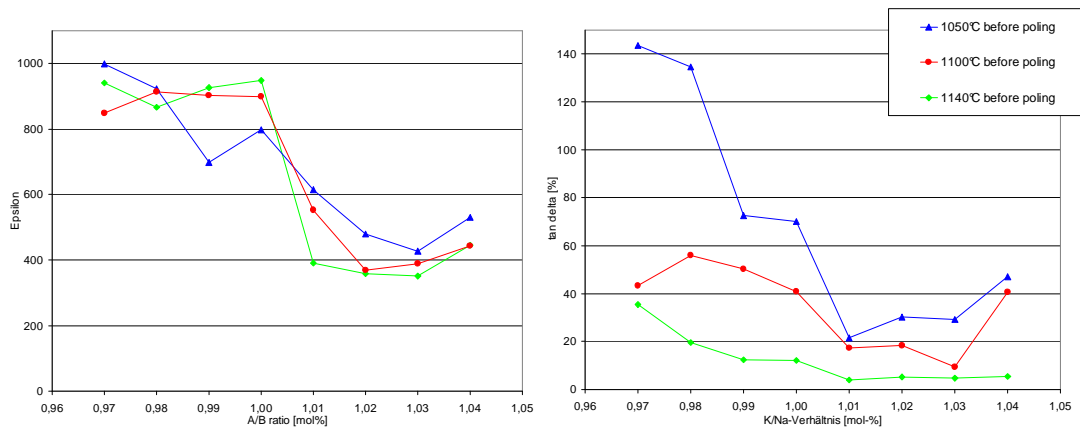
Fig. 79: relative dielectric constant and dielectric losses of 0.97 [(K$_{0.47}$Na0$_{.53}$)$_{0.94-x}$Li$_{0.06}$] (Nb$_{0.94}$Ta$_{0.06}$)O$_3$ – 0.03 SCNN15 prepared with KN$_{2.7}$ and NN$_{-0.4}$
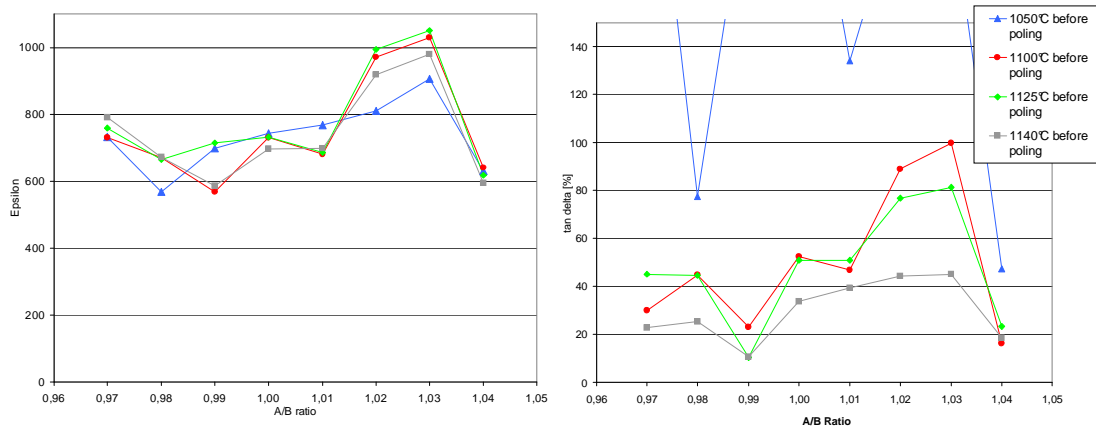
Fig. 80: relative dielectric constant and dielectric losses of 0.97 [(K$_{0.47}$Na$_{0.53}$)$_{0.94-x}$Li$_{0.06}$] (Nb$_{0.94}$Ta$_{0.06}$)O$_3$ – 0.03 SCNN15 prepared with KN$_{1.4}$ and NN$_{-0.4}$
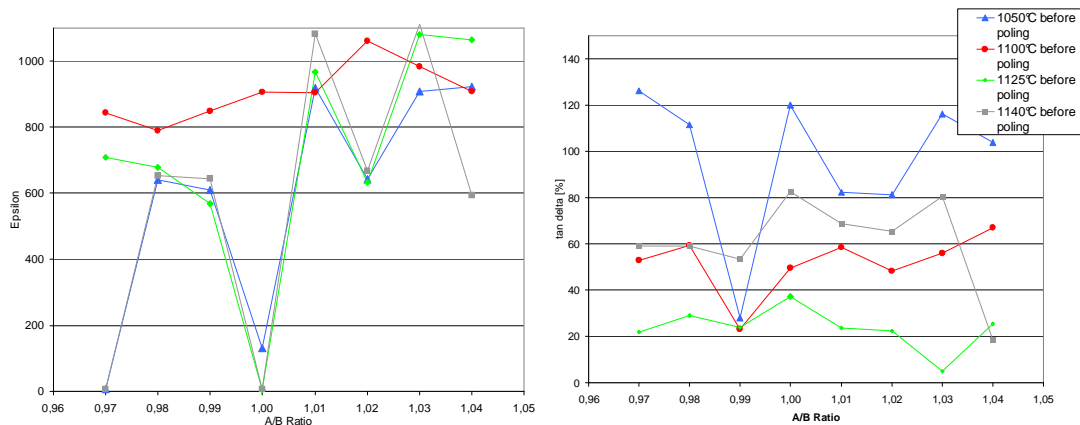
Fig. 81: relative dielectric constant and dielectric losses of 0.97 [(K$_{0.47}$Na$_{0.53}$)$_{0.94-x}$Li$_{0.06}$] (Nb$_{0.94}$Ta$_{0.06}$)O$_3$ – 0.03 SCNN15 prepared with KN$_{2.7}$ and NN$_{-0.7}$

The dielectric constants as well as the dielectric losses are different for all the libraries.

After measurements of the dielectric properties, the piezoelectric coefficients were measured, shown in Fig. 83. For these experimental series a new tool has been

employed to display the results. The automated d_{33}^* measuring machine was fully operating and the software Spotfire® was utilised to plot the results. In the automated d_{33}^* measuring machine two limiting parameters are employed to apply the electric field: either the electric field applied on the sample or the current passing through it. The amplifier used for the measurement of d_{33}^* allows a maximum current of 1 mA; if the current passes this limit no electric field is applied.

Fig. 82: capacity in function of the temperature for 0.97 [(K$_{0.47}$Na$_{0.53}$)$_{0.96}$Li$_{0.06}$] (Nb$_{0.94}$Ta$_{0.06}$)O$_3$ − 0.03 SCNN15 prepared from different precursors

Fig. 83: d_{33}^* of 0.97 [(K$_{0.47}$Na$_{0.53}$)$_{0.94-x}$Li$_{0.06}$] (Nb$_{0.94}$Ta$_{0.06}$)O$_3$ − 0.03 SCNN15 prepared from different precursors

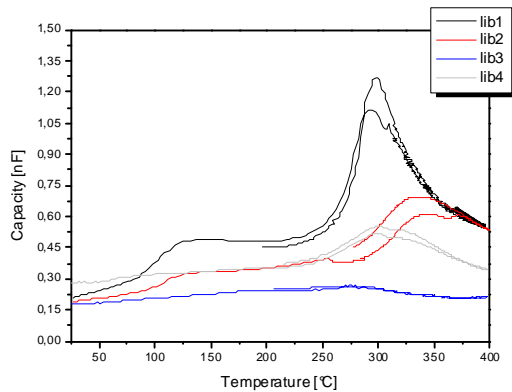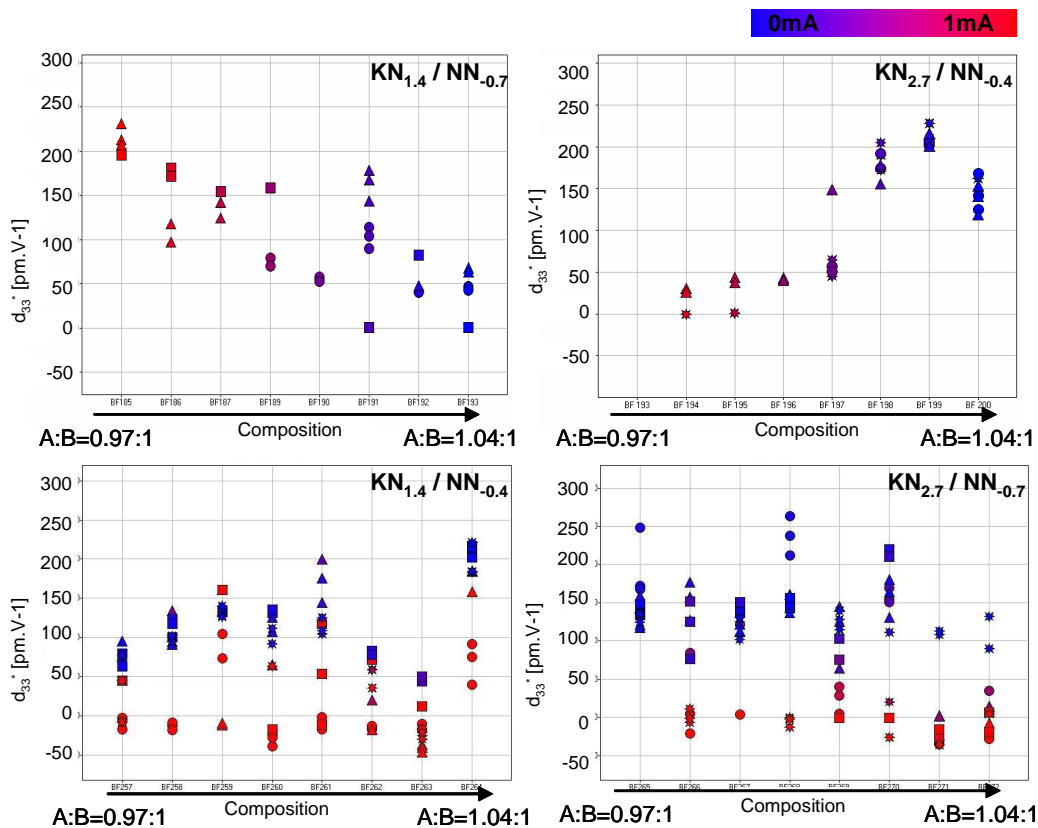The Curie temperature is the last parameter to be measured. Fig. 82 shows the curve measured on one sample of the composition $0.97 [(K_{0.47}Na_{0.53})_{0.96}Li_{0.06}] (Nb_{0.94}Ta_{0.06})O_3$ – 0.03 SCNN15 from each library.

c. Discussion

The influence of the precursor combination in this experimental series is significant. The first library, processed with $KN_{1.4}$ and $NN_{-0.4}$, shows stable values of the relative dielectric constant only for sintering at 1050℃. The va lues of ε_r of the samples sintered at higher temperatures are also higher but more scattered. The values of the dielectric losses are rather low, scattered and the minimum is situated for A/B=1.02.

The plots of the values of ε_r and tan δ of the second library, processed with $KN_{2.7}$ and $NN_{-0.4}$ follow the same profile, and both sink with higher A/B ratio. The values are lower for samples sintered at higher temperatures. The lowest value of the dielectric losses is attained for A/B ratio of 1.01 and at the same time the relative dielectric constant is about 500.

In the results of the third library, processed with $KN_{1.4}$ and $NN_{-0.4}$ the tendency visible is the same for ε_r as well as for tan δ, i.e. a peak is present around A/B=1.03, except for the samples sintered at 1050℃. High dielectric losses are often related to high conductivity therefore, in this library for high SCNN15 contents; it is difficult to discern the contribution to the relative dielectric constant from the material itself or from the conductivity. For lower A/B ratios, the losses are lower and therefore, the values of ε_r are more representative of the material properties.

The last library was processed with the more non-stoichiometric precursors, i.e. with $KN_{2.7}$ and $NN_{-0.7}$. The results of the relative dielectric losses are rather scattered except for the samples sintered at 1100℃. A slight tendency i s visible for the dielectric losses and the samples sintered at 1125℃ show the lowest losses. All the samples had lower losses for A/B=0.99 but the lowest losses were measured for the samples sintered at 1125℃ having A/B ratio of 1.02. The samples having A /B ratios higher than 1 had high relative dielectric constants.

As well as the dielectric values, the values of $d_{33}{}^*$ measured of the different libraries which are supposed to have the same compositions are totally different. For the two first libraries the values do not as strongly depend on the sintering temperature as the two last libraries. In fact the opposite tendency is detectable: for the library processed

with $KN_{1.4}$ and $NN_{-0.7}$ the values of d_{33}^{*} sink with increasing A/B ratios and for the library processed with $KN_{2.7}$ and $NN_{-0.4}$, a peak for A/B=1.03 is present.

For the second library the plot of the d_{33}^{*} values shows the opposite behaviour to that of ε_r and $\tan\delta$ and furthermore the current passing through the sample decreases with increasing A/B ratio. This tendency is distinguishable for the two first libraries. The d_{33}^{*} maximum measured for the two first libraries is almost the same: 225 pm/V.

The d_{33}^{*} values of the two last libraries are rather scattered. The curve of the dielectric measurement for the third library (processed with $KN_{1.4}$ and $NN_{-0.7}$) can be connected with the d_{33}^{*} measurement; i.e. the losses increase with increasing A/B ratio and the current passing through the samples also increases with the A/B ratio. The curve of the d_{33}^{*} values of the fourth library does not show a clear tendency either. The highest piezoelectric coefficient measured was 250 pm/V for A/B ratio of 1.

The profile of the curves of the dielectric constant as function of the temperature should be the same as they are measured on samples having the same composition. For the samples from the two first libraries the orthorhombic-tetragonal phase formation revealed in a previous chapter is present at 125°C, whereas the curve is flat in this area for the samples from the two last libraries. The Curie temperature is shifted to higher temperatures for the libraries 1, 2 and 3 (300°C for the library 1 and 3, 340°C for the library 2) and for the fourth library the curve is also flat, but a detailed view shows that the Curie temperature is situated around 270°C.

Such high differences cannot be explained only by the different stoichiometries, other parameters concerning the precursors are investigated to control the quality of the samples produced. The parameters investigated for the different precursors powders were the specific surface area determined by the BET method (results Robert Bosch GmbH), the grain size distribution measured in water and the purity determined by X-ray analysis (results Robert Bosch GmbH). The results are summarised in Table 12.

Table 12: properties of different precursors

	Lot Nr.	Potassium/Sodium excess (mol%)	BET $(m^2.g^{-1})$	XRD Presence of external phase	Grain size distribution (d_{50} in µm)
KN	20051001	+2.7	4.23	+	1.05
	20051105	+1.4	4.31	+	0.96
NN	20060205	-0.7	2.33	+	2.64
	20051115	-0.4	4.67	+++	0.98

The precursors employed show important differences for the properties measured. To reduce the differences concerning the specific surface area and the grain size distribution in the next experimental series the powders were previously ground.

The third experimental series was focussed on the relations between precursor combinations, lack of stochiometry of the weight composition and the resulting properties. The high values of 290 pm/V measured during the discovery of the new material system could not be reproduced as previously but similar values were measured (250 pm/V). However, no correlation between the high values measured and the precursors used was found. No real difference of importance between the precursors could be determined. For the two first libraries and for the fourth of this experimental series the dielectric losses were lower for higher A/B ratios, this has not necessarily a direct consequence on the values of the piezoelectric coefficient but the properties measured on samples having low tan δ are more reliable as the ε_r measured is an intrinsic property of the material and during the $d_{33}{}^*$ measurement the current remains under the limiting value given by the amplifier and the risk of spark shortening is also lower. Thereof, a slight alkali excess should improve the properties of KNN-LT-SCNN15. To verify this, further experimental series with KNN-LT-based powders with an alkali excess were prepared as basis for further investigations.

4. Fourth Experimental Series: Evaluation of alkali elements excess

a. Experimental

From the last experimental series it is though that a small potassium and sodium excess into KNN-based ceramics could improve the properties. Therefore, to try to reproduce the first results, the preparation method was the same as used during the discovery of new KNN-based ceramics, i.e. powders from the $(K,Na,Li)(Nb,Ta)O_3$ system were classically prepared and then used as base for further doping with SCNN15. The KNN was doped with 6 mol% LT as we conclude from the first experimental series and two NN as well as two KN were tested simultaneously.

Thereof, 4 powders were prepared: 2 with 1 mol% sodium and potassium excess prepared from two different sodium and potassium niobates and 2 with 2 mol% sodium and potassium excess prepared from the same powders (see Table 13).

Table 13: Research libraries for the fourth experimental series

Basic material system	K/Na Excess	Precursor combinations		SCNN15 Doping	Library
$[(K_{0,47}Na_{0,53})_{0,95}Li_{0,06}]$ $(Nb_{0,94}Ta_{0,06})O_3$	1 mol%	$KN_{1.4}$ / $NN_{-0.4}$	LKNNT1.1	0-7 mol%	1
		$KN_{2.7}$ / $NN_{-0.7}$	LKNNT1.2		2
$[(K_{0,47}Na_{0,53})_{0,96}Li_{0,06}]$ $(Nb_{0,94}Ta_{0,06})O_3$	2 mol%	$KN_{1.4}$ / $NN_{-0.4}$	LKNNT2.1		3
		$KN_{2.7}$ / $NN_{-0.7}$	LKNNT2.2		4

The first two libraries prepared from LKNNT having 1 mol% sodium and potassium excess were investigated and then the two other libraries prepared from a LKNNT having 2 mol% were studied.

The composition of the LKNNT selected was $[(K_{0.47}Na_{0.53})_{0.95}Li_{0.06}]$ $(Nb_{0.94}Ta_{0.06})O_3$, as stated before, it contains 1 mol% alkali element excess, i.e. 0.5 mol% excess sodium and 0.5 mol% excess potassium. Two powders with these compositions were classically prepared; one with a potassium niobate having 1.4 mol% potassium excess regarding niobium ($KN_{1.4}$) and with a sodium niobate having 0.4 mol% sodium deficit regarding niobium ($NN_{-0.4}$), called powder LKNNT1.1, the second powder was prepared with a potassium niobate having 2.7 mol% potassium excess regarding niobium ($KN_{2.7}$) and with a sodium niobate having 0.7 mol% sodium deficit regarding niobium ($NN_{-0.7}$), called LKNNT1.2. These powders were subsequently doped with SCNN15 between 0 and 7 mol% with 1 mol% steps.

b. Results: 1 mol% sodium and potassium excess

The preparation of these powders allows reducing the differences concerning the specific surface area and the grain size distribution. Fig. 84 shows the particle size distribution of different powders. Typical curves of a sodium niobate and lithium carbonate were added to see the benefits of previous grinding of the powders on the particle size distribution. The grinding of Li_2CO_3, KN, NN and KT (and eventually Nb_2O_5, K_2CO_3 and Na_2CO_3) allows a unimodal particle size distribution of all powders. When the powders were ground at the same time, with similar grinding medium (ZrO_2-

spheres) and in similar grinding cup, the particle size of both powders for the binary libraries was approximately the same allowing a better mixing of both powders in the Speedmixer®.
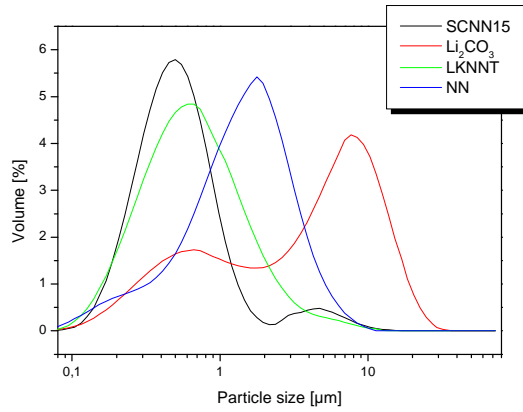
Fig. 84: particle size distríbution of different powders

The results of the dielectric measurements for the library prepared with LKNNT1.1 are shown in Fig. 85 and those for the library prepared with LKNNT1.2 are shown in Fig. 86.

Fig. 85: relative dielectric constant and dielectric losses of 1-x $[(K_{0.47}Na_{0.53})_{0.95}Li_{0.06}]$ $(Nb_{0.94}Ta_{0.06})O_3 - x$ SCNN15 prepared from LKNNT1.1

Fig. 86: relative dielectric constant and dielectric losses of 1-x [(K$_{0.47}$Na$_{0.53}$)$_{0.95}$Li$_{0.06}$] (Nb$_{0.94}$Ta$_{0.06}$)O$_3$ – x SCNN15 prepared from LKNNT1.2

The Fig. 87 shows the d$_{33}$* measured in function of the compositions, i.e. of the concentration of SCNN15, furthermore, the colour displays the maximal current measured. Both diagrams show a maximum for different compositions. The library prepared with LKNNT1.1 shows a maximum for 1 mol% SCNN15 about 225 pm/V and the maximum of the second one is situated for 4 mol% SCNN15 with a value of d$_{33}$*=160 pm/V.
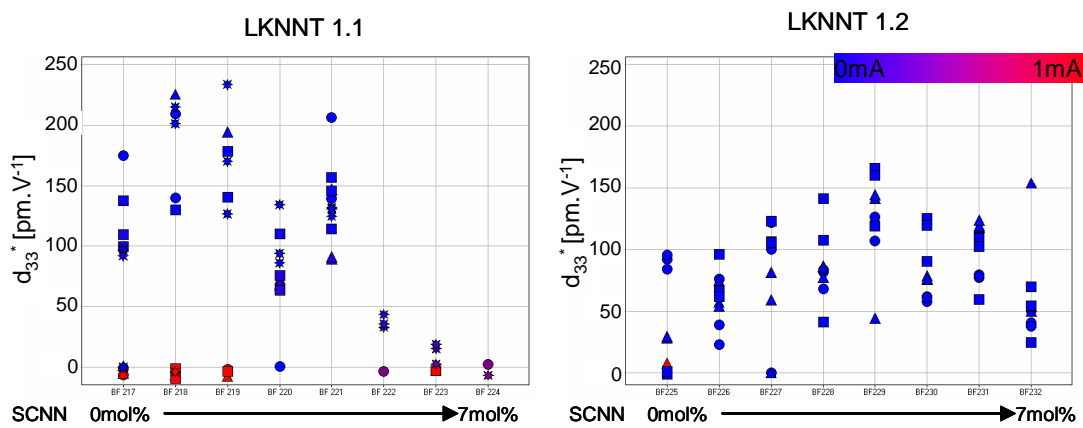
Fig. 87: d$_{33}$* of 1-x [(K$_{0.47}$Na$_{0.53}$)$_{0.95}$Li$_{0.06}$] (Nb$_{0.94}$Ta$_{0.06}$)O$_3$ – x SCNN15

Nevertheless to understand the reason of higher properties for samples containing 1 up to 2 mol% SCNN15 with LKNNT1.1, microstructure images were collected by means of SEM. The evolution of the microstructure depending on the SCNN15 content is visible in Fig. 88.
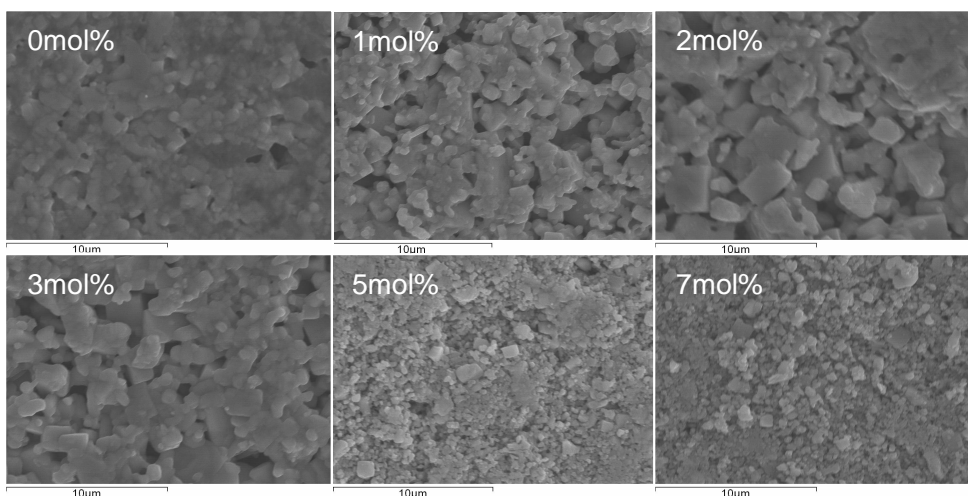
Fig. 88: microstrucure of 1-x [(K$_{0.47}$Na$_{0.53}$)$_{0.95}$Li$_{0.06}$] (Nb$_{0.94}$Ta$_{0.06}$)O$_3$ – x SCNN15 prepared from LKNNT1.1

The Curie temperature was measured for samples containing different doping levels as shown in Fig. 89.
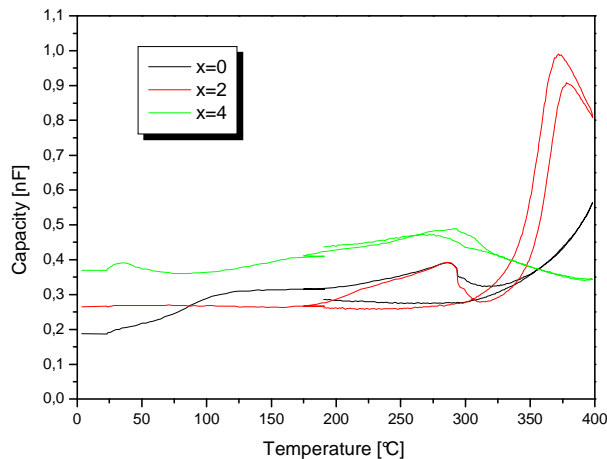
Fig. 89: Curie temperature of 1-x [(K$_{0.47}$Na$_{0.53}$)$_{0.95}$Li$_{0.06}$] (Nb$_{0.94}$Ta$_{0.06}$)O$_3$ – x SCNN15 prepared from LKNNT1.1

c. Results: 2 mol% sodium and potassium excess

The second part of the investigation was pursued with two LKNNT powders having 2 mol% potassium and sodium excess, therefore its formula was [(K$_{0.47}$Na$_{0.53}$)$_{0.96}$Li$_{0.06}$](Nb$_{0.94}$Ta$_{0.06}$)O$_3$. The precursors employed to prepare both powders were the same as previously, i.e. one powder was prepared with a potassium niobate having 1.4 mol% potassium excess regarding niobium and with a sodium niobate having 0.4 mol% sodium deficit relative to niobium, called powder LKNNT2.1 and the second powder was prepared with a potassium niobate having 2.7 mol% potassium excess relative to niobium and with a sodium niobate having 0.7 mol% sodium deficit relative to niobium, called LKNNT2.2. Both LKNNT were doped with SCNN15 between 0 and 7 mol%. The results of the dielectric measurement are displayed in the Fig. 90 for the library prepared from LKNNT2.1 and in the Fig. 91 for the library prepared from LKNNT2.2.
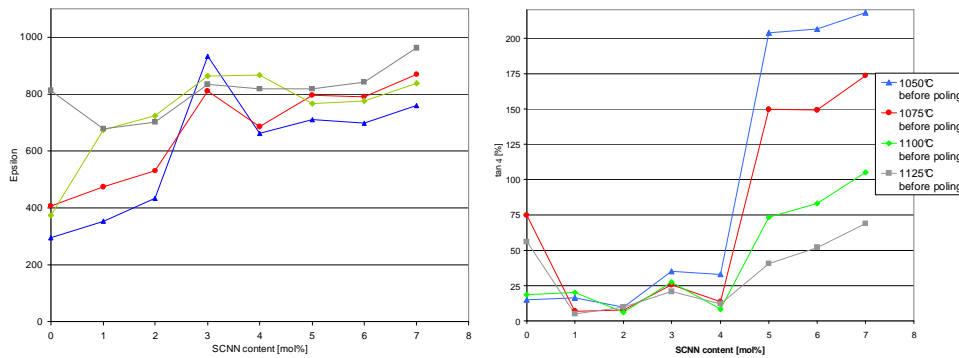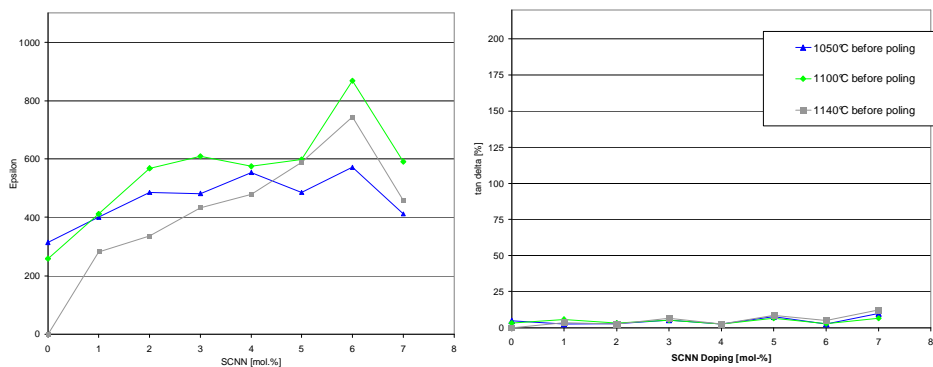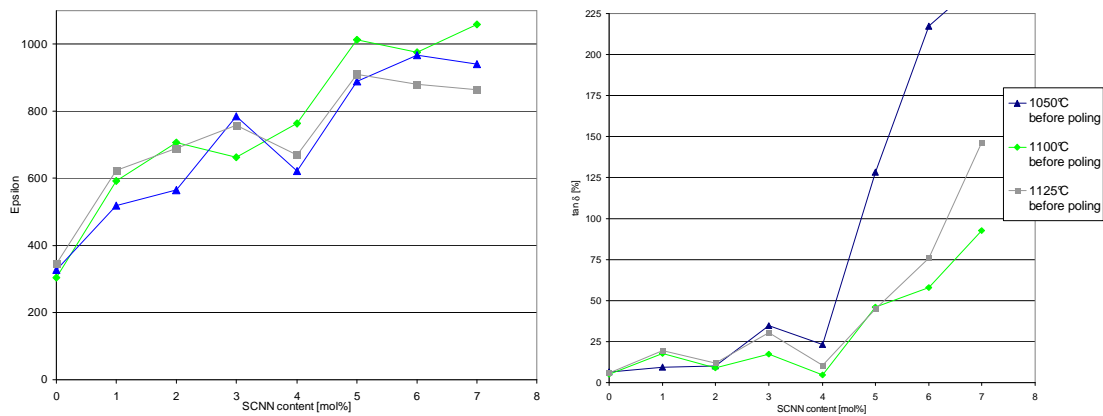
Fig. 90: relative dielectric constant and dielectric losses of 1-x [(K$_{0.47}$Na$_{0.53}$)$_{0.96}$Li$_{0.06}$] (Nb$_{0.94}$Ta$_{0.06}$)O$_3$ – x SCNN15 prepared from LKNNT2.1
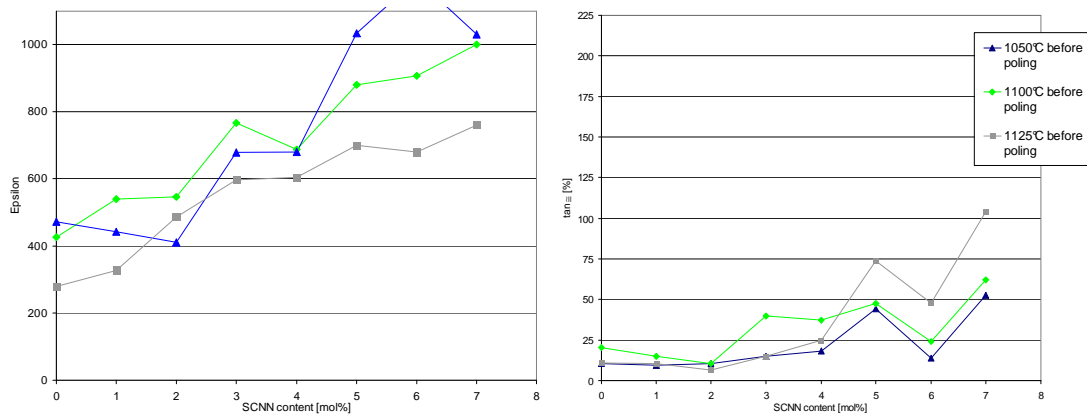
Fig. 91: relative dielectric constant and dielectric losses of 1-x [(K$_{0.47}$Na$_{0.53}$)$_{0.96}$Li$_{0.06}$] (Nb$_{0.94}$Ta$_{0.06}$)O$_3$ – x SCNN15 prepared from LKNNT2.2
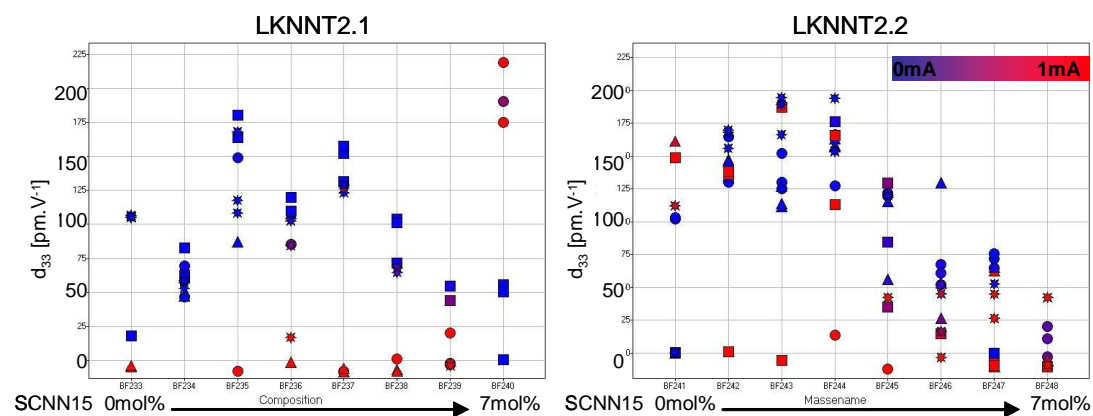
Fig. 92: d$_{33}$* of 1-x [(K$_{0.47}$Na$_{0.53}$)$_{0.96}$Li$_{0.06}$](Nb$_{0.94}$Ta$_{0.06}$)O$_3$ - x SCNN15 prepared with different precursors

The values of d_{33}^* of both libraries which are plotted in Fig. 92 are scattered. However a maximum is visible for both about 2 mol% SCNN15 doping as it was the case for the other libraries of this experimental series.

The diagram of the capacitance in function of the temperature of samples of the compositions 1-x $[(K_{0.47}Na_{0.53})_{0.95}Li_{0.06}](Nb_{0.94}Ta_{0.06})O_3 - x$ SCNN15 prepared from the two different LKNNT with 2 mol% sodium and potassium excess is displayed in Fig. 93.
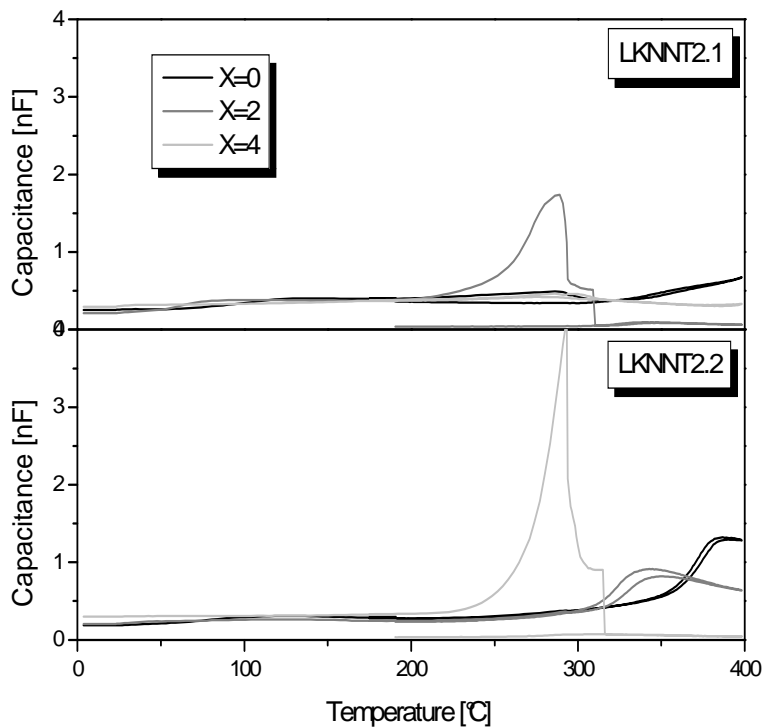
Fig. 93: Capacitance in function of the temperature 1-x $[(K_{0.47}Na_{0.53})_{0.96}Li_{0.06}](Nb_{0.94}Ta_{0.06})O_3$ - x SCNN15 prepared with different precursors

d. Discussion

The library prepared with LKNNT1.1 shows dramatically high dielectric losses for high doping level (<4 mol%) and these are moreover dependent on the sintering temperature. For lower sintering temperatures the losses are higher, since the samples are not as dense as samples sintered at higher temperatures. Samples containing between 1 and 4 mol% SCNN15 show satisfying dielectric properties; the relative dielectric constants are situated between 400 and 900 and the losses are under 25%.

The library prepared with LKNNT1.2 shows a different behaviour concerning the relative dielectric constant and the dielectric losses. The dielectric constant are generally not as high as the previous library and a peak for 6 mol% SCNN is present where the value attains 800. The losses are low and independent of the SCNN15 content.

In both libraries it is possible to see a positive effect of the addition of SCNN15 to LKNNT prepared from KN and NN precursors: the dielectric constants are higher for doped samples and the losses are partially lower. To see if the results of the dielectric measurement are really satisfying, the piezoelectric coefficient d_{33}^{*} must be also measured and the influence of the SCNN15 doping must be evaluated.

The morphology and shape of the grains is different to those observed during the first phase of the development of new material systems (see Chapter 7.2). The density of the samples seems to be rather constant with the increase of the doping content. The average crystallite size increases between 0 and 2 mol% SCNN15 from 1 to 3μm and then decreases for 3 mol% and more SCNN15 to 0.5 μm. The microstructure analysis of samples from the library prepared from LKNNT1.1 shows that the doping with 2 mol% leads to more homogenous grain size distribution as well as larger grains.

The behaviour observed with the samples during the Curie temperature measurements from this experimental series is similar to those observed during the first phase of development of this material system. For high level of doping (4 mol% SCNN15 in Fig. 89) a peak of low intensity is visible around 280℃ which indicates the Curie temperature of this sample. For the non-doped sample a shoulder around 125℃ appeared, which can be interpreted as the orthorhombic to tetragonal phase transformation, whereas for the samples doped with 2 mol% SCNN15, this shoulder is not present. Both non-doped and 2 mol%-doped samples show a peak around 280℃ during heating which was not present during cooling. The non-doped sample seems to have a Curie temperature higher than 400℃ and the 2 mol%-doped samples a Curie temperature around 370℃ (see Fig. 89). The dopants have the same effect onto KNN-based ceramics as on other piezoelectric materials, i.e. the Curie temperature sinks with the doping level. Additionally, the addition of this doping seems to lead to the disappearance or the shifting of the orthorhombic-tetragonal phase transformation as no shoulder is visible on the curve of the doped samples. Therefore it seems that this dopant shifts the both transitions temperatures of KNN.

In the second part of the fourth experimental series the evolution of the values of the relative dielectric constant and the dielectric losses for two libraries of the same

composition is rather similar. The relative dielectric constant ε_r increases with the SCNN15 content and the dielectric losses are dramatically high in the library prepared from LKNNT2.1 for SCNN15 contents exceeding 4 mol%. The dielectric losses of the library prepared from LKNNT2.2 are not as high after 4 mol% SCNN15 doping but a slight increase is visible. As it is the case for the libraries prepared with 1 mol% sodium and potassium excess the library prepared with the precursors $KN_{2.7}$ and $NN_{-0.7}$ the values of the dielectric losses are lower than the values of the dielectric losses of the library prepared with the precursors $KN_{1.4}$ and $NN_{-0.4}$.

The behaviour of samples having the same theoretical composition is different. The non-doped samples prepared from LKNNT2.1 shows a Curie temperature higher than 400°C whereas the sample prepared with LKNNT2.2 shows its maximal capacitance at about 380°C. The 2 mol%-doped LKNNT2.1 shows a maximum about 280°C and the sample with the same composition prepared with LKNNT2.2 has a Curie temperature of 340°C. The sample doped with 4 mol% SCNN15 prepared from LKNNT2.1 shows a weak maximum about 280°C, whereas the sample with the same doping level but prepared from LKNNT2.2 shows a net capacitance maximum at the same temperature.

In this experimental series the morphology of the precursors cannot be the cause of the difference between the results of four libraries as both LKNNT were ground before being used as starting powder for a binary library with SCNN15 and they show a narrow grain size distribution. One of the only parameter which could cause such differences is the stoichiometry of the precursors and thereof, the presence of unidentified phases together with the perovskite phases.

The excess of alkali elements into TB-doped KNN shows positive effects on the sample quality. The conductivity of the samples proportional to the maximal amperage measured during d_{33}^{*} measurement was lower for these experimental series than in the previous ones. Moreover, it has been shown that the dielectric and piezoelectric properties of KNN-based ceramics improved with the addition of SCNN15 for all libraries of this experimental series. The high temperature behaviour is rather different for samples having the same compositions from the different libraries. In both cases the Curie temperature decreases with SCNN15 doping.

5. Conclusion

The goal was the optimisation of one of the most promising lead-free compositions developed in a previous phase, SCNN15-doped LKNNT. However reproduction problems were rapidly met, which were partly attributed to a different processing route on one side and to the use of different niobate precursors on the other hand. Despite these reproduction problems some improvements regarding the LT doping could be accomplished in the first part and it has been observed that 6 mol% LT into SCNN15-doped KNN leads to superior properties. Other experimental series were studied to try to understand the relationship between the precursor compositions, their combination and the properties measured for the piezoelectric samples. It has been found that a sodium excess of about 1-2 mol% in the sodium niobate precursor allows to improve the properties of KNN-based samples. The third experimental series focussed on the lack of stochiometry between A and B sites and four libraries were carried out with the same compositions and different precursor combinations. The properties measured were different for all libraries but a slight improvement of the sample quality could be detected through the measurement of the dielectric losses for samples having an excess of alkaline elements (A/B > 1). Therefore, in the last experimental series 4 different starting KNN powders with 1 and 2 mol% sodium and potassium excess as well as 6 mol% LT were prepared and doped with SCNN15. The quality of the samples improved and the maximal current measured for the majority of the sample was lower than 1mA. The 4 libraries showed the same tendencies, a peak of the piezoelectric coefficient at 1-2 mol% SCNN15.

The optimisation of the LKNNT-SCNN15 carried out in this part did not allow to reproduce the sample with the same quality as first discovered, but some parameters are now assessed to achieve superior material properties:

- the NN-precursor employed should have a sodium excess of about 1 mol%

- sodium and potassium excess into KNN of 1 mol%

- LT content of 6 mol%

- SCNN15 content of 1-2 mol%

- narrow particle size distribution of the different powders before calcination

Despite the reproduction difficulties met during the optimisation of the material composition, satisfying properties could be constantly measured like a relative dielectric constant ε_r about 700, dielectric losses tan δ about 0.1 and a large piezoelectric coefficient d_{33}^* of 225 pm/V.

IX.   Experimental

1. Sample preparation

The samples were prepared with the method described in the chapter 6. The throughput of the compositions was not high enough to require the use of software and they were individually determined. The programming of a software was difficult due to the use of precursors with different stochiometry. For example to produce $[(K_{0.47}Na_{0.53})_{0.94}Li_{0.06}](Nb_{0.84}Ta_{0.1}Sb_{0.06})O_3$ from the precursors $KN_{1.4}$ and $NN_{-0.6}$, if the alkali ions had been provided only by the precursors to avoid the use of carbonates, the quantity of niobium would have been too high as shown in Table 14.

Table 14: composition calculation (1)

Precursor	Quantity (mol)	Alkali ions (mol)	Niobium ions (mol)
$KN_{1.4}$	0.4357	0.4418	0.4357
$NN_{-0.6}$	0.5015	0.4982	0.5015
Sum		0.94	0.9372

Therefore, the quantity of precursors had to be adjusted and it was decided that each precursor should deliver the same amount of niobium. Hence the maximal quantity of precursor was fixed out 0.42 mol and the rest of alkali ions were inserted as carbonates as shown in Table 15.

After calculation of each composition, the final stochiometry was controlled by means of Excel. After the determination of the stochiometry; the weight of each raw material for the 8 compositions of a library was calculated and recorded.

Table 15: composition calculation (2)

Raw material	Quantity (mol)	Alkali ions (mol)	Niobium ions (mol)
$KN_{1.4}$	0.42	0.42588	0.42
$NN_{-0.6}$	0.42	0.41723	0.42
Na_2CO_3	0.080972	0.08097	
K_2CO_3	0.01592	0.01592	
Sum		0.94	0.84

The powders were weighted per hand up to the fourth decimal place to find a balance between precision and time spend. The weighting up to the second decimal induced a maximal error of 15 mol % and the weighting up to the third decimal a maximal error of 2 mol % as shown in

Table 16 as example of the composition $0.97[(K_{0.47}Na_{0.53})_{0.95}Li_{0.06}](Nb_{0.94}Ta_{0.06})O_3 - 0.03$ SCNN15 prepared from the raw materials $KN_{1.4}$, $NN_{-0.6}$, Li_2CO_3, Ta_2O_5, Na_2CO_3 and SCNN15.

The error was amplified for raw materials with a lower molar weight like sodium and lithium carbonates. The truncation at the third decimal was considered acceptable for almost all components except sodium carbonate. The control of the stochiometry is crucial for KNN-based ceramics, therefore, an approximation of 2 mol% was not acceptable and the weighting should be made with a precision up to the fourth decimal which deliver admissible results without loosing a lot of time.

After weighting of the powders in 50ml plastic cup adapted for Speed-mixer® they were mixed for 1 min at 2000 revolution/minute with 20ml alcohol as homogenising liquid. Tests were pursued to determine the best parameter as shown in Fig. 94. The dry mixed powders were not homogenous, white and black grains (from KN, NN and CuO) could be distinguished. The homogenisation with alcohol gave better results. The mixing time of only 30s was not sufficient to break all the agglomerates, and it is only after 1min that the homogeneity of the powders seemed to be sufficient.

After mixing the powders were dried and inserted in 10x20x10mm³ alumina calcination crucibles. The small size of the calcination crucibles allows the parallel calcination of all powders at the same time in one oven.

Table 16: molar error induced by weighting precision

Raw material	Quantity for 0.1mol (mol)	Weight	Min. weight 3 decimal	Max. weight 3 decimal	Min. mol	Max. mol	Error
$KN_{1.4}$	0.04271	7,8030	7,802	7,804	0,042701	0,042718	±0.03%
$NN_{-0.6}$	0.04846	8,0152	8,015	8,016	0,048456	0,048472	±0.02%
Li_2CO_3	0.00582	0,2150	0,214	0,216	0,005793	0,005848	±0.5%
Ta_2O_5	0.00582	1,2859	1,285	1,286	0,005816	0,005820	±0.07%
Na_2CO_3	0.00069	0,0385	0,038	0,039	0,000683	0.000700	±2%
SCNN15	0.003	3,0217	3,021	3,022	0.002999	0.003000	±0.005%

Raw material	Quantity for 0.1mol (mol)	Weight	Min. weight 2 decimal	Max. weight 2 decimal	Min. mol	Max. mol	Error
$KN_{1.4}$	0.04271	7,8030	7,80	7,81	0,042696	0,04275	±0.1%
$NN_{-0.6}$	0.04846	8,0152	8,01	8,02	0,048436	0,048496	±0.07%
Li_2CO_3	0.00582	0,2150	0,21	0,22	0,005684	0,005955	±2.5%
Ta_2O_5	0.00582	1,2859	1,28	1,29	0,005793	0,005839	±0.5%
Na_2CO_3	0.00069	0,0385	0,03	0,04	0,000566	0.000755	±15%
SCNN15	0.003	3,0217	3,02	3,03	0.002998	0.003008	±0.07%

Fig. 94: Powder mixing with Speedmixer

After the calcination the powders were ground in a planetary ball milling machine. The maximal throughput of the planetary ball milling machine is 8 powders parallel ground into 80 ml zirconium oxide grinding cup. The optimal grain size in function of the grinding medium was given by the constructor (Fritsch GmbH) and they recommended 30 10 mm diameter zirconium oxide ball for the 80 ml grinding cups. The powders were grinded during 3 hours to obtain an optimal grain size repartition as shown in Fig. 95.
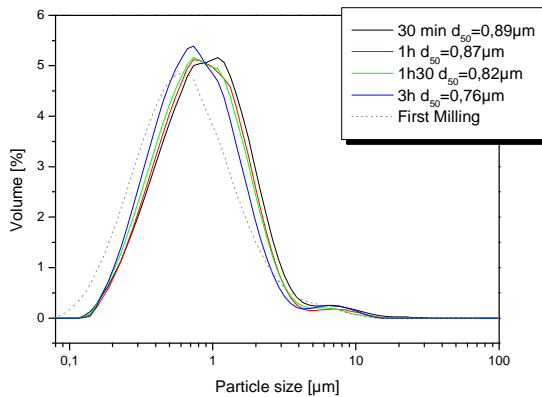

Fig. 95: Particle size distribution after different milling time

The pressing took place in specially designed silicon moulds as shown in Fig. 16. Due to the pressing in a isostatic press, the powders did not need the presence of any binder to be pressed. One composition filled in one mould produce 20 samples of each new composition. After filling of the moulds, they were sealed in a plastic bag and put in the cavity of a wet bag isostatic press (Dieffenbacher, Isomat CIP-Anlage). They were pressed up to 3000 bar during 1 min. No variations of these parameters were done as they were the typical parameters adjusted for this press.

To avoid the diffusion effect of the samples with the sintering medium or sintering plate, 5 samples of each composition were pilled up on a platinum foil and were encapsulated in a zirconium oxide sintering boat. The boat was placed in an oven and the desired temperature programme was carried out.

For the characterisation the samples, their surfaces had to be parallel ground. To maintain the throughput and to achieve the same thickness for all samples of a library (which is later important for the measurement of d_{33}^{*}) all the samples of a library were glued by means of wax on the grinding plate and parallel ground on both side of the samples.

The metallization of the samples was carried out by means of silver vapour deposition. The samples were placed in a silicon matrix, which sustains them in the silver vapour deposition machine (Leybold-Heraeus). A silicon matrix could contain the half of a library (48 samples) and to contact them around 1g of silver was necessary.

2. Characterisation

a. Electro-mechanical characterisation

All the produced samples were electrically characterised as stated in the chapter $. The measurement of the relative dielectric constant was achieved by the measurement of the capacitance with a capacitance bridge (Wayne Kerr Automatic Precision Bridge B905). To obtain the value of the relative dielectric constant, the thickness and diameter of the sample must be taken into account. Equation 1.15 defines the calculation of the relative dielectric constant of the material.

$$C = \varepsilon_0 \times \varepsilon_r \times \frac{A}{t}$$ (1.15)

where C is the capacitance measured, ε_0 is the permittivity of the air = $8.85.10^{-12}$ F/m, A is the area of the electrode and t the thickness of the sample.

The dielectric losses are measured at the same time. They are determined as the tangent of the phase loss during the measurement of the capacitance.

In the literature the piezoelectric coefficient d_{33}, which is measured via the direct piezoelectric signal, is often used to asses the material properties. However, as the goal of the project was to find a replacement for PZT in the actuator industry, the large signal piezoelectric coefficient d_{33}^*, which is measured with the indirect piezoelectric response was selected. The measurement of d_{33}^* with a robot was described in a previous chapter.

The definition of d_{33} is the current developed by a material in the poling direction submitted to a force in the poling direction per unit length; its unity is the C/N. The definition of d_{33}^* is the strain developed in the poling direction under an applied electric field in the poling direction per length unit and its unity is m/V. Both d_{33} represent the piezoelectric coefficient measured via direct or indirect piezoelectric effect. The goal of this project was to find new materials to replace PZT in the actuator industry; where the

large signal piezoelectric coefficient is often used. Therefore to asses the piezoelectric material properties d_{33}^* was measured.

For the measurement, the thickness of the samples is needed as d_{33}^* is a coefficient relative to unit length. As all the samples of a library are ground together the thickness is the same for all samples and is known. After silver vaporisation on the surface of the samples these are put onto a plate containing wells and the automated measurement of a whole library can be carried out. The description of the d_{33}^* measurement robot is described in chapter 4.2.6.

b. Curie temperature

The Curie temperature of each composition was measured with bulk samples. Up to ten samples could be parallelly positioned in an oven between two contacts protected by alumina and heated up to the desired temperature with the selected ramp. The capacitances were recorded at constant time intervals.

After measurement the data were processed with Origin and the temperature of maximal capacitance is the Curie temperature of the sample.

c. X-ray analysis

The X-ray analysis (Siemens SD500) was carried out on selected sintered samples, calcinated powder and on raw materials to analyse the phases present qualitatively as well as quantitatively. The diffractogrammes were recorded in an angular zone of $[10°, 80°]_{2\theta}$ with an increment of $0.02°$ and a measuring time of 5sec for each step. The acceleration voltage was 40 kV and the current at the anode was 15mA.

After record of the diffractogrammes the data were analysed and compared with ASTM data (American Society of Testing and Measuring). The qualitative measurements were carried out comparing the location of the reflexes and the quantitative measurements were carried out comparing their intensity.

d. Dilatometer measurement

Dilatometer measurements (Netschz DIL402PC) were carried out in order to observe the behaviour of the samples during sintering. Powders of the selected samples were filled in silicon barrels with dimensions of 8 mm diameter and 10 mm height. These small barrels were subsequently uniaxially pressed up to 3000 bar to obtain pellets having the same properties in all directions. Subsequently the pellets were grinded to obtain plane parallel surfaces.

Afterwards the samples were placed in the dilatometer and held with an alumina stem fixed to an inductive sensor. The dilatometer measurements took place in a temperature range from 25℃ to 1150℃ with a ramp o f 10 K.min^{-1}.

e. Microstructure analysis by means of SEM

For the study of the microstructure the samples were first gradually polished up to 1µm and thermally etched. The chemical etching on KNN-based samples was not easy as the niobium oxide is chemically extremely stable; therefore, thermal etching was carried out at a temperature of about 100℃ lower th an the sintering temperature.

After etching the samples were glued on a support. To impeach electrical charging of the surface of the sample through the electron beam, the samples were sputtered with platinum. After the sample preparation, the microstructure analyses were carried out by means of a scanning electron microscope.

The secondary electron detector (Hitachi S-4100) allows taking different micrographs of the samples. To analyse the crystallite size distribution about 200 grains were detected in different areas of the sample to ensure that all the distributions were considered.

f. Differential Scanning Calorimetry (DSC)

The DSC (Netzsch DTA404PS Eos) was used to detect the phase transformation during calcination and sintering. DSC is a thermo-analytical technique in which the difference of heat amount required to increase the temperature of a sample and a reference as function of the temperature is measured. The reference sample used was made of aluminum oxide which has a linear heat capacity over a large range of temperatures. The sample as well as the reference were placed in platinum crucible and heated up to 1200℃ at a heating rate of 10 K/m in.

g. Specific Surface Area (SSA)

The SSA determine the total specific external and internal surface area of disperse or porous solids by measuring the amount of physically adsorbed nitrogen according to the method of Brunauer, Emmett and Teller[181] (BET method).

h. Grain size distribution

The grain size distribution was analysed via laser diffraction analysis (Malvern Instruments). The apparatus allows the grain size distribution of wet powders; therefore, the powders were mixed with distilled water and dispergator and homogenised 2 min with ultra-sounds. Consequently the solution was measured for 1 min.

3. Data management

All the data concerning the production of the samples as well as their properties measured were recorded in a database created for the design of the plates and the properties measured. The databases as well as the table used for the download of the results were created by the project partner of the chair of Technical Chemistry at the University of Saarbrücken. The download of the information was divided on two parts. First the processing of the samples was recorded in the database with help of a specially designed excel sheet. Then the measured properties were also registered in another specially designed Excel sheet and also downloaded in the same database. The overview on all the registered samples could be done connecting the database to a visualising software, Spotfire®.

a. Samples Processing

Different powders were used to process the samples. The first step was to record of the powders in the database. A dummy samples should be created to enlist the powders, i.e. the dummy sample was recorded per hand in the database as well as the powders composing it. For each powder used, the stochiometry is recorded as shown

in Fig. 96. The precursor registered in this example is $KNbO_3$ (Lot. 20070612). From the X-ray fluorescence analysis given by the provider, the stochiometry calculated was $K_{0.992}Nb_1O_{3-\delta}$. As the sum of the compounds except oxygen should be 100%, the composition of this precursor was calculated and this compound contained 49.98 mol% potassium and 50.02 mol% niobium. The composition is written as _P:Nb/50,02-K/49,98-.

Fig. 96: Data import for new chemicals

At the same time the raw materials are recorded in the database, different processing must also be recorded with the same dummy sample. In the database different processing steps (Method) could be chosen like pipetting, coating, milling, etc. To process the bulk samples, variations were introduced in the method as calcination and sintering temperature, dwell and ramp. Few methods were often used as KNN-based materials calcine and sinter about the same temperatures.

After recording of the raw materials (new chemicals) and methods in the database the sample compositions and processing can be downloaded. The number of samples is rather high to register them as single samples in the database. Therefore, an Excel sheet with all the samples processed in a library was developed in parallel to the database. Libraries are composed of 8 different compositions, processed with 4 different parameters and 3 samples per composition and processing are available, that means that a library contains 96 samples. In the Excel sheet a sequential number is given to all samples (S2_001_XXXX), the number of the sample in the library, the composition by the chemicals employed and their content, the method, operator, date of synthesis and the X and Y position in the d_{33}^* robot. The Fig. 97 gives an overview of this Excel sheet. The boxes marked in blue are those to fill.

Fig. 97: Excel sheet employed to download the samples compositions and processing of one library

The composition of the samples is given in mol % and must be calculated for each new composition. For example, to prepare the following composition $0.97[(K_{0.47}Na_{0.53})_{0.95}Li_{0.06}](Nb_{0.94}Ta_{0.06})O_3 - 0.03$ SCNN15 the quantity of each powder is calculated and normalised as shown in Table 17.

Table 17: normalisation of composition

Chemical	Lot. Number	Quantity for 1 mol (mol)	Mol. %
KN	20051105	0.427125	42.42
NN	20060205	0.484675	48.13
Li_2CO_3		0.0291	2.89
Ta_2O_5		0.0291	2.89
K_2CO_3		0.00692	0.69
SCNN15		0.03	2.98

b. Results

After filling the Excel sheet for the samples processing, it can be downloaded in the database. Each sample is recorded with a sequential number as well as X and Y coordinates, which must be used to record the properties measured of the samples. To download the properties, an Excel sheet must be also created. The sample name is then changed to S2_001_XXXX X=x Y=y. For the evaluation of the properties, different key parameters were measured and a selection of them was done and these were recorded in the database. The relative dielectric constant and dielectric losses before and after poling, d_{33}^{*} by 1 and 2 kV/mm and the Curie temperature were always

recorded. Additional parameters could also be recorded as the coercive field and the remnant polarisation.

Remark	Nummer	Eps_v	tan_v_in_Prozent	Eps_n	tan_n_in_Prozent	d33_[pm_V-1]_1kVmm-1	d33_[pm_V-1]_2kVmm-1	TkC[10-6_pro_K]	Tcurie_in_dC	Ec	Pr	Operator	Date_of_measurement	X-Par	Y-Par
X	1	709,00	64,09									AC	24.4.2006	1	1
X	2	747,00	66,17									AC	24.4.2006	2	1
X	3	728,00	69,30									AC	24.4.2006	3	1
OK	4	740,00	68,95			164,94	163,54					AC	24.4.2006	4	1
X	5	695,00	57,81									AC	24.4.2006	5	1
X	6	802,00	73,57									AC	24.4.2006	6	1
OK	7	705,00	47,06	715,00	34,78		116,95					AC	24.4.2006	7	1
OK	8	733,00	40,55	673,00	32,21	184,66	114,15					AC	24.4.2006	8	1
OK	9	797,00	41,93	707,00	29,78	190,46	114,15					AC	24.4.2006	9	1
OK	10	699,00	25,61	658,00	22,86	224,24	150,39					AC	24.4.2006	10	1
OK	11	701,00	25,94	646,00	22,27	175,31	124,16					AC	24.4.2006	11	1
OK	12	706,00	26,72	656,00	24,26	202,38	152,62					AC	24.4.2006	12	1
OK	13	769,00	29,14	683,00	21,07	191,89	128,90					AC	24.4.2006	1	2
OK	14	794,00	29,47	699,00	21,09	173,84	123,02					AC	24.4.2006	2	2
OK	15	912,00	41,37	777,00	28,28	178,42	112,56					AC	24.4.2006	3	2
OK	16	741,00	22,22	698,00	20,41	166,74	126,48					AC	24.4.2006	4	2
OK	17	721,00	19,88	673,00	16,97	189,06	135,99					AC	24.4.2006	5	2
OK	18	802,00	28,18	727,00	21,68	172,37	142,03					AC	24.4.2006	6	2
OK	19	802,00	14,30	762,00	13,93	214,70	184,64					AC	24.4.2006	7	2
OK	20	776,00	12,94	733,00	12,75	190,08	174,06					AC	24.4.2006	8	2
OK	21	786,00	14,34	743,00	13,68	213,69	173,46					AC	24.4.2006	9	2
OK	22	853,00	30,31	709,00	16,51	147,58	111,16					AC	24.4.2006	10	2
OK	23	873,00	29,07	726,00	15,91	131,05	104,00					AC	24.4.2006	11	2
OK	24	836,00	29,05	720,00	17,94	146,40	103,95					AC	24.4.2006	12	2
OK	25	1714,00	191,58	5,00	7,91	121,82	126,51					AC	3.5.2006	1	3
OK	26	1390,00	138,98	265,00	8,07	193,96	216,89					AC	3.5.2006	2	3
OK	27	1231,00	139,58	526,00	15,15	193,80	119,90					AC	3.5.2006	3	3
X	28	1144,00	117,63	5,00	18,10							AC	3.5.2006	4	3
OK	29	1867,00	120,98	3,00	7,95	116,14	102,87					AC	3.5.2006	5	3
OK	30	1176,00	115,74	469,00	19,58	142,36	136,96					AC	3.5.2006	6	3
OK	31	1035,00	55,61	670,00	11,96	181,98	159,48					AC	3.5.2006	7	3
OK	32	894,00	54,94	568,00	13,31	181,68	159,42					AC	3.5.2006	8	3
OK	33	876,00	52,41	583,00	9,85	174,65	154,49					AC	3.5.2006	9	3
OK	34	948,00	70,97	5,00	9,65	132,90	115,04					AC	3.5.2006	10	3
OK	35	936,00	58,31	597,00	20,63	180,48	152,79					AC	3.5.2006	11	3
OK	36	938,00	62,13	543,00	13,60	157,91	152,79					AC	3.5.2006	12	3
OK	37	960,00	48,58	624,00	6,92	133,98	107,13					AC	3.5.2006	1	4
OK	38	968,00	49,51	635,00	9,34	157,91	134,47					AC	3.5.2006	2	4
OK	39	1017,00	58,27	651,00	14,02	176,90	133,86					AC	3.5.2006	3	4
OK	40	916,00	40,95	636,00	12,36	167,34	152,85					AC	3.5.2006	4	4
OK	41	995,00	52,10	651,00	12,81	159,10	149,20					AC	3.5.2006	5	4
OK	42	881,00	41,64	642,00	12,13	161,50	149,14					AC	3.5.2006	6	4
OK	43	989,00	31,09	764,00	8,96	198,58	186,27					AC	3.5.2006	7	4
OK	44	944,00	26,84	736,00	9,41	199,94	200,96					AC	3.5.2006	8	4
OK	45	917,00	24,32	724,00	5,91	232,08	231,31					AC	3.5.2006	9	4
OK	46	1077,00	42,22	700,00	13,25	116,04	103,48					AC	3.5.2006	10	4
OK	47	1007,00	35,75	747,00	13,05	126,80	121,74					AC	3.5.2006	11	4
OK	48	1058,00	39,87	744,00	13,11	138,77	118,65					AC	3.5.2006	12	4
OK	49	809,00	54,08		17,73	128,43	107,31					AC	8.5.2006	1	5
OK	50	867,00	80,34	544,00	22,66	105,62	92,64					AC	8.5.2006	2	5
OK	51	883,00	104,30		24,07	147,63	126,44					AC	8.5.2006	3	5

Fig. 98: Excel sheet for properties download

After download of the results all the samples could be found in the database with their identification number and their X and Y place. The composition, sintering program and the properties of all samples were consultable.

The complete database could be connected to Spotfire® for a fast visualisation of all data available concerning the samples processing as well as results. For individual libraries the visualisation of the results was carried out by direct import of the Excel sheet into Spotfire®.

c. Data mining

The data mining was carried out with help of the visualisation software Sportfire®. As stated before two modes of visualisation were available, through connection with the database or by direct import of the results.

The presentation of most of the results was done by direct import of the results from the Excel sheet into Sportfire®. The advantage is a quick import and evaluation of the results. During this work the samples were classified by composition in the x-axis. Then in the y-axis one of the key parameters was given and, in colour, a second property appeared (often the combination was ε_r / tan δ or d_{33}^{*} at 2kV/mm / I max). The shape of the plots indicated the sintering temperature. 3D visualisation was also possible but they are not reported in this work as their visualisation is difficult.

X. Overview and Further Developments

The aim of this work was to develop a high throughput experimentation method for the screening of bulk lead-free piezoelectric ceramics via mixed-oxide route. The established route allows the evaluation of different parameters like doping and sintering during processing. Moreover a large amount of key parameters could be screened for a complete characterisation of the samples. With this method new doping systems for lead-free piezoelectric ceramics were developed and optimised. The goals of this work were the following:

Set up of a HTE route for bulk samples produced from mixed-oxide

Production of libraries for the evaluation of the influence of composition as well as sintering parameters

Construction of a HT characterisation machine for piezoelectric samples

Automated characterisation of the samples and properties evaluation

The set up of the HTE processing route for bulk materials presented different challenges:

Few automated powder dosing systems were available.

The homogenisation of powders is difficult.

In the case of piezoelectric ceramics, the powders need to be pressed and sintered.

To solve these different problems, the first step of the processing (powders dosing) was carried out per hand which on one hand slows the production of samples but which on the other hand allows more flexibility regarding the library design. After dosage, the powders were mixed and subsequently calcined. Ensuing the powders were parallel grinded and dried. Finally the powders of different compositions were parallel pressed into pellets and sintered.

In this case it is difficult to talk about a high throughput experimentation route as the sample preparation is not fully automated and it is not an innovative processing route. The method developed consisted in a deep parallelisation of different steps of a classical preparation. The throughput of this parallelised method is 4 times higher than the classical preparation

High throughput experimentation often requires high throughput screening. Piezoelectric samples need two electrodes on flat parallel surfaces to ensure a homogeneous propagation of the electric field applied during measurement. Accordingly the samples were plane polished in parallel after sintering and the whole surfaces were contacted by means of silver vapour deposition. Afterwards the key properties of the samples (ε_r, tan δ, d_{33}^{*} and T_C) could be automatically determined at a fast rate. The evaluation of the results was improved by the use of the visualisation software Spotfire®. The characterisation of a library can be called "High Throughput".

The sample production and characterisation allowed the evaluation of 10 new compositions having suffered four different sintering programs which is normal for a second screening.

The accelerated production method was tested on two known material systems, a PZT and a KNN-based ceramics.

For the PZT-based material system, a Zr/Ti variation was applied to find the morphotropic phase boundary. The method was successful as the MPB could be found with the measurement of ε_r and the values of d_{33}^{*} measured were almost as high as the values measured on conventionally processed samples.

To process the KNN-based material system improvements had to be carried out on the present method as follows:

Use of $KNbO_3$ and $NaNbO_3$ precursors.

Insertion of a new steps in the processing, i.e. the mixing with Speedmixer® and calcination before high energy milling.

For this material system the method was also successful with results for the values of the measured properties close to the values found in the literature.

The method has been successfully tested with two different material systems, the values obtained for the dielectric and piezoelectric measurement allowed the

identification of the MPB and interesting composition areas. Therefore the method could be applied to discover new materials.

The HTE phase of material discovery was applied to KNN-based materials. The throughput of the method was too slow to permit using it as a material discovery method and it was focussed on the discovery of new doping system for KNN.

The KNN doping with copper and germanium delivered promising results in the HTE phase. The losses were limited (<0.02), ε_r was low and d_{33}^* up to 200 pm/V could be measured. However the reproducibility of the satisfying results (in particular concerning d_{33}^*) was not totally controlled and problems were met during the upscaling. Larger quantities of the most promising composition could not be produced with the same properties measured during the HTE phase.

The doping of KNN with lithium and tantalum was investigated not as a new material but as a starting composition for further doping. It has been seen that tungsten-bronze compounds could be promising doping materials for KNN-based piezoelectric ceramics. Three compounds having different dielectric and piezoelectric properties were selected and tested as doping for KNN between 0.5 and 5 mol%. The dielectric constants of the SBN and BNN-doped KNN were constant with low values and both showed a peak in the d_{33}^* measurements of respectively 300 pm/V for 3 mol% SBN and 230 pm/V for 1.5 mol% BNN doping. The value of the Curie temperature and the orthorhombic-tetragonal phase transformation were reduced from respectively 400 and 200℃ for pure KNN to about 300 and 100℃ for SBN a nd BNN doped-KNN. The KNN-doping with SCNN15 showed a slight different behaviour concerning the dielectric and piezoelectric properties. The values of the dielectric losses were low, the values of the dielectric constant increase with the doping content and two peaks in the d_{33}^* values were identified at 250 and 300 pm/V, for 0.5 and 3 mol% doping. The influence of the tungsten-bronze doping could be also detected through the measurement of the capacitance in function of the temperature, where the reduction of the orthorhombic-tetragonal phase transformation as well as the Curie temperature to respectively 280 and 120℃ could be identified. The crystallite size dist ribution in the sintered samples was also altered by the tungsten-bronze doping.

The doping with tungsten-bronze can create A-site vacancies in KNN improving its ability to sinter and its dielectric as well as piezoelectric properties as it is the case for PZT.

The processing method being close of a conventional processing, the optimisation of promising composition discovered could be also carried out on the same way.

During the first experimental series the lithium and tantalum content were adjusted and different processings were tested. The non-expected results pointed out problems concerning the use of different batch of $KNbO_3$ and $NaNbO_3$ precursors. The dielectric properties were incoherent and the d_{33}^* maximum measured was 200 pm/V. However it could be established through the measurement of the dielectric losses that a content of 6 mol% lithium and tantalum in solid solution into SCNN-doped KNN provided a better quality to the samples as the losses attained their lowest level for this composition.

The second experimental series was focussed on the precursor problematic by producing in the same libraries samples with the same composition but produced from starting powders having different stoichiometries. No results concerning the stoichiometry of $KNbO_3$ could be delivered but it was arrest that an excess of 1 up to 2 mol% sodium in $NaNbO_3$ improved the piezoelectric properties.

In the third experimental series the excess or deficit of sodium and potassium was evaluated in respect to an electronically neutral composition. Four libraries with the same final compositions were processed with four different precursor combinations. Despite the same end compositions of all samples from the libraries their behaviours were different, the maximum for different parameters being at different locations. However, it could be seen that an excess of 1 or 2 mol% sodium and potassium in respect to an electronically neutral composition improved the quality of the samples. The highest d_{33}^* measured on the samples from this experimental series was 225 pm/V.

Before the processing of the fourth experimental series, four basics powders with 1 and 2 mol% sodium and potassium excess, using two different precursors combinations were milled. These powders were used as basic compositions for further doping with SCNN between 0 and 7 mol%. The quality of the samples from these libraries was improved and several samples were measured. A tendency for higher d_{33}^* could be observed for SCNN doping between 1 and 3 mol% where the values for d_{33}^* reached 225 pm/V.

During this phase of optimisation of the first promising compositions, the high results previously measured could not be reproduced. However, parameters achieving superior performances could be arrested:

Lithium and tantalum content of 6 mol%

SCNN15 content between 1 and 3 mol%

Use of $NaNbO_3$ having a sodium excess about 1 or 2 mol%

Excess or 1 mol% sodium and potassium regarding the neutral composition

The successfully established method for piezoelectric samples preparation and characterisation allows a throughput of about 10 new compositions per week. With this method new doping for KNN-based ceramics could be developed and optimised.

XI. Literature

[1] B. Jaffe, W.R. Cook, H. Jaffe "*Piezoelectric ceramics*" Academic Press Limited, London (1971) 1-5

[2] P. Duran, C. Moure "Piezoelectric ceramics" Mat. Chem. Phys. **15** [3-4] (1986) 193-211.

[3] N. Setter *et al.* "*Piezoelectric Material Devices*", EPFL, Switzerland (2002) 29-66

[4] EU Directive 2002/96/EC

[5] Y. Saito, H. Takao, T. Tani, T. Nonoyama, K. Takatori, T. Homma, T. Nagaya, M. Nakamura "Lead-free piezoceramics" Nature **432** (2004) 84-87.

[6] J.N. Cawse "*Experimental Design for Combinatorial and High Throughput Materials Development*", John Wiley & Sons, inc., Publication, New Jersey 2003

[7] B. Wessler, V. Jéhanno, W. Rossner, W.F. Maier "Combinatorial Synthesis of thin film libraries for microwave dielectrics" Appl. Surf. Sci. **223** (2004) 30-34.

[8] R.C. Pullar, Y. Zhang, L. Chen, S. Yang, J.R.G. Evans, N.McN. Alford "Manufacture and and measurement of combinatorial libraries of dielectric ceramics, Part I: Physical characterisation of $Ba_{1-x}Sr_xTiO_3$ libraries" J. Eur. Ceram. Soc. (2007), doi:10.1016/j.jeurceramsoc.2007.02.114 and "Part II: Dielectric Measurement of $Ba_{1-x}Sr_xTiO_3$ libraries" J. Eur. Ceram. Soc. (2007), doi:10.1016/j.jeurceramsoc.2007.04.008.

[9] Y. Xu "*Ferroelectric Materials and Their Applications*" Elsevier Science Pub. Co., Amsterdam (1991) 1-36.

[10] J.F.J. Brons "*Impedance Spectroscopy: Basics and Selected Applications to Heterogenous Systems*", Delft University of Technology (1998)

[11] B. Jaffe, W.R. Cook, H. Jaffe "*Piezoelectric ceramics*" Academic Press Limited, London (1971) 53-114

[12] N. Setter *et al.* "*Piezoelectric Material Devices*", EPFL, Switzerland (2002) 1-27.

[13] B. Jaffe, W.R. Cook, H. Jaffe "*Piezoelectric ceramics*" Academic Press Limited, London (1971) 7-21.

[14] K. Ruschmeyer *et al.* "*Piezokeramik, Grundlagen, Werkstoffe, Applikationen*" Expert Verlag, Renningen (1994) 1-35.

[15] N. Setter *et al.* "*Piezoelectric Material Devices*", EPFL, Switzerland (2002) 1-29.

[16] B. Jaffe, W.R. Cook, H. Jaffe "*Piezoelectric ceramics*" Academic Press Limited, London (1971) 115-133.

[17] H. Huang, Z. Tianshu, J.Ti. Oh, P. Hing "Effect of A-Site Substitution of Calcium on Zr-Rich Lead Zirconate Titanate" Ferroelectrics **274**, (2002) 55-65.

[18] A. Garg, T. C. Goel "Mechanical and electrical properties of PZT ceramics (Zr:Ti=0.4:0.6) related to Nd^{3+} Addition" Materials and Science Engineering B, **60** (1999) 128-132.

[19] A. Garg, D.C. Agrawal "Effect of rare earth (Er, Gd, Eu, Nd and La) and bismuth additives on the mechanical and piezoelectric properties of lead zirconate titanate ceramics" Materials science and Engineering B **86** (2001) 134-143.

[20] W. Rossner, K. Lubitz, G. Tomandl "Densification and Crystallite growth in PZT Ceramics with Variable Neodymium Content" Silicates Industrials **4-3** (1985) 31-34.

[21] V. Koval, C. Alemany, J. Briančin, H. Bruncková, K. Saksl "Effect of PMN modification on structure and electrical response of xPMN–(1–x)PZT ceramic systems" J. Eur. Ceram. Soc. **23** [7] (2003) 1157-1166.

[22] C. H. Lu, W. J. Hwang "Phasic and Microstructural Developments of $Pb(Ni_{1/3}Nb_{2/3})O_3$ prepared by the Columbite Precursor Process" Ceramics International **22** (1996) 373-379.

[23] Z. Gui, H. Hu, L. Li, X. Zhang "Influence of Additives on Sintering Processing and Properties of High Performance Piezoelectric Ceramics" Sintering '91. Proc.5th Int.Symp.on Science & Technology of Sintering Vancouver, 23-26 July 1991.

[24] F. Bamière, K. Benkert, M. Radanielina, C. Schuh, M.J. Hoffmann „Low temperature sintering and high piezoelectric properties of strontium doped PNZT–PNN ceramics processed via the columbite route" J. Eur. Ceram. Soc. doi:10.1016/j.jeurceramsoc.2007.02.001

[25] S.E. Park, T.R. Shrout "Ultrahigh strain and piezoelectric behavior in relaxor based ferroelectric single crystals" J. Appl. Phys. **82** [4] (1997) 1804-1811.

[26] C. Tănăsoiu, E. Dimitriu, C. Miclea "Effect of Nb, Li Doping on structure and Piezoelectric Properties of PZT Type ceramics" J. Eur. Ceram. Soc. **19** (1999) 1187-1190.

[27] H. Jaffe, D.A. Berlincourt "Piezoelectric transducer materials" Proceeding of the IEEE **53** [10] (1965) 1372-1386.

[28] M. Kondo, K. Kurihara "Piezoelectric properties and the applications of $Pb(Ni_{1/3}Nb_{2/3})O_3$-$PbTiO_3$-$PbZrO_3$ Ceramics" Key Engineering Materials **248** (2003) 15-18.

[29] T.C. Goel, P.K.C. Pillai, H.D. Sharma, A.K. Tripathi, A. Tripathi, C. Pramila, A. Govindan "Effects of rare earth doping on the piezo and pyro electric properties of Lead Zirconate Titanate (PZT)" Electroceramics, 1994. (ISE 8), 8th International Symposium on

[30] G. Helke, S. Seifert, Cho S. J. "Phenomenological and structural properties of piezoelectric ceramics based on $xPb(Zr,Ti)$ O_3-(1-x)$Sr(K_{0.25}Nb_{0.75})O_3$ (PZT/SKN) solid solutions" J. Eur. Ceram. Soc. **19** [6] (1999) 1265-1268.

[31] Y. Xu, "*Ferroelectrics Materials and Their Applications*" Elsevier Science Pub. Co., Amsterdam (1991) 247-276.

[32] B. Jaffe, W.R. Cook, H. Jaffe "*Piezoelectric ceramics*" Academic Press Limited, London (1971) 214-235.

[33] L. E. Croos, D. Viehland "Piezoelectricity in Tungsten Bronze Crystals" Ferroelectrics **160** (1994) 265-276.

[34] S. Nishiwaki, J. Takahashi, K. Kodaira "Effect of additives on microstructure development and Ferroelectric Properties of $Sr_{0.3}Ba_{0.7}Nb_2O_6$ Ceramics" Jpn. J. Appl. Phys. **33** (1994) 5477-5481.

[35] S. Nishiwaki, J. Takahashi, K. Kodaira, M. Kishi "Morphotropic Phase Boundary and Dielectric Properties of V_2O_5-Containing $Sr_xBa_{1-x}Nb_2O_6$ (0.2≤x≤0.4) Ferroelectrics" Jpn. J. App. Phys. **35** (1996) 5137-5140.

[36] M. Kim, J.H. Lee, J.J. Kim, H. Y. Lee, S.H. Cho "Origin of Abnormal Grain Growth in Tungsten Bronze Structured Ferroelectric $Sr_xBa_{1-x}Nb_2O_6$ Ceramics" Jpn. J. App. Phys. **41** (2002) 7048-7052.

[37] Q. W. Huang, L. H. Zhu, J. Xu, P.L. Wang, H. Gu, Y.B. Cheng "Effect of V_2O_5 on sintering behaviour, microstructure and dielectric peoperties of textured $Sr_{0.4}Ba_{0.6}Nb_2O_6$ ceramics" J. Eur. Ceram. Soc. **25** (2005) 957-962.

[38] D. U. Spínola, I.A. Santos, L.A. Bássora, J.A. Eiras, D. Garcia "Dielectric properties of Rare Earth Doped (Sr, Ba)Nb_2O_6 Ceramics" J. Eur. Ceram. Soc. **19** (1999) 1111-1114.

[39] R.R.Neurgaonkar, J.R. Oliver, W.K. Cory "Piezoelectricity in Tungsten Bronze Crystals" Ferroelectrics **160** (1994) 265-276.

[40] R. J. Xie, Y. Akimune "Lead-free piezoelectric ceramics in the (1-x) $Sr_2NaNb_5O_{15}$ − x $Ca_2NaNb_5O_{15}$ (O.05 ≤ x ≤ 0.35) system" J. Mater. Chem. **12** (2002) 3156-3161.

[41] R. J. Xie, Y. Akimune, R.P. Wang, K. Matsuo, T. Sugiyama, N. Hirosaki "Spark Plasma Sintering of Tungsten Bronze $Sr_{2-x}Ca_xNaNb_5O_{15}$ (x=0.1) Piezoelec Ceramics: I Processing and Microstructure" J. Am. Ceram. Soc. **85** [11] (2002) 2725-2730.

[42] S. C. Abrahams, P. B. Jameson, J. L. Bernstein "Ferroelectric Tungsten Bronze-Type Crystal structure. III. Potassium Lithium Niobate $K_{(6-x-y)}Li_{(4+x)}Nb_{(10+y)}O_{30}$" J. Chem. Phys. **54** [6] (1971) 2355-2363.

[43] A. Zegzouti, A. Abalhassain, M. Elaatmani, J. Ravez, J.P. Chaminade "Elaboration et caractérisation de cristaux dérivés de $K_3Li_2Nb_5O_{15}$" J. Phys. III France **6** (1996) 727-735.

[44] P. Wang, S. L. Xu, J. H. Lee, J. J. Kim, S. H. Cho, H.Y. Lee "Microstructure and dielectric Properties of Tungsten Bronze Structured KLN and BNN Ceramics: TiO2 Effect" Int. J. Modern Phys. B. **17** [8, 9] (2003) 1267-1272.

[45] B. Jaffe, W.R. Cook, H. Jaffe "*Piezoelectric ceramics*" Academic Press Limited, London (1971) 213-235

[46] S. P. Yordanov, I. Ivanov, Ch. P. Carapanov "Dielectric Properties of the ferroelectric $Bi_2Ti_2O_7$ Ceramics" J. Phys. D: Appl. Phys. **31** (1998) 800-806.

[47] H. Nagata, Y. Fujita, H. Enosawa, T. Takenaka "Piezoelectric properties of Grain oriented Nb- or V- Doped $Bi_4Ti_3O_{12}$ Ceramics" Key Engineering Materials **248** (2003) 7-10.

[48] T. Tani, T. Kimura "Reactive-templated grain growth processing for lead-free piezoelectric ceramics" Advances in Applied Ceramics **105** (2006) 55-63.

[49] J.T. Lewis "The piezoelectric effect" Electrical Insulation and Dielectric Phenomena, 2005. CEIDP '05. 2005 Annual Report Conference on, 16-19. oct. 2005, 717-720.

[50] V.P. Pavlović, M.V. Nikolić, Z. Nikolić, G. Branković, Lj. Živković, V.B. Pavlović, M.M. Ristić "Microstructural evolution and electric properties of mechanically activated BaTiO3 ceramics" J. Eur. Ceram. Soc. **27** (2007) 575-579.

[51] B. Jaffe, W.R. Cook, H. Jaffe "*Piezoelectric ceramics*" Academic Press Limited, London (1971) 53-114

[52] S. Guillemet-Fritsch, M. Boulos, B. Durand, V. Bley, T. Lebey "Electrical characterisation of $BaTiO_3$ ceramics from hydrothermal prepared powders" J. Eur. Ceram. Soc. **25** (2005) 2749-2753.

[53] B.L. Chen, T.W. Button, M. Gabbay, G. Fantozzi, M. Maglione "Oxygen Vacncy Relaxation and Domain Wall Hysteresis Motion in Cobalt-Doped Barium Titanate Ceramics" J. Am. Ceram. Soc. **88** [4] (2005) 907-911.

[54] J.G. Fisher, B.K. Lee, A. Brancquart, S.Y. Choi, S.J. Kang "Effect of Al_2O_3, dopant on abnormal grain growth in $BaTiO_3$" J.Eur. Ceram. Soc. **25** (2005) 2033-2036.

[55] Z.C. Li, B. Bergman "Electrical properties and ageing characteristics of BaTiO3 ceramics doped by single dopants" J. Eur. Ceram. Soc. **25** (2005) 441-445.

[56] J. Jeong, E.J. Lee, Y.H. Han "Defect chemistry and electrical degradation of $BaTiO_3$ co-doped with Ho and Mn" J. Eur. Ceram. Soc. **27** (2007) 1159-1163.

[57] R. Von der Mühll, A. Simon, H. Khemakhem, J. Ravez "Pyroelectric and piezoelectric properties of new lead-free ceramics with compositions $Ba_{1-x}Na_xTi_{1-x}Nb_xO_3$" Ann. Chim. Sci. Mat. **26** (2001) 127-130.

[58] S. Priya, A. Ando,Y. Sakabe "Nonlead perovskite materials:$Ba(Li_{1/4}Nb_{3/4})O_3$ and $Ba(Cu_{1/3}Nb_{2/3})O_3$" J. Appl. Phys. **94** [2] (2003) 1171-1177.

[59] H. Nagata, N. Koizumi, N. Kuroda, I. Igarashi, T. Takenaka "Lead-free Piezoelectric Ceramics of $(Bi_{1/2}Na_{1/2})TiO_3$-$BaTiO_3$-$BiFeO_3$ Systems" Ferroelectrics **229** (1999) 273-278.

[60] K. Sakata, Y. Masuda "Ferroelectric and antiferroelectric properties of $(Bi_{0.5}Na_{0.5})TiO_3$-$SrTiO_3$ solid solution ceramics" Ferroelectrics **7** (1974) 347-349.

[61] Y. M. Chiang, G.W. Farrey, A.N. Soukhojak "Lead-free high-strain single crystal piezoelectrics in the alkaline-bismuth-titanate perovskite family" Appl. Phys. Letter **73** [25] (1998) 3683-3685.

[62] C. Y. Kim, T. Sekino, K. Niihara "Sysnthesis of Bismuth Sodium Titanate Nanosized Powders by Solution / Sol-Gel Process" J. Am. Ceram. Soc. **86** [9] (2003) 2464-2467.

[63] M. L. Zhao, C.L. Wang, W. L. Zhong, J. F. Wang, Z. F. Li "Grain-Size Effect on the Dielectric Properties of $(Bi_{0.5}Na_{0.5})TiO_3$" Chin. Phys. Lett. **2** [20] (2003) 290-293.

[64] X.X. Wang, S.W. Or, X.G. Tang, H.L.W. Chan, P.K. Choy, P.C.K. Liu "TiO_2-nonstochiometry dependence on piezoelectric properties and depolarization temperature of $(Bi_{0.5}Na_{0.5})_{0.94}Ba_{0.06}TiO_3$ lead-free ceramics" Sol. Stat. Comm. **134** [10] (2005) 659-663.

[65] K. Fuse, T. Kimura "Effect of Particle Size of Starting Materials on Microstructure Development in Textured $(Bi_{1/2}Na_{1/2})TiO_3$" J. Am. Ceram. Soc. **89** [6] (2006) 1957-1964.

[66] T. Tani, T. Kimura "Reactive-templated grain growth processing for lead-free piezoelectric ceramics" Adv. Appl. Ceram. **105** (2006) 55-63.

[67] D.M. Lin, D.Q. Xiao, J.G. Zhu, P. Yu, H.J. Yan, L.Z. Li, W. Zhang "The relations of sintering conditions and microstructures of $[Bi_{0.5}(Na_{1-x-y}K_xLi_y)_{0.5}]TiO_3$ piezoelectric ceramics" Cryst. Res. Technol. **39** [1] (2004) 30-33.

[68] D.Q. Xiao, D.M. Lin, J.G. Zhu, P. Yu "Investigation on the design and synthesis of new systems of BNT-based lead-free piezoelectric ceramics" J. Electroceramics **16** [4] (2006) 271-275

[69] K. Yoshii, Y. Hiruma, H. Nagata, T. Takenaka "Electrical Properties and Depolarisation Temperature of $(Bi_{1/2}Na_{1/2})TiO_3$-$(Bi_{1/2}K_{1/2})TiO_3$ lead-free piezoelectric Ceramics" Jpn. J. Appl. Phys. **45** [5B] (2006) 4493-4496.

[70] S.H. Choy, X.X. Wang, H.L. Chan, C.L. Choy "0.75 $(Bi_{1/2}Na_{1/2})TiO_3$-0.2 $(Bi_{1/2}K_{1/2})TiO_3$-0.05 $BaTiO_3$ Lead-Free Ceramics with Addition of CeO_2" Ferroelectrics **336** (2006) 69-79.

[71] H. Nagata, T. Takenaka "Additive effects on electrical properties of $(Bi_{1/2}Na_{1/2})TiO_3$ ferroelectric ceramics" J. Eur. Ceram. Soc. **21** (2001) 1299-1302.

[72] J.H. Cho, Y.H. Lee, B.J. Chu, B.I. Kim, H.T. Chung "Processing and Properties of Piezoelectrics based on BNT (Bi, Na)TiO_3" Key Engineering Materials **264-268** (2004) 1321-1324

[73] T. Takenaka, K.I. Maruyama, K. Sakata „ $(Bi_{1/2}Na_{1/2})TiO_3$-$BaTiO_3$ system for lead-free piezoelectric ceramics" Jpn. J. Appl. Phys. **30** (1991) 2236-2239.

[74] B.J. Chu, D.R. Chen, G.R.Li, Q.R. Yin „Electrical properties of $Na_{1/2}Bi_{1/2}TiO_3$-$BaTiO_3$ ceramics" J. Eur. Ceram. Soc. **22** (2002) 2115-2121.

[75] D. Lin, D. Xiao, J. Zhu, P. Yu "Piezoelectric and ferroelectric properties of lead-free $[Bi_{1-y}(Na_{1-x-y}Li_x)]_{0.5}Ba_yTiO_3$ ceramics" J. Eur. Ceram. Soc. **26** (2006) 3247-3251.

[76] Y. Hiruma, R. Aoyagi, H. Nagata, T. Takenak "Piezoelectric Properties of $BaTiO_3$-$(Bi_{1/2}NK_{1/2})TiO_3$ Ferroelectric Ceramics" Jpn. J. Appl. Phys. **43** [11A] (2004) 7556-7559.

[77] H. Nagata, M. Yoshida, Y. Makiuchi, T. Takenaka "Large Piezoelectric Constant and High Curie Temperature of Lead-Free Piezoelectric Ceramic Ternary System Based on Bismuth Sodium Titanate–Bismuth Potassium Titanate–Barium Titanate near the Morphotropic Phase Boundary" Jpn. J. Appl. Phys. **42** (2003) 7401-7403.

[78] Y. Li, W. Chen, Q. Xu, J. Zhou, X. Gu, S. Fang "Electromechanical and dielectric properties of $Na_{0.5}Bi_{0.5}TiO_3$-$K_{0.5}Bi_{0.5}TiO_3$-$BaTiO_3$ lead-free ceramics" Mat. Chem. Phys. **94** (2005) 328-332.

[79] H. Ishii, H. Nagata, T. Takenaka "Morphotropic Phase Boundary and Electrical Properties of Bismuth Sodium Titanate-Potassium Niobate Solid Solution Ceramics" Jpn. J. Appl. Phys. **40** (2001) 5660-5663.

[80] T. Takenaka, T. Okuda, K. Takegahara "Lead-free piezoelectric ceramics based on $(Bi_{1/2}Na_{1/2})TiO_3$-$NaNbO_3$" Ferroelectrics **196** (1997) 175-178.

[81] B. Jaffe, W.R. Cook, H. Jaffe *Piezoelectric ceramics* Academic Press Limited, London (1971) 185-212

[82] N. Setter *et al.* "*Piezoelectric Material Devices*", EPFL, Switzerland (2002) 355-388.

[83] T. Imai, S. Yagi "Introducing Protons into Potassium Tantalate Niobate Single Crystals" Jpn. J. Appl. Phys. **38** (1999) 729-736.

[84] S. Wada, K, Muraoka, H. Kakemoto, T. Tsurimi, H. Kamagai "Enhanced Piezoelectric Properties of Potassium Niobate Single Crystals by Domain Engineering" Jpn. J. Appl. Phys. **43** [9B] (2004) 6602-6700.

[85] S. Wada, A. Seike, T. Tsurimi "Poling Treatment and Piezoelectric Properties of Potassiun Niobate Ferroeletric Single Crystals" Jpn. J. Appl. Phys. **40** (2001) 5690-5697.

[86] H. Birol, D. Damjanovic, N. Setter "Preparation and Characterisation of $KNbO_3$ Ceramics" J. Am. Ceram. Soc. **88** [7] (2005) 1754-1759.

[87] S. Toyoda, K. Fujiura, M. Sasaura, K. Enbutsu, A. Tate, M. Shimokozono, H. Fushimi, T. Imai, K. Manaba, T. Matsuura, T. Kurihara "Low-Driving-Voltage Electro-optic Modulator with Novel $KTa_{1-x}Nb_xO_3$ Crystals Waveguide" Jpn. J. Appl. Phys. **43** [8B] (2004) 5862-5866.

[88] J. Venkatesh, V. Sherman, N. Setter "Synthesis and Dielectric Characterisation of Potassium Niobate Tantalate Ceramics" J. Am. Ceram. Soc. **88** [12] (2005) 3397-3404.

[89] K. Kakimoto, I. Masuda, H. Ohsato "Ferroelectric and Piezoelectric Properties of $KNbO_3$ Ceramics Containing small amount of $LaFeO_3$" Jpn. J. Appl. Phys. **42** (2003) 6102-6105.

[90] A. Molak, A.Onoder, H. Yamashita "Dielectric and Optical Studies of the Low-Temperature Phase in $NaNbO_3$: Effect of Manganese Dopant" Jpn. J. Appl. Phys. **31** (1992) 3221-3224.

[91] L.A. Reznitchenko, A.V. Turik, E.M. Kuznetsova, V.P. Sakhnenko "Piezoelectricity in NaNbO3 ceramics" J. Phys.: Condens. Matter. **13** (2001) 3875.3881.

[92] T. Wada, K. Tsuji, T. Saito, Y. Matsuo "Ferroelectric $NaNbO_3$ Ceramics Fabricated by Spark Plasma Sintering" Jpn. J. Appl. Phys. **42** (2003) 6110-6114.

[93] M. Kosec, D. Kolar "On activated sintering and electrical properties of $NaKNbO_3$" Mat. Res. Bull. **10** (1975) 335-340.

[94] E. Ringgaard, T. Wurlizer "Lead-free piezoceramics based on alkali niobates" J. Eur. Ceram. Soc. **25** (2005) 2701-2706.

[95] V. Lingwal, B.S. Semwal, N.S. Panwar "Dielectric preperties of $Na_{1-x}K_xNbO_3$ in orthorhombic phases" Bull. Mater. Sci. **26** (2003) 619.625.

[96] H. Birol, D. Damjanovic, N. Setter "Preparation and characterisation of $(K_{0.5}Na_{0.5})NbO_3$ ceramics" J. Eur. Ceram. Soc. **26** (2006) 861-866.

[97] J.F. Li, K. Wang "Ferroelectric and Piezoelectric Properties of Fine-Grained $Na_{0.5}K_{0.5}NbO_3$ Lead-Free Piezoelectric Ceramic Prepared by Spark Plasma Sintering" J. Am. Ceram. Soc. **89** [2] (2006) 706-709.

[98] Y. Shiratori, A. Magrez, C. Pithan "Particle size effect on the crystal structure symmetry of $K_{0.5}Na_{0.5}NbO_3$" J. Eur. Ceram. Soc. **25** (2005) 2075-2079.

[99] E. Hollenstein, D. Damjanovic, N. Setter "Temperature stability of the piezoelectric properties of Li-modified KNN ceramics", J. Eur. Ceram. Soc. (2007), doi:10.1016/j.eurceramsoc.200702100

[100] F. Tang, H. Du, Z. Li, W. Zhou, S. Qu, Z. Pei "Preparation and properties of $(K_{0.5}Na_{0.5})NbO_3$-$LiNbO_3$ ceramics" Trans. Nonferrous Met. Soc. China **16** (2006) 466-469.

[101] M.H. Francombe, B. Lewis "Structural and Electrical Properties of Silver Niobate and Silver Tantalate" Acta Crys. **11** (1958) 175-178.

[102] K.H. Ryu, J.A. Cho, T. K. Song, M.H. Kim, S.S. Kim, H.S. Lee, S.J. Jeong, J.S. Song, K.S. Choi "Microstructure and Piezoelectric Properties of Lead-Free Niobate Ceramics" Ferroelectrics **338** (2006) 57-63.

[103] E. Hollenstein, M. Davis, D. Damjanovic, N. Setter „Piezoelectric properties of Li- and Ta-modified $(K_{0.5}Na_{0.5})NbO_3$ ceramics" Appl. Phys. Lett. **87** (2005) 182905.

[104] Y. Zhen, J.F. Li "Normal Sintering of (K, Na)NbO_3-Based Ceramics: Influence of Sintering Temperature on Densification, Microstructure, and Electrical Properties" J. Am. Ceram. Soc. **89** [12] (2006) 3669-3675.

[105] Y. Guo, K. Kakimoto, H. Oshato "$(Na_{0.5}K_{0.5})NbO_3$-$LiTaO_3$ lead-free piezoelectric ceramics" Mat. Lett. **59** (2005) 241-244.

[106] Y. Saito, H. Takao "High Performance Lead-Free Piezoelectric Ceramics in the (K,Na)NbO_3-$LiTaO_3$ Solid Solution System" Ferroelectrics **338** (2006) 17-32

[107] S. Zang, J.F. Wang, H.C. Chen, W.B. Su, C.M. Wang, P. Qi, B.Q. Ming, J. Du, L.M. Zheng "Perovskite $(Na_{0.5}K_{0.5})_{1-x}(LiSb)_xNb_{1-x}O_3$ lead-free piezoeceramics" Appl. Phys. Lett. **88** (2006) 212908.

[108] Y. Saito, H. Takao, T. Tani, T. Nonoyama, K. Takatori, T. Homma, T. Nagaya, M. Nakamura "Lead-free piezoceramics" Nature **432** (2004) 84-87.

[109] J. Yoo, K. Lee, K. Chung, S. Lee, K. Kim, J. Hong, S. Ryu, C. Lhee "Piezoelectric and Dielectric properties of (LiNaK)(NbTaSb)O3 Ceramics with variation in Poling Temperature" Jpn. J. Appl. Phys. **45** [9B] (2006) 7444-7448.

[110] B. Malic, J. Bernard, J. Holc, D. Jenko, M. Kosec "Alkaline-earth doping in (K,Na)NbO_3 based piezoceramics" J. Eur. Ceram. Soc. **25** (2005) 2707-2711.

[111] S. Tashiro, K. Ishi, T. Wada "Fabrication of $(Sr_xK_{0.5-x}Na_{0.5-x})NbO_3$ Piezoelectric Ceramics and Effects of MnO Addition on Their Piezoelectric Properties" Jpn. J. Appl. Phys. **45** [9B] (2006) 7449-7454.

[112] Y. Chang, Z. Yang, X. Chao, R. Zhang, X. Li "Dielectric and piezoelectric properties of alkaline-earth doped $(K_{0.5}Na_{0.5})NbO_3$ ceramics" Mat. Lett. **61** (2007) 785-789.

[113] Y. Guo, K. Kakimoto, H. Ohsato "Structure and Electrical Properties of Lead-free $(Na_{0.5}K_{0.5})NbO_3$-$BaTiO_3$ Ceramics" Jpn. J. Appl. Phys. **43** [9B] (2004) 6662-6666.

[114] Y. Shimojo, R. Wang, T. Sekiya, K. Matsuzaki "Dielectric and Piezoelectric Properties of $MeTiO_3$ (Me = Ba and Sr) Modified (K,Na)NbO_3" J. Kor. Phys. Soc. **46** [1] (2005) 48-51.

[115] Y. Guo, K.I. Kakimoto, H. Ohsato "Dielectric and piezoelectric properties of lead-free $(Na_{0.5}K_{0.5})NbO_3$-$SrTiO_3$ ceramics" Solid State Communication **129** (2004) 279-284.

[116] R. Wang, R.J. Xie, K. Hanada, K. Matsuaki, H. Bando, M. Itoh "Phase Diagram and enhanced piezoelectric properties in the strontium titanate doped potassium-sodium niobate solid solution" Phys. Stat. Sol. (a) **202** (2005) R57-R59.

[117] M. Matsubara, T. Yamagushi, K. Kikuta, S.I. Hirano "Siniterability and Piezoelectric Properties of $(K,Na)NbO_3$ Ceramics with Novel Sintering Aid" Jpn. J. Appl. Phys. **43** [10] (2004) 7159-7163.

[118] M. Matsubara, T. Yamaguchi, K. Kikuta, S.I. Hirano "Sintering and Piezoelectric Properties of Potassium Sodium Niobate Ceramics with Newly developed Sintering Aid" Jpn. J. Appl. Phys. **44** [1A] (2005) 258-263.

[119] M. Matsubara, T. Yamaguchi, K. Kikuta, S.I. Hirano "Effect of Li Substitution on the Piezoelectric Properties of Potassium Sodium Niobate Ceramics" Jpn. J. Appl. Phys. **44** [8] (2005) 6136-6142.

[120] R. Zuo, J. Rödel, R. Chen, L. Li "Sintering and Electrical Properties of Lead-Free $Na_{0.5}K_{0.5}NbO_3$ Piezoelectric Ceramics" J. Am. Ceram. Soc. **89** [6] (2006), 2010-2015.

[121] S.H. Park, C.W. Ahn, S. Nahm, J.S. Song "Microstructure and Piezoelectric Properties of ZnO-added $(Na_{0.5}K_{0.5})NbO_3$ Ceramics" Jpn. J. Appl. Phys. **43** [8B] (2004), L1072-L1074.

[122] Utilisation manual from Fritsch Company for Planetary ball milling machine (http://www.fritsch.de)

[123] Utilisation manual from Martin Christ GmbH for Freeze-Dryer (http://www.martinchrist.de)

[124] L.B. Kong "PZT Ceramics formed directly from oxides via reactive sintering", *Materials Letters*, **51** (2001) 95-100

[125] W. Rossner, K. Lubitz and G. Tomandl "Densification and Crystallite Growth in PZT Ceramics with variable Neodymium Content" Silicates Industriels **3-4** (1985) 31-34.

[126] R.B. Atkin and R. M. Fulrath "Point Defects and Sintering of Leadzirconate-Titanate" J. Am. Ceram. Soc. **54** (1971) 265-270.

[127] W. Rossner: "Sinterverhalten und elektrische Eigenschaften von Neodym dotierter Bleizirkonat-Titanat-Keramik, hergestellt nach dem Mixed-Oxide-Verfahren", PhD thesis University of Erlangen-Nürnberg, Erlangen, 1985

[128] T. R. Shrout, P. Papet, S. Kim and G-S. Lee "Conventionally prepared submicrometer lead-based perovskite powders by reactive calcination" J. Am. Ceram. Soc **73** (1990) 1862-1867.

[129] C. H. Lu, W. J. Hwang "Phasic and Microstructural Developments of $Pb(Ni_{13}Nb_{23})O_3$ Prepared by the Columbite Precursor Process" Ceramics International 22 (1996) 373-379.

[130] C. Schuh, M. Kulig, K. Lubitz "AG DOPING OF RARE EARTH MODIFIED PZT" in Electroceramics V, edited by J.L. Baptista, J.A. Labrincha, P.M. Vilarinho (Aveiro (Portugal), 1996) Book 1, 201-204

[131] W.D. Kingery "Densification during sintering in presence of a liquid phase, I. Theory and II. Experimental" J. App. Phys. 30 (1959)

[132] L.B. Kong "PZT Ceramics formed directly from oxides via reactive sintering", *Materials Letters*, **51** (2001) 95-100.

[133] A. I. Kingon and J. B. Clark "Sintering of PZT Ceramics, I: Atmosphere Control and II: Effect of PbO Content on Densification Kinetics", J. Am. Ceram. Soc. **66** (1983) 253-270

[134] US 2005/0006618 A1 (M. Nanao [JP] et al.) 13 January 2005

[135] B. Malic, J. Bernard, J. Holc, D. Jenko and M. Kosec "Alkaline-Earth doping in $(K,Na)NbO_3$ based piezoceramics" J. Eur. Ceram. Soc. **25** (2005) 2707-2711.

[136] Y. Guo, K.-I. Kakimoto, H. Ohsato "$(Na_{0.5}K_{0.5})NbO_3$-$LiTaO_3$ lead-free piezoelectric ceramics" Materials Letters **59** (2005) 241-244.

[137] A.M. Glazer, H.D. Megaw "Studies of the Lattice Parameter and Domains in the Phase transitions of $NaNbO_3$" Acta Crys. **A29** (1973) 489-494

[138] Jaffe cook jaffe, KNN phase diagramm B. Jaffe, W.R. Cook, H. Jaffe "*Piezoelectric ceramics*" Academic Press Limited, London (1971) 213

[139] G. Shirane, R. Newnham, R. Pepinsky, "Dielectric properties and phase transition of NaNbO3 and (K, Na)NbO3" Phys. Rev., **96** [1] (1954) 581-588

[140] A. Shigemi, T. Wada "Enthalpy of Various Pahses and Formation Energy of Pooint defects in Perovskite-Type $NaNbO_3$ by frist Principles Calculation" Jpn. J. App. Phys. **43** [9B] (2004) 6793-6798

[141] J. Attia, L. Bellaiche, P. Gemeiner, B. Dkhil and B. Malic, "Study of potassium-sodium-niobate alloys: A combined experimental and theoretical approach" J. Phys. IV France, **128** (2005) 55-60

[142] H.R. Rukmini, R.N.P. Choudhary and V.V. Rao "Effect of doping pairs (La,Na) on structural and electrical properties of PZT ceramics" Mat. Chem. Phys. **55** (1998) 108-114.

[143] M. Kosec, D. Kolar, "On activated sintering and electrical properties of $NaKNbO_3$", Mat. Res. Bull. **10**, 335-340 (1975)

[144] R.E. Jaeger, L. Egerton, "Hot Pressing of Potassium-Sodium Niobate" J. Am. Ceram. Soc. **42** [9] (1962) 438-442

[145] R. Wang, R. Xie, T. Sekiya and Y. Shimojo, "Fabrication and Characterisation of Potassium-Sodium Niobate Piezoelectric Ceramics by Spark Plasma Sintering Method" Mater. Res. Bull. **39** (2004) 1709-1715

[146] M. Matsubara, T. Yamaguchi, K. Kikuta, S. Hirano, "Sintering and Piezoelectric Properties of Potassium Sodium Niobate Ceramics with Newly Developed Sintering Aid", Jap. J. of App. Phys. **44** [1A] (2005) 253-263.

[147] E. Boucher, D. Guyomar, L. Lebrun, B. Guiffard, G. Grange, "Effect of (Mn, F) and (Mg, F) co-doping on dielectric and piezoelectric properties of lead zirconate titanate ceramics", J. App. Phys., **92** [9] (2002) 5437-5442.

[148] Y. Saito, H. Takao "High Performance Lead-Free Piezoelectric Ceramics in the $(K,Na)NbO_3$ Solid Solution System" Ferroelectrics **338** (2006) 17-32.

[149] US 2004/0214723 A1 (T. Nonoyama [JP] et al.) 28 October 2004

[150] E. Hollenstein, M. Davis, D. Damjanovic, N. Setter , „Piezoelectric properties of Li- and Ta-modified $(K_{0.5}Na_{0.5})NbO_3$ ceramics", App. Phys. Letter **87** (2005) 182905

[151] Y. Zhang, J. Wang, J. Du, W. Su, G. Zang, C. Wang, P. Qi, X. Liang, „Preparation and performances of Niobate-tantalate Lead-free Piezoelectric Ceramics", Electronic Component and materials, **23** [11] (2004) 11-12.

[152] Y. Guo, K. Kakimoto, H. Ohsato, "$(Na_{.5}K_{.5})NbO_3$-$LiTaO_3$ lead-free piezoelectric ceramics" Mat. Lett. **59** (2005) 241-244.

[153] Y. Saito, H.Takao "High Performances Lead-Free Piezoelectric Ceramics in the $(K,Na)NbO_3$-$LiTaO_3$ Solid Solution System", Ferroelectrics 38 (2006) 17-32.

[154] R.J Xie, Y. Akimune, „Lead-free piezoelectric ceramics in the $(1-x)$ $Sr_2NaNb_5O_{15}$-x $Ca_2NaNb_5O_{15}$ $(0.05 \leq x \leq 0.35)$ system", J. Mat. Chem. **12** (2002) 3156-3161.

[155] P. Wang, S.L. Xu, J. H. Lee, J.J. Kim, S. H. Cho, „Microstructure and dielectric properties of tungsten bronze structured KLN and BNN ceramics: TiO_2 effect", Intern. J. Mod. Phys. B **17** [8,9] (2003) 1267-1272.

[156] S. Nishiwaki, J. Takahashi, K. Kodaira, „Effect of additives on Microstructure Development and Ferroelectric Properties of $Sr_{.3}Ba_{.7}Nb_2O_6$ Ceramics", Jpn. J. App. Phys. **33** (1994) 5477-5481.

[157] Q. W. Huang, L. H, Zhu, J. Xu, P.L. Wang, H. Gu, Y.B. Cheng, "Effect of V_2O_5 on sintering behaviour, microstructure and dielectric properties of textured $Sr_{0.4}Ba_{0.6}Nb_2O_6$ ceramics" J. Eur. Ceram. Soc. **25** (2005) 057-962.

[158] B. Jaffe, W.R. Cook, H, Jaffe *"Piezoelectric ceramics"* Academic Press Limited, London (1971) 135-183.

[159] B. Malic, J. Bernard, J. Holc, D. Jenko, M. Kosec, „Alkaline-Earth Doping in $(K, Na)NbO_3$ Based Piezoeceramics", J. Eur. Ceram. Soc. **25** (2005) 2707-11.

[160] H. Birol, D. Damjanovic, N. Setter, "Preparation and characterisation ok (K0.5Na0.5)NbO3", J. Eur. Ceram. Soc. **26** (2006) 861-866.

[161] B. Jaffe, W.R. Cook, H, Jaffe *"Piezoelectric ceramics"* Academic Press Limited, London (1971) 185-212.

[162] M. Matsubara, T. Yamaguchi, W. Sakamoto, K. Kikuta, T. Yogo, S. Hirano, "Processing and Piezoelectric Properties of Lead-free (K, Na) (Nb, Ta)O_3 Ceramics", J. Am. Ceram. Soc. **88** [5] (2005) 1190-1196

[163] A. Garg, D.C. Agrawal „Effect of rare earth (Er, Gd, Eu, Nd and La) and bismuth additives on the mechanical and piezoelectric properties of lead-zirconate-titanate ceramics", Mat. Sci. Eng. **B86** (2001) 134-143.

[164] W. Rossner, K, Lubitz, G. Tomandl "Densification and Crystallite Growth in PZT Ceramics with variable Neodymium Content", Silicates Industriels **3-4** (1985) 31-34.

[165] M. Drofenik, D. Makovec, I. Zajc and H. T. Langhammer "Anomalous Grain Growth in Donor-Doped Barium Titanate with Excess Barium Oxide" J. Am. Ceram. Soc. **85** (2002) 653-660.

[166] A. Garg, T.C. Goel "Mechanical and electrical properties of PZT ceramics (Zr:Ti=0.40:0.60) related to Nd^{3+} Addition", Mat. Sci. Eng. **B60** (1999) 128-132.

[167] S. Tashiro, K. Ishi, T. Wada "Fabrication of $(Sr_xK_{0.5-x}Na_{0.5-x})NbO_3$ Piezoelectric Ceramics and Effects of MnO Addition on their Piezoelectric Properties" Jpn. J. Appl. Phys. **45** [9B] (2006) 7449-7454.

[168] A.I. Kington, J.B. Clark "Sintering of PZT Ceramics: II, Effect of PbO Content on Densification Kinetics", J. Am. Ceram. Soc., **66** [4] (1980) 256-260.

[169] R.B. Atkin, R.M. Fulrath "Point Defect and Sintering of Lead Zirconate-Titanate", J. Am, Ceram. Soc., **54** (1971) 265-270.

[170] B. Jaffe, W.R. Cook, H, Jaffe *"Piezoelectric ceramics"* Academic Press Limited, London (1971) 237-251.

[171] Y. Saito, H. Takao "High Performances Lead-Free Piezoelectric Ceramics in the $(K,Na)NbO_3$-$LiTaO_3$ Solid Solution System" Ferroelectrics, **338** (2006) 17-32.

[172] H. Birol, D. Damjanovic, N. Setter "Preparation and characterisation of $(K_{0.47}Na_{0.53})NbO_3$ ceramics" J. Eur. Ceram. Soc. **26** (2006) 861-866.

[173] R.J. Xie, Y. Akimune, R.P. Wang, K. Matsuo, T. Sugiyama, N. Hirosaki "Spark Plasma Sintering of Tungsten Bronze $Sr_{2-x}Ca_xNaNb_5O_{15}$ (x=0.1) Piezoelectric Ceramics: I, Processing and Microstructure" J. Am. Ceram. Soc., 85 [11] (2002) 2725-2730.

[174] G. Ravi, R. Jayavel, S. Takekawa, M. Nakamura and K. Kitamura "Effect of niobium substitution in stoichiometric lithium tantalate (SLT) single crystals" J. Crys. Growth, **250** [1-2] (2003) 146-151.

[175] Y. Zhen, J.F. Li "Normal Sintering of (K, Na)NbO_3-Based Ceramics: Influence of Sintering Temperature on Densification, Microstructure, and Electrical Properties" J. Am. Ceram. Soc. **89** [12] (2006) 3669-3675.

[176] H. Chen, J. Long, Z. Meng: "Effect of Zr/Ti ratio on the properties of PMMN–PZT ceramics near the morphotropic phase boundary", Mat. Sci. and Eng. B, **99** [1-3], 433-436 (2003)

[177] M. Kosec, A. Bencan Golob, J. Bernard, J. Fisher, J. Holc, D, Jenko, B. Malic "Towards Better Performances of Piezoelectric Ceramics Based on Alkaline Niobates", 10th International Conference and Exhibition of the European Ceramic Society, Berlin, June 17-21, 2007

[178] R.J. Xie, Y. Akimune "Lead-free piezoelectric in the $(1-x)Sr_2NaNb_5O_{15} - xCa_2NaNb_5O_{15}$ (0.05 ≤ x ≤ 0.35) system" J. Mat. Chem. **12** (2002), 3156-3161.

[179] H.R. Rukmini, R.N.P. Choudhary, V.V. Rao "Effect of doping pairs (La,Na) on structural and electrical properties on PZT ceramics" Mat. Chem and Phys. **55** (1998) 108-114.

[180] M. Matsubara, T. Yamaguchi, W. Sakamoto, K. Kikuta, T. Yogo, S. Hirano "Processing and Piezoelectric Properties of Lead-Free (K,Na)(Nb,Ta)O$_3$ Ceramics" J. Am. Ceram. Soc., **88** [5] (2005) 1190-1196.

[181] ISO 8213:1986, Chemical products for industrial use - Sampling techniques - Solid Chemical products in the form of particles varying from powders to coarse lumps